ELECTRONIC COMPONENTS & APPLICATIONS

VOL.8 - No.4

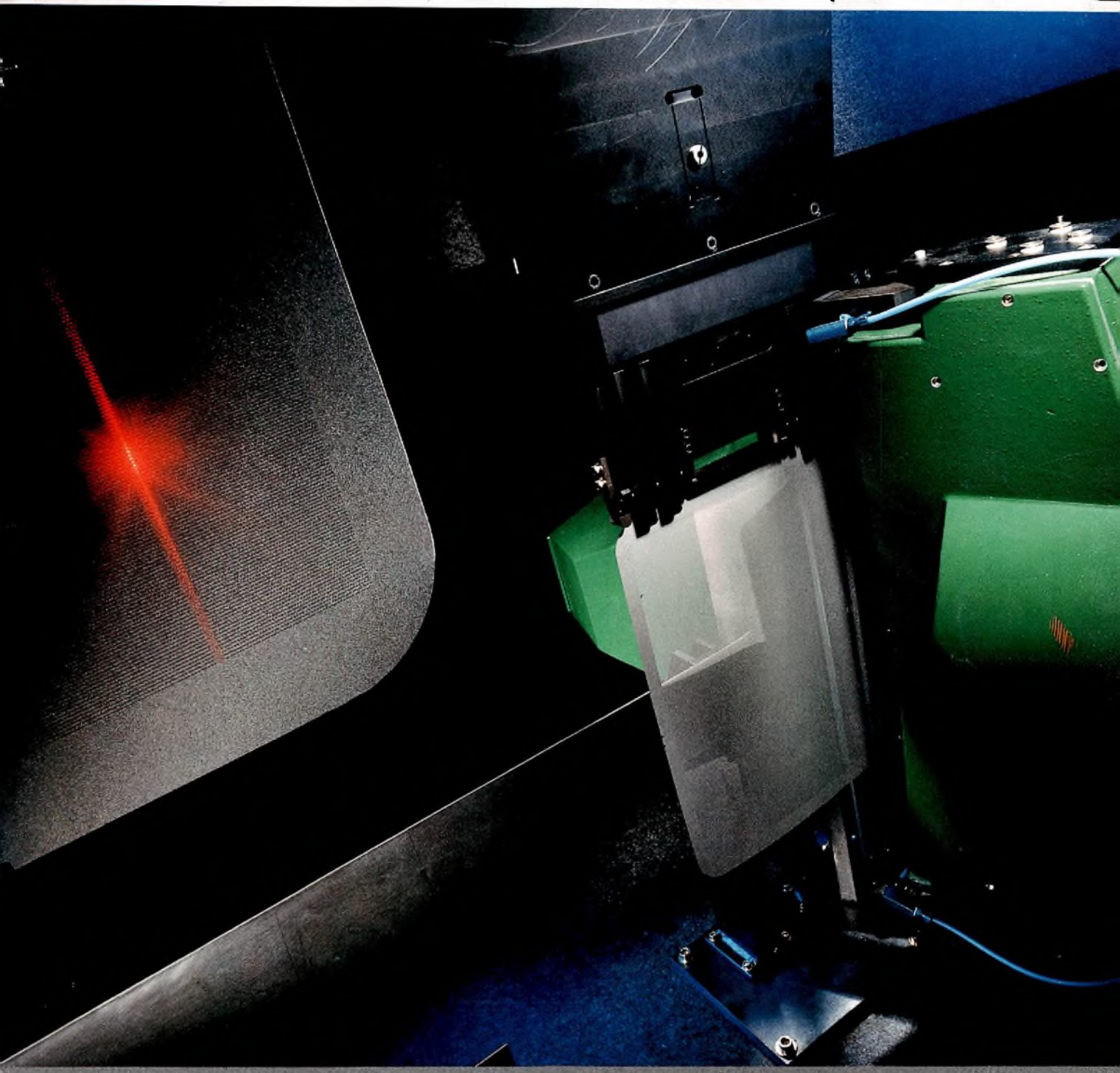

Philips Components

PHILIPS

ISSN 1041 – 6219

Electronic components & applications

Volume 8, No. 4

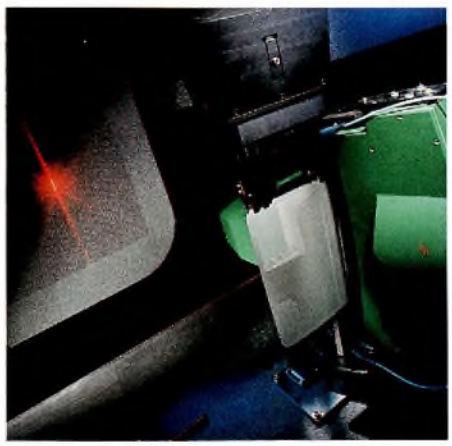

Philips' 45AX flat-square colour picture tube is a precision component, far removed from the simple monochrome CRT from which it evolved. Its design and manufacture, a fine blend of the electrical and mechanical engineers' skills. Skills that are apparent in every element of its construction. Like its unique ART (aberration-reducing triode) gun with oblique-injection – designed with the latest CAD techniques for optimum electron-optical behaviour. Located and aligned in the tube with better than 200 µm accuracy to provide outstanding stability and focusing precision. And its shadow mask – manufactured with micron precision – every one of its several hundred thousand apertures individually laser scanned (see photo) for accuracy. And mounted on its revolutionary corner suspension system (see article on page 215), to provide excellent temperature compensation and immunity from microphony. Without doubt an innovative product at the very forefront of display technology, providing a level of picture quality and fidelity undreamed of just a few years ago.

Contents

SAL capacitors for automotive applications

EVERT DEKKER

Philips made its first car lamps more than 50 years ago, and ever since then it's been manufacturing high quality electronic components for automotive use. As the largest supplier of electronic components in the world, Philips offers automotive manufacturers both a broad product range and expertise in specialist areas such as surface mounting and Application Specific IC (ASIC) design. Its Automotive Centre in Detroit, with a work force of over 200, highlights its commitment to provide technical support for all aspects of automotive electronics.

Capacitors are among the most traditional of electronic components, and have always been important to the automotive industry. Of the various types available, the solid aluminium (SAL) range is particularly suited to the harsh automotive environment because of the following features:

- no inherent failure mechanisms
- temperature range −40 to +175 °C
- ability to withstand mechanical shock and vibration
- high tolerance to ripple currents
- ability to withstand reverse voltages
- low-drift characteristics.

This article describes the construction and properties of solid aluminium electrolytic capacitors, and highlights their automotive applications.

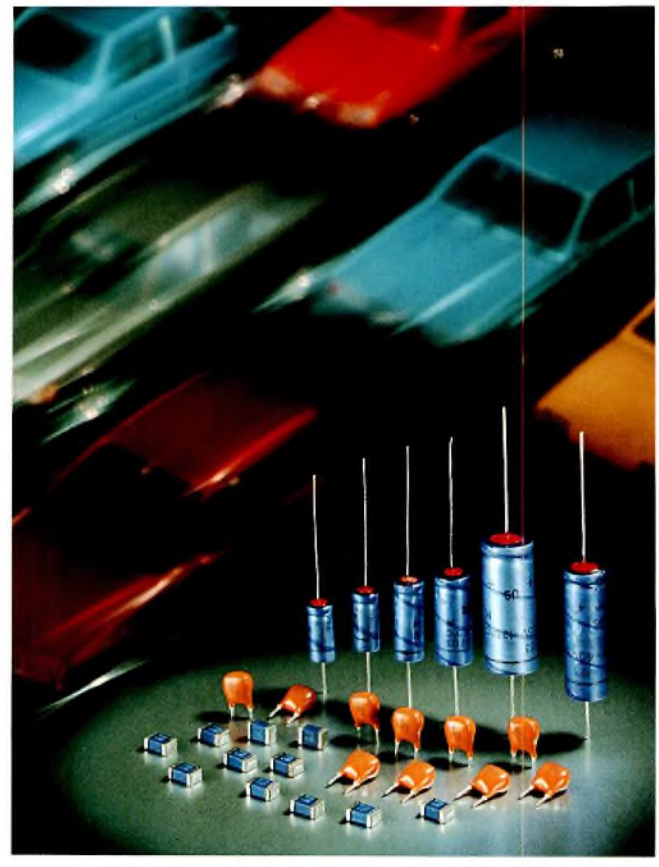

SAL capacitors are an important part of the electronic systems in a modern car

CONSTRUCTION OF SAL CAPACITORS

Capacitors are available for either general use or professional use, but for the harsh automotive environment, the professional category is preferred. Car applications require low voltages (4 to 40 V) and moderate capacitances (0.1 to 2000 μF). Three types of electrolytic capacitor (Ref.1) are available for these applications:

- non-solid aluminium, with an aluminium anode and a liquid or gel electrolyte cathode
- solid tantalum, with a tantalum anode and a solid semiconductor cathode
- solid aluminium (SAL), with an aluminium anode and a solid semiconductor cathode.

This section describes the construction of SAL electrolytics and discusses the relative merits of the three types of capacitor in automotive applications.

Wound-foil capacitors

Figure 1 is a schematic showing typical internal constructions of wound-foil capacitors. A wound aluminium foil covered with a dielectric oxide layer forms the anode, and a second aluminium foil functions as the cathode - see Fig.1(a). In non-solid electrolytics, the separator is paper impregnated with electrolyte as a solution or a gel. In solid aluminium electrolytics, the separator is a glass fibre impregnated with powdered manganese dioxide, which acts as a semiconductor. An alternative construction for capacitors with solid electrolyte is given in Fig.1(b). The main difference is a silver epoxy layer on a graphite base used at the cathode.

Non-solid electrolytes evaporate during storage and use and have a relatively short lifetime, but good stability. Their internal resistance increases at low temperature, thus reducing storage capacity. Although they easily resist short-duration surge currents, they are not stable to reverse voltages. Some of the limitations of non-solid electrolytics have been overcome with solid tantalum capacitors. These have high capacitance per unit volume, an internal resistance which is not strongly temperature dependent, and operate up to 125 °C, with, however, a voltage derating above 85 °C to avoid short-circuits. Because the electrolyte does not evaporate, their useful life is long. The electrolyte must be protected from humidity with a metal case or epoxy coating. Disadvantages of solid tantalum capacitors are that they're not suitable for applications involving reverse voltages or surge currents, they need to be protected with a series resistance of 3 Ω/V against a dynamic charge (Refs 2 – 4), and they may be damaged by mechanical shock or vibration. These limitations restrict the use of non-solid aluminium and solid tantalum capacitors in automotive applications.

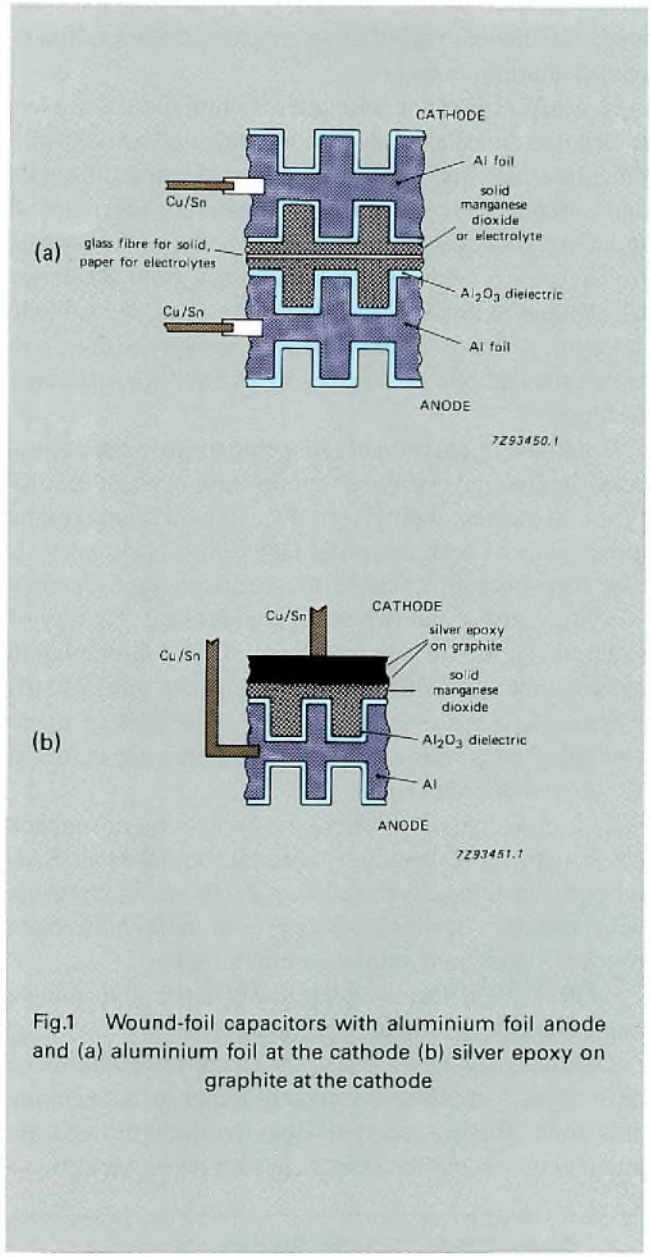

Fig.1 Wound-foil capacitors with aluminium foil anode and (a) aluminium foil at the cathode (b) silver epoxy on graphite at the cathode

SAL capacitors are less well known than their tantalum counterparts. Their construction combines features from non-solid aluminium and solid tantalum technologies. Lifetime, capacitance and resistance of SAL capacitors are about the same as for solid tantalum. They do not need to be voltage derated below 125 °C, can withstand surge currents, as well as reverse voltages, and do not require a series resistance for protection under a dynamic charge (Ref.5). These characteristics make then ideal for automotive applications.

Axial SALs

SAL capacitors with axial terminations in a metal case have been around for some time. Their CV product (Ref.6) has been greatly increased by using new, highly etched aluminium foil, which has a much larger surface area, and hence retains a higher charge, than ordinary etched aluminium foil.

In a SAL capacitor with etched aluminium foil electrodes, the anode assembly is manufactured by cold-welding the anode foil onto the anode pin. Aluminium anode and cathode foils and separator foils are then wound round the anode pin. The connection between the cathode foil and case is made by an ultrasonically-welded cathode tab, shown in Fig.2. For smaller case sizes, the cathode connection has been modified as shown in Fig.3, in which the ceramic disc serves as an anvil for ultrasonic welding.

Continual improvements are being made in the design, construction and chemical composition of axial electrolytics, to increase their CV product. Table 1 compares the dimensions of SAL and solid tantalum capacitors. SAL case type 1 is slightly larger than tantalum type B, otherwise the sizes of the two types are identical. By way of example, at a working voltage of 10 V, solid tantalum electrolytics are available with capacitances up to 220 μF, whereas SALs are available with capacitances up to 1000 μF. The working voltage of tantalum capacitors at 125 °C is reduced to 6.3 V.

SAL case types 1 to 4 have the same or higher capacitance than their tantalum equivalents, whereas SAL types 5 and 6 have capacitances which are unattainable with tantalum technology and until now have been restricted to the non-solid aluminium region.

Table 2 gives the complete capacitance and voltage ranges for SALs with axial terminations.

Finally, a new range of SAL axial capacitors has been developed, with an epoxy end-fill rather than a ceramic disc anvil (Fig.4), and with case sizes and termination pitches compatible with tantalum case types A and B.

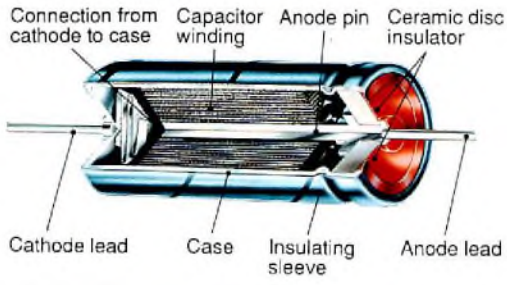

Fig.2 121-series of SAL capacitors, with coiled connection from cathode to case

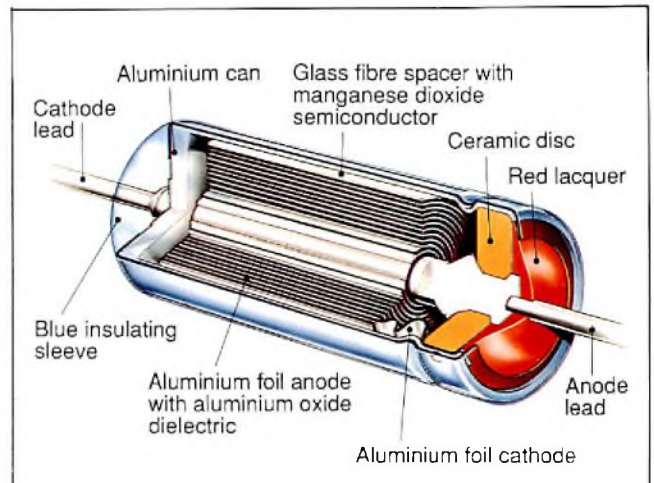

Fig.3 123-series of SAL capacitors with ceramic sealed construction

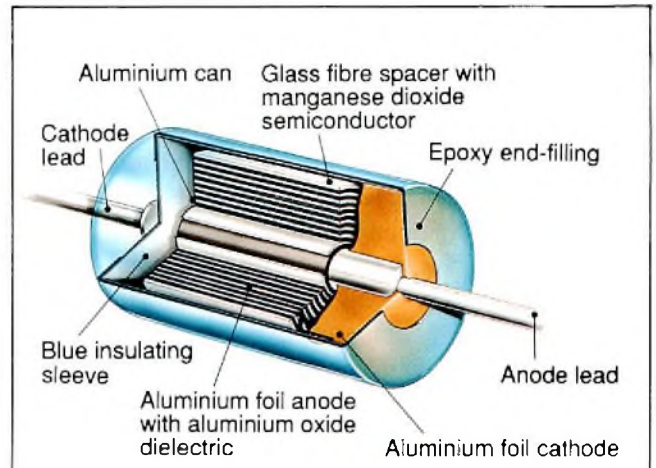

Fig.4 125-series of SAL capacitors with epoxy end-fill construction

TABLE 1
Sizes of solid tantalum and SAL capacitors.

Material	Case type	Diameter (mm)	Length (mm)
tantalum	B	5	15
SAL	1	6.5	15
tantalum	C	7.5	20
SAL	2A	7.5	20
tantalum	D	9	22.5
SAL	4	9	22.5
SAL	5	10	31.5
SAL	6	10	31.5

TABLE 2
Nominal capacitance C (μF) and rated voltage U_R (V) of SAL capacitors.

C_{nom} (μF)	U_R (V) at 125 °C							
	4	6.3	10	16	20	25	35	40
2.2							1	1
3.3							1	1
4.7							1	1
6.8							1	1
10				1	1	1	2A	2A
15				1	1	1	2A	2A
22				1		2A	2A	4
33			1	2A		2A	4	4
47		1	1	2A	2A	2A	4	5
68	1	1	2A	2A		4	5	5
100	1		2A	4	4	4	6	6
150		2A	4	4	5	5	6	
220	2A		4	5	5	6		
330		4	5	5	6	6		
470	4		5	6	6			
680		5	6	6				
1000	5	6	6					
1500	6	6						
2200	6							

Note: Dimensions of the various case types are given in Table 1.

Radial and surface mount SALs

Capacitors with radial terminations are smaller than those with axial terminations. Figure 5 shows the traditional construction of radial SAL capacitors. These have a thick aluminium anode foil, etched to increase capacitance, anodized to obtain the oxide dielectric, and folded to reduce volume. Solid manganese dioxide semiconductor is deposited on the anode foil, followed by layers of graphite and silver acrylate to provide a connection for the cathode lead. The anode lead is welded onto the anode stem, and the element covered with a lacquer coating.

Design and construction of radial SAL capacitors are being improved continually. For example, thinner foil (allowing a larger number of anode platelets) and increased etching improve the CV product. New flanged leads limit contamination by lacquer on one side, but also allow flux to flow past the leads in through-hole PCB applications (Fig.6).

A similar construction is used in chip capacitors for surface mounting (Fig.7). The capacitor is encased in a blue thermoset plastic outer case, filled with epoxy and closed by soldered copper caps. The cathode is attached to the terminal by a silver epoxy adhesive. Table 3 gives dimensions for the various case sizes of surface mount SAL capacitors, and Table 4 summarizes capacitance and voltage ranges for surface mount and radial lead versions.

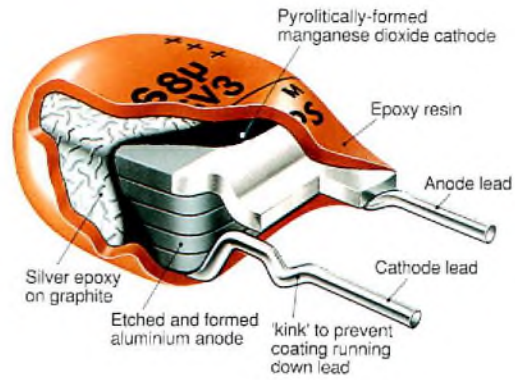

Fig.5 Traditional construction of radial SAL capacitors

TABLE 3
Dimensions of surface mount SAL capacitors

case size	H_{max}	W_{max}	L_{max}
20	3.0	4.5	6.7
30	3.5	5.8	6.7
40	4.1	5.8	6.7
50	4.1	7.9	6.7
60	5.2	7.9	6.7

Note: Dimensions are identified in Fig.7

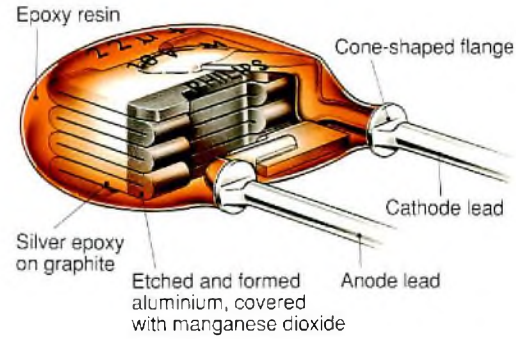

Fig.6 Improved construction of radial SAL capacitors

TABLE 4
Nominal capacitance C_{nom} (μF) and rated voltage U_R (V) for surface mount and radial SAL capacitors.

C_{nom} (μF)	U_R for surface mount (V)					
	4	6.3	10	16	20	25
	U_R for radial leads (V)					
	6.3	10	16	25	35*	40*
0.22						20
0.33					20	30
0.47					30	40
0.68				20	30	40
1.0				20	40	50
1.5				20	50	60
2.2			20	30	60	60△
3.3			20	40	60△	
4.7		20	30	50		
6.8		20	30	60		
10	20	30	40	60△		
15		30	50			
22	30	40	60△			
33	40	50				
47	50	60				
68	60					

* up to 85 °C; from 85 to 125 °C this value is 30V
△ under consideration

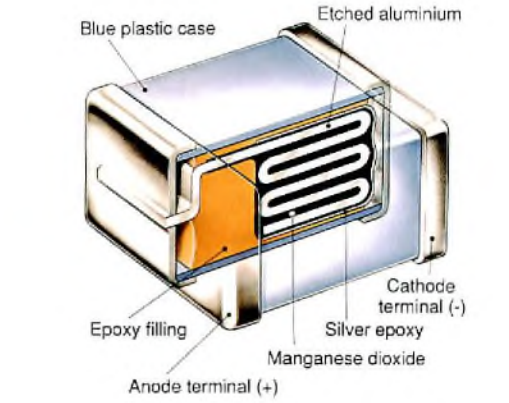

construction

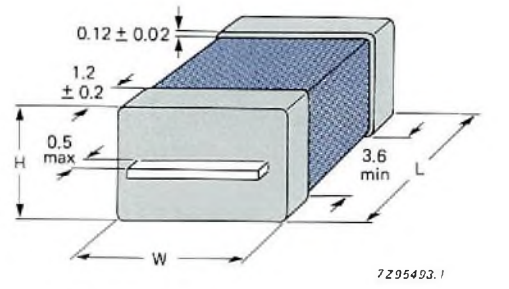

dimensions (in mm)

Fig.7 Surface mount SAL capacitors

AUTOMOTIVE APPLICATIONS

Putting electronics into cars means using components and assemblies under very demanding operating conditions, a fact not always fully appreciated in the past by component suppliers or automotive manufacturers. Components need to be rugged, completely reliable, able to withstand the effects of hot oil and water, able to work from sub-zero temperatures upwards, and able to tolerate a wide variety of electrical loads.

Extensive testing (summarized in the Appendix) of SAL capacitors shows that they not only survive under very hostile conditions, but continue to function very well. Additionally: testing has so far failed to reveal any failure mechanisms. In fact, these capacitors can actually improve with age, as the leakage current decreases during the life of the capacitor. This is in total contrast to both non-solid aluminium and solid tantalum electrolytics, which have intrinsic failure mechanisms that ultimately result in the breakdown of the capacitor.

Further advantages are that the electrical and thermal characteristics of SAL electrolytics remain constant throughout a very long life, and they can tolerate a variety of electrical loads. These characteristics make SAL capacitors ideal for the demanding operating conditions of the automotive environment.

In 1970 a car had less than $20 of electronic equipment. By 1985 electronics cost about $500 in each car, and by 1992 they are likely to cost close to $1500 per car, which means a projected annual growth rate of 15% for the next few years. Capacitors are an important part of this market.

Because capacitors are used in almost every section of the automotive industry and in virtually every part of a vehicle, it is not possible to cover all of the applications. This section highlights current applications of SAL capacitors in cars (Fig.8).

SAL capacitors are ideally suited to the harsh environment of the engine, and are used, for example, to protect microprocessors and microcontrollers against transient electrical disturbance, in the fuel injection and ignition systems, in ignition timing, and to preheat diesel fuel (making it easier to start the engine). They are also used in sensors for oil and fuel levels.

Safety is a vital concern in all automotive applications, and SAL capacitors are part of many safety features, including the automated braking system. In addition they provide back-up power for the seat belt tightener (Fig.9) and inflatable air bag, in case the normal electrical supply is disconnected as a result of an accident.

To prevent interference, it is necessary to suppress electrical noise to almost every electric component, and SAL capacitors are used extensively in this role, for example, on motors for the windscreen wiper, radiator fan and fuel pump.

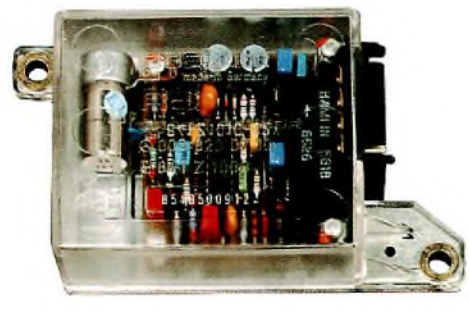

Fig.9 Sensor to increase seat belt tension at the start of a collision

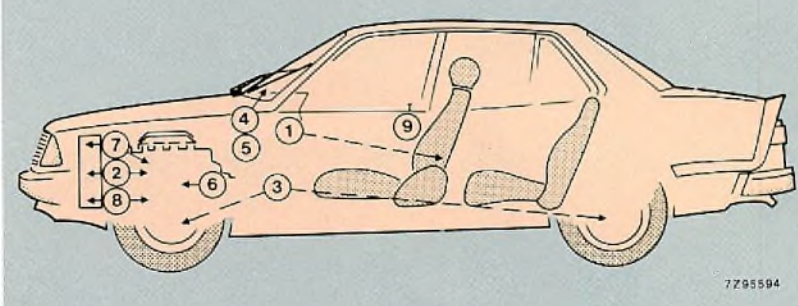

application

1. Crash sensor for seat belt stretching device
2. Electronic fuel injection
3. Automated braking system
4. Timer for windscreen wiper
5. Suppression capacitor for wiper
6. Electronic ignition
7. Suppression capacitor for fuel pump
8. Ignition timer
9. Remote control central doorlock

Fig.8 Some current applications of SAL capacitors in the car

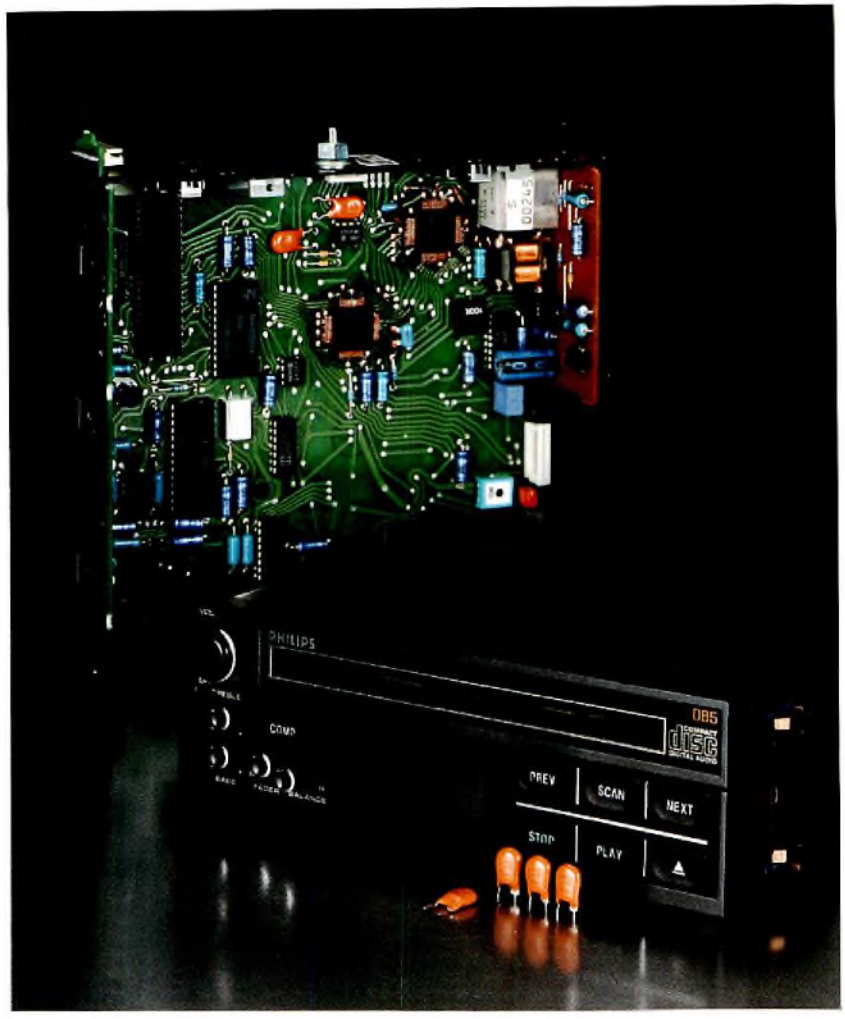

Fig.10 A CD player is part of every high quality car entertainment system

Other uses include:

- control of the direction indicators
- remote monitoring of tyre pressures
- electronic control of the heating/ventilation system
- the CD player (Fig.10)
- the power supply and circuitry of the CARIN* car navigation system
- advanced, high technology display systems (Fig.11).

Fig.11 Integrated opto-electronic driver information displays use SAL electrolytics (courtesy of Bosch GmbH)

* Philips' Car Information and Navigation (CARIN) system links a microprocessor with the data storage capacity of CD to provide an electronic pilot, which supplies information to the driver as spoken instructions supported by simple schematic diagrams.

Increasing concern about safety, pollution, economy and reliability is causing a revolution in automotive design. It is no longer sufficient for a car to be fast, aesthetically appealing and comfortable. It must also be economical, efficient, competitively priced, reliable and unquestionably safe. Electronic components and systems, including SAL capacitors, play a vital and expanding role in helping car manufacturers to achieve these goals.

Philips' SAL capacitors are approved by the European Space Agency, and are used in the Ariane rocket. They are equally well suited to the rugged environment of space and the harsh conditions encountered in automotive applications.

APPENDIX

Test conditions and results for SAL capacitors

Temperature and endurance tests

Initially, the standard endurance test temperature for SAL electrolytics was 85 °C, but this was subsequently raised to 125 °C at rated voltage. Large numbers of SALs have been measured over a period of years, as part of our quality assurance programme. Results are analyzed by normal statistical methods, such as the Weibull distribution (Ref.7), which plots cumulative frequency (per cent samples less than a given value) against some property of a system. Figure 12 shows Weibull plots of change in capacitance against cumulative frequency for various durations. Figures 13 and 14 show Weibull plots for dissipation factor and leakage current, respectively, for various durations.

Table 5 summarizes test conditions that are in current use, and shows that temperature limits are being increased continually.

TABLE 5
Test conditions for SAL capacitors.

Temperature (°C)	Duration (h)	Purpose
125	5000	qualification approval
125	20000	standard quality control
125	45000	occasional quality control
155	2000	qualification approval
155	5000	pending qualification approval
155	20000	standard quality control
175	2000	search for limits (radial leads)
200	2000	search for limits (axial leads)
260	0.01	soldering test for SMDs
300	0.1	search for limit of SMDs
190-250	>250	actual use for axial leads

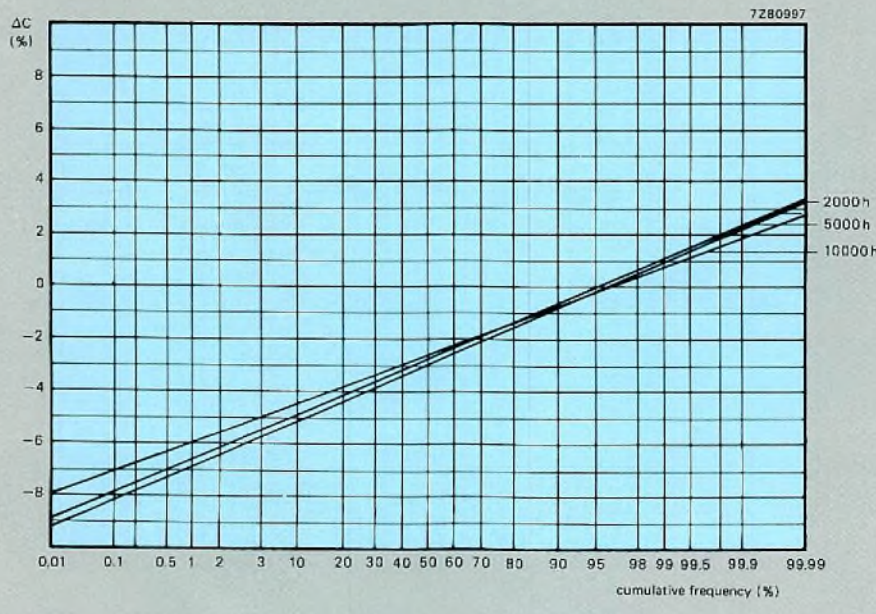

Fig.12 Weibull plots showing change in capacitance (ΔC) as a function of duration of test

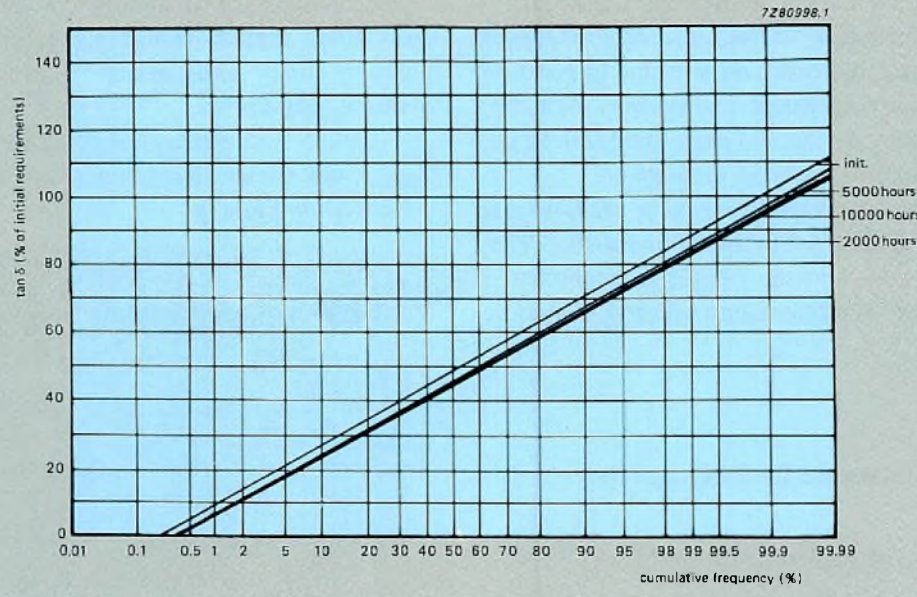

Fig.13 Weibull plots showing dissipation factor (tan δ) as a function of duration of test

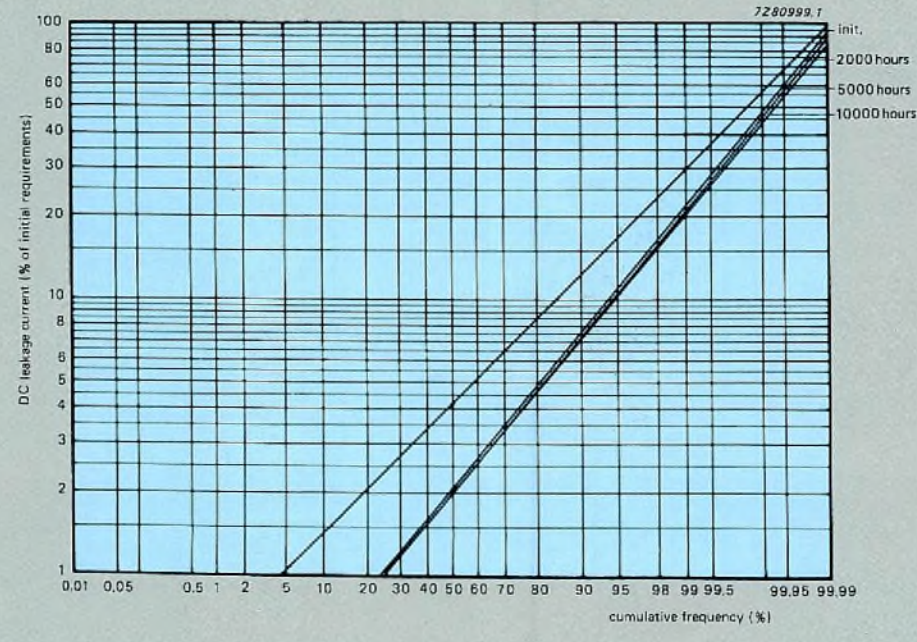

Fig.14 Weibull plots showing leakage current as a function of duration of test

Qualification tests are carried out routinely at 155 °C. Capacitor limits for radial leads are determined at 175 °C owing to the internal solder connection. Axial leads have welded electrical connections which are stable up to 200 °C, although the thermoplastic sleeving becomes ineffective above about 175 °C.

Surface mount versions use a thermoset plastic encapsulation for greater thermal stability and to prevent solder from adhering to the case. Typical measured temperature profiles for soldering SMDs are given in Fig.15 for wave and in Fig.16 for reflow methods. Since SMDs are immersed under the solder in the wave method, they must withstand molten solder for up to 1 min.

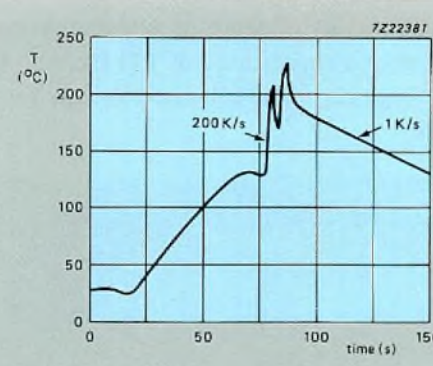

Fig.15 Measured temperature profile at the immersion point, for double-wave soldering

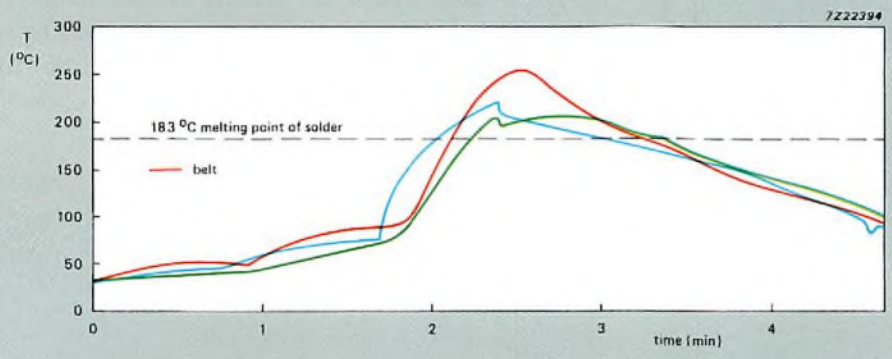

hot belt

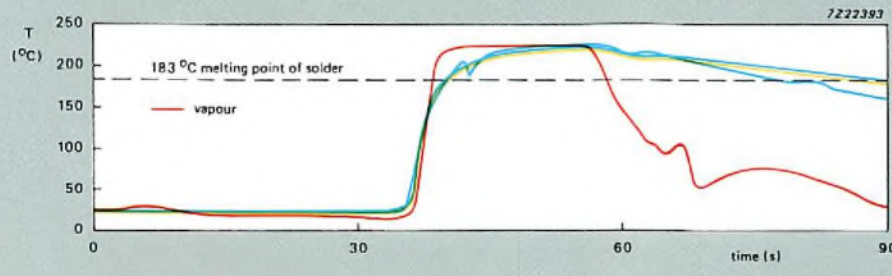

vapour phase

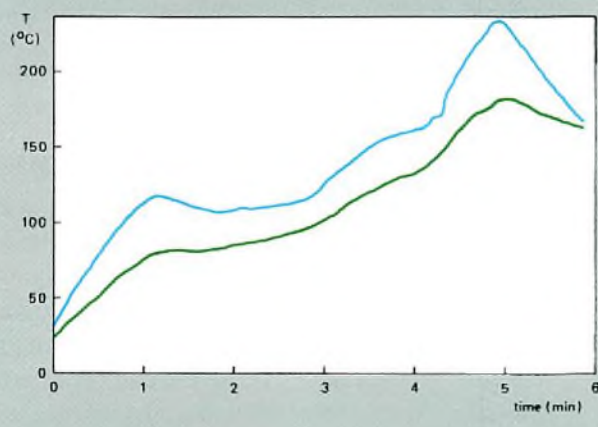

infrared

Fig.16 Measured temperature profiles for reflow soldering
small SMD
large SMD

Figure 17 shows the influence of temperature on axial SAL capacitors at a capacitance of 100 Hz, and Fig.18 shows the leakage current at full rated voltage for radial SAL capacitors.

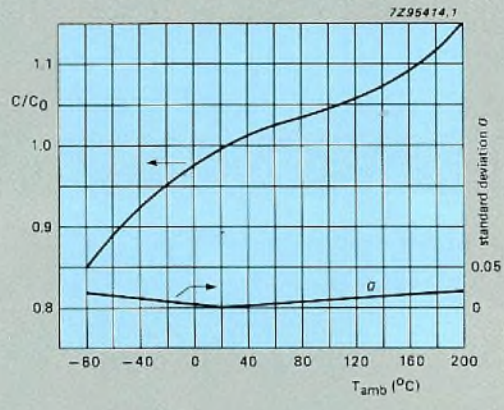

Fig.17 Capacitance of axial SAL capacitors as a function of temperature at 100 Hz (C_0 = capacitance at 25 °C)

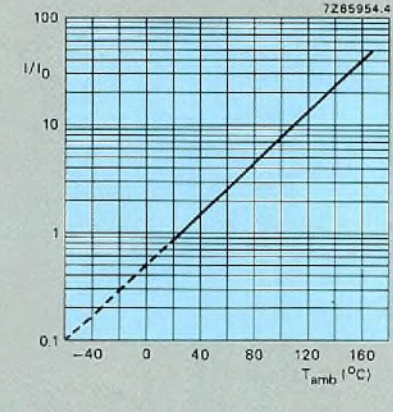

Fig.18 Leakage current of radial SAL capacitors as a function of temperature (I_0 = DC leakage current at 25 °C)

Thermal shock

In the standard thermal shock test, capacitors are cycled five times from −55 to +125 °C. For axial capacitors, the test is extended to 100 cycles, with the following additional requirements:

- no change in leakage current
- <10% variation in capacitance
- <60% change in dissipation factor and impedance.

For radial SAL capacitors, the temperature variation is reduced to a maximum of 90 °C in the range −55 to +125 °C, but the number of cycles is increased to 1400. Surface mount versions must withstand thermal shock caused by dipping in molten solder at 260 to 300 °C, followed by rapid cooling.

Surge voltage and reverse voltage

Surge voltage for extended periods is limited to 15% of the rated voltage. If the surge only lasts for milliseconds, then 2 to 3 times the rated voltage can be applied, and even larger surges can be tolerated for microseconds.

DC voltage cycles are limited to 30% of the rated voltage in the reverse direction and 100% of the rated voltage in the forward direction (Fig.19), for 2000 h. Up to 80% reverse voltage is allowed during AC operation.

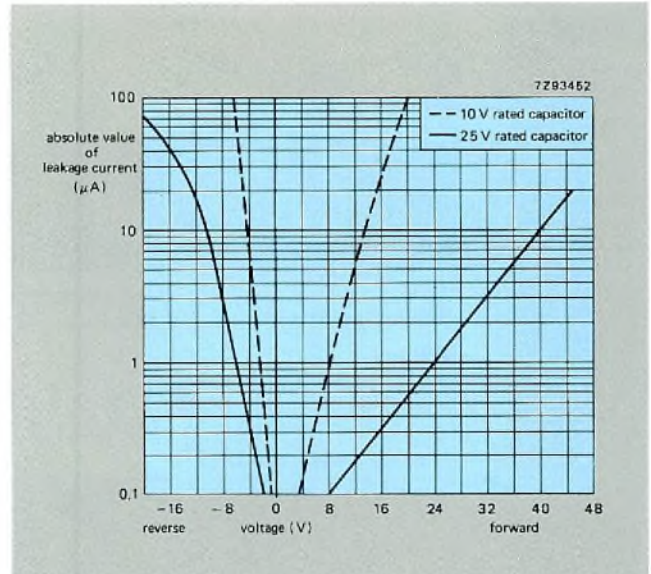

Fig.19 Leakage current in forward and reverse directions for axial SAL capacitors

Charge/discharge and ripple currents

Aluminium electrolytics can be charged and discharged without a current-limiting series resistor. Although the standard charge/discharge test involves 1 million cycles, this does not adequately represent conditions of use, and some types of non-solid aluminium electrolytics pass the standard test but fail in use. So the number of test cycles is usually extended to 4 million, to represent application conditions. When charge/discharge occurs several times per second, the currents become ripple currents.

Because ripple current increases the internal temperature and is accompanied by a ripple voltage, it is a stress parameter, which is therefore useful for accelerated testing. For example, a combination of ripple current, temperature and DC voltage can be used in a step-stress test (Ref.8) to assess the reliability of a new component. In this test several parameters are applied simultaneously, and the value of each parameter is increased in steps. For comparison, a component whose behaviour under the test conditions is well established is tested at the same time. Philips' 121-series of SAL electrolytics, available since 1971, is a suitable standard product that can be compared with the 123-series. Table 6 shows electrical data for the 123- and 121-series of capacitors at the start of the test, and Table 7 gives the step-stress measurements on these capacitor types, for the same case size.

Table 7 demonstrates that the performance of the two types is identical. Furthermore, it also shows that the devices have not been tested to their limits, although this is desirable to provide failed samples that can be examined to determine failure mechanisms, which can in turn be used to improve quality (Ref.8). Analysis from step-stress tests have enabled measures to be taken to increase specifications for CV product, ripple current, leakage current and temperature limit (Ref.9).

Vibration test

The standard test for the ability of a capacitor to withstand mechanical vibration is to accelerate at 10g, while vibrating at frequencies of 10 to 500 Hz. Test conditions are extended to 2000 Hz at 10g for normal SAL capacitors, and to 3000 Hz at 50g for special axial versions with a partial epoxy filling. Maximum acceleration that can be tolerated is about 100g.

TABLE 6
Electrical data for SAL electrolytics under test

	nominal capacitance	U_R	max. RMS ripple current at T_{amb} = 125 °C	max. leakage current at U_R after 1 min.	max. tan δ	max. ESR	max. impedance at 100 kHz
device [1] 2222 121 13331	330 µF	6.3 V	430 mA	150 µA	0.18	1.1	0.2
device [2] 2222 123 13102	1000 µF	6.3 V	760 mA	440 µA	0.18	0.36	0.2

REFERENCES

1. E.H.L.Dekker and P.S.Friedrich, 'Small electrolytic capacitors compared', Electronic Components and Applications, 4 , (3), 158-62 (1982).
2. J.Hasegawa and K.Morimoto, 'Characteristics and failure analysis of solid tantalum capacitors', NEC Research and Development, 50 , 79-94 (1978).
3. A.Cooke-Sanderson, 'Failure mechanisms in tantalum capacitors', Electronics Industry, 6 , 57-58 (1980).
4. J.D.Moynihan, 'Unshackle the solid tantalum capacitor', Proceedings 29th Electronic Components Conference, Cherry Hill, pp.303-8, IEEE (1979).
5. J.Brettle and N.F.Jackson, 'Failure mechanisms in solid electrolytic capacitors', Electrocomponents Science and Technology, 3 , 233-46 (1977).
6. E.H.L.J.Dekker and H.Schmickl, 'Advances in solid aluminium electrolytic capacitor technology', Electronic Components and Applications, 3, (4), 206-9 (1981).
7. R.A.Brown and F.J.Hinnenkamp, Journal of the Electrochemical Society, 123, (6), 886 (1976).
8. E.H.J.L.Dekker and H. Schmickl, 'Multiple-step stress testing proves the reliability of solid aluminium capacitors', Electronic Components and Applications, 8, (3), 137-44 (1988).
9. E.H.L.J.Dekker and C.J.Lasance, 'Thermal and electrical analysis of solid aluminium capacitors', Active and Passive Electronic Components, 12, 167-86 (1987).

TABLE 7

Step-stress test results for axial solid aluminium capacitors

stress step		1	2	3	4	5	6	7	8	9	10	11	physical
time (h)		24	24	24	72	24	24	24	24	72	24	24	limit
stress factor	*device*[1])												
DC voltage (V)	[1]	6.3	6.8	7.3	7.8	8.3	8.8	9.3	9.8	10.3	10.8	11.3	28.8[2])
	[2]	6.3	6.8	7.3	7.8	8.3	8.8	9.3	9.8	10.3	10.8	11.3	11.5
ambient temperature (°C)	[1]	125	130	135	140	145	150	155	160	165	170	175	175[3])
	[2]	125	130	135	140	145	150	155	160	165	170	175	175
RMS ripple current (mA)	[1][6])	342	380	420	1240	1340	1440	1500	1500	1500	1525	1540	1370[4])
	[2]	940	1040	1140	1240	1340	1440	1540	1640	1740	1840	1940	1290
RMS ripple voltage (V)	[1]	1.5	1.65	1.8	5.24	5.61	5.9	6.0	6.0	6.0	6.0	6.0	12.4[5])
	[2]	1.24	1.34	1.47	1.65	1.77	1.9	2.1	2.1	2.2	2.38	2.56	0.1
peak ripple voltage (V)	[1]	2.1	2.3	2.5	7.4	7.9	8.3	8.5	8.5	8.5	8.5	8.5	17.5[5])
	[2]	1.8	1.9	2.1	2.3	2.5	2.7	3.0	3.0	3.1	3.4	3.6	0.2
sum of DC voltage + peak ripple voltage as multiplier on U_R	[1]	1.3	1.4	1.6	2.4	2.6	2.7	2.8	3.0	3.0	3.1	3.1	4.6
	[2]	1.3	1.4	1.5	1.6	1.7	1.8	2.0	2.1	2.1	2.3	2.4	1.8
measured results[7])													specification[8])
leakage current as multiplier on CV	[1]	0.006	0.006	0.005	0.004	0.003	0.003	0.002	0.002	0.001	0.002	0.002	
	[2]	0.025	0.024	0.024	0.017	0.017	0.015	0.013	0.012	0.012	0.018	0.018	0.1
$\triangle C$ as a % of initial capacitance at 100 kHz	[1]	−2.2	−2.7	−3.1	−7.3	−9.6	−11.0	−13.6	−14.9	−16.1	−15.7	−15.3	
	[2]	−2.2	−2.9	−3.3	−4.2	−4.4	−4.9	−5.2	−5.5	−5.7	−5.9	−6.2	10%
tan δ (dissipation factor as a % at 100 Hz)	[1]	4.4	4.5	4.8	6.6	9.8	9.0	9.9	9.5	10.0	9.8	8.6	
	[2]	17.2	17.2	17.0	16.8	18.6	18.2	18.5	18.4	18.2	18.6	16.5	22%
impedance at 100 kHz (mΩ)	[1]	93	94	91	83	87	82	84	86	90	92	80	
	[2]	150	147	141	132	138	136	139	134	137	141	128	240

[1]) Device type [1] – Axial lead solid aluminium capacitor series 121, 330 µF, $U_R = 6.3$ V.
Device type [2] – Axial lead solid aluminium capacitor series 123, 1000 µF, $U_R = 6.3$ V.
[2]) Voltage limit is 60% of the anode foil forming voltage.
[3]) Temperature limit: at 175 °C discolouration of the tin and insulation occurs, the capacitors can electrically go beyond this temperature.
[4]) Ripple current limit is derived from an inner temperature 20 °C higher than ambient.
[5]) Peak ripple voltage limit is the difference between limit value and applied value of the voltage.
[6]) For the 330 µF reference capacitor (device [1]), the ripple current setting was hampered by power supply limitations.
[7]) Average of six samples.
[8]) Specified requirements after 125 °C endurance tests. Wider margins apply for higher temperatures.

Redesign of small-signal switching diodes in SOT packages

CHRIS HARTMAN and MICHIEL HILLEN

When small-signal diodes were first used in surface mount transistor encapsulations (SOT packages), the existing diode technology (originally developed for glass diodes) was simply married to the existing plastic transistor encapsulation, causing some design shortcomings. For example, with the conventional Ti/Pt/Au metallization deposited on top of the thick insulation necessary for glass envelopes, there can be insufficient 'step' coverage which can crack the gold layer, allowing Au/Si alloys to form. In addition, glass diode chips have high phosphorus content (necessary for gettering) and this can corrode the metallization. To avoid these possible shortcomings, and to improve the quality, we have completely redesigned our small-signal diodes in SOT23 and SOT143 packages. The redesign combines the latest in diode technology with standard transistor technology.

This article discusses the relative merits and reliability of the new and old designs.

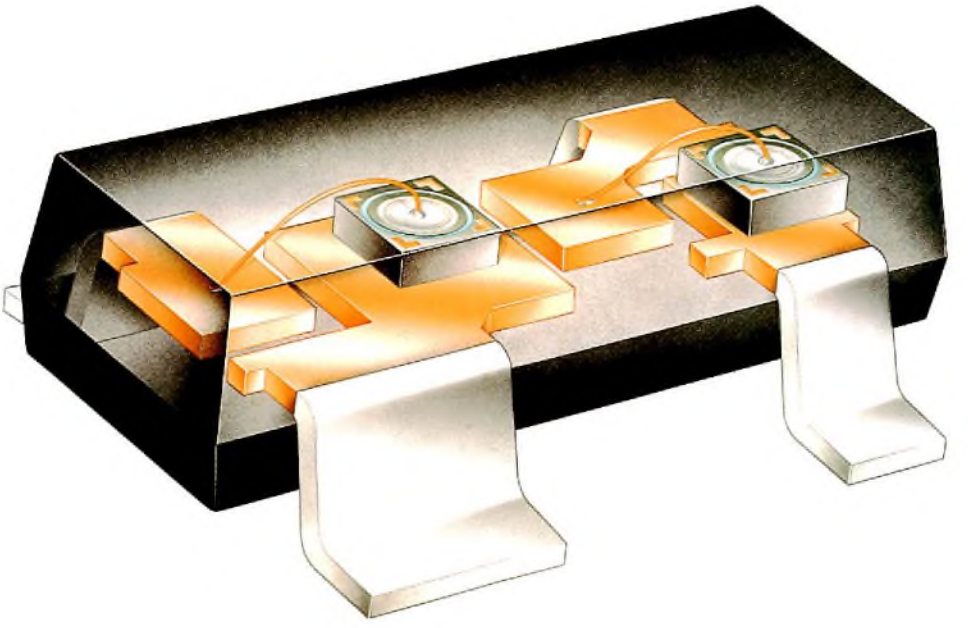

BAV23 small-signal diodes in SOT143 encapsulation

DESIGN IMPROVEMENTS

Figure 1 shows the old and new chip designs.

The main features of the redesign are:

- Greatly improved passivation, resulting from silicon nitride passivation, which completely encloses the active areas of the crystal, and reduces phosphorus doping of the top oxide layer. This improves resistance to moisture and other contaminants, thus increasing reliability.
- A single layer of aluminium replaces the Ti/Pt/Au triple-layer as the top metallization, reducing the complexity, making deposition easier and improving reliability.
- Recognition marks and changing the shape of the contacts makes it easier to align and bond the crystals with automatic bonding machines, improving attachment quality.

Passivation

Glass encapsulation, although providing a hermetic seal, allows sodium diffusion from the glass into the chip, necessitating high phosphorus doping to getter the sodium. Because the new plastic encapsulation does not contain sodium, there is no sodium diffusion and hence the phosphorus in the top oxide layer can be significantly reduced, though some is still required as a getter. Since phosphorus reacts to produce phosphate glass which is hygroscopic, reducing the phosphorus level improves reliability.

Because plastic encapsulation does not provide a hermetic seal, the whole of the active area (except for the bonding wire) is sealed with an inert silicon nitride layer to isolate the crystal from the environment.

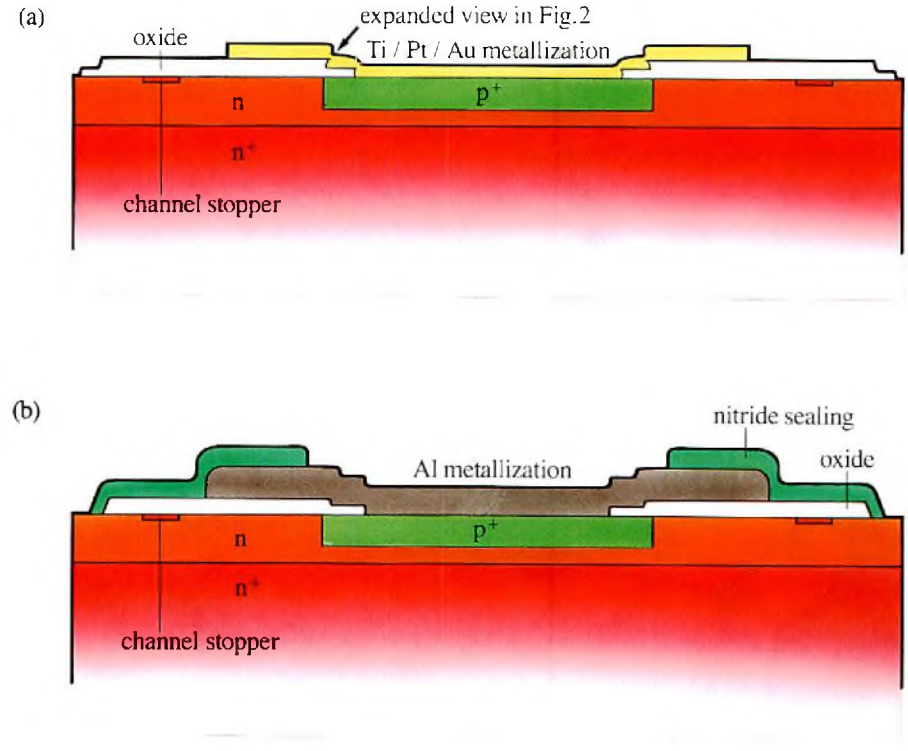

Fig.1 Comparison of (a) old and (b) new chip designs of small-signal diodes (schematic and not to scale)

Aluminium metallization

Although gold is well-established as a contact on silicon, it has two main drawbacks: it has poor adhesion and forms alloys with silicon. To overcome these drawbacks, it is necessary to deposit successive layers of titanium (improves adhesion), platinum (acts as a barrier) and gold. (Fig.2). Three depositions increase the complexity and make poor metallization more likely. As a result, the metallization tends to crack (unless special precautions are taken), and when this happens gold diffuses into the silicon, forming alloys which can reduce reliability or even cause failure.

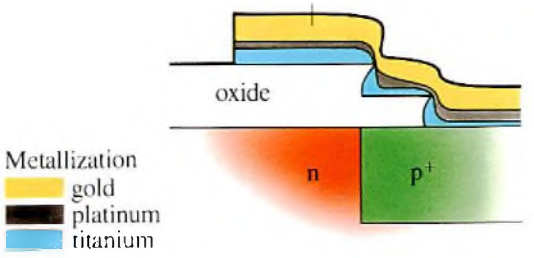

Fig.2 Ti/Pt/Au metallization showing worst-case step coverage in the old chip design

In the new process the Ti/Pt/Au metallization on the top electrode is replaced by aluminium, which is the standard metallization in ICs and transistors. Aluminium adheres well, does not form alloys with silicon, and can be deposited in a single operation. Since the new metallization gives the same electrical performance at normal operating temperatures, aluminium metallization is now standard for our small-signal diodes.

The new diodes meet the worldwide specification for maximum junction temperature ($T_{j\,max}$) of 150 °C, although this is 25 °C lower than for gold types. A $T_{j\,max}$ of 150 °C is, however, sufficient for all normal circuit operations.

Recognition marks

As part of the redesign we have introduced recognition marks (Fig.3) on all symmetrical crystals, to make alignment easier and more reliable, which in turn makes automated wire bonding more straightforward. Also, the shapes of some of the contacts have been changed to make them asymmetric (Fig.4), and this again makes alignment and bonding more reliable.

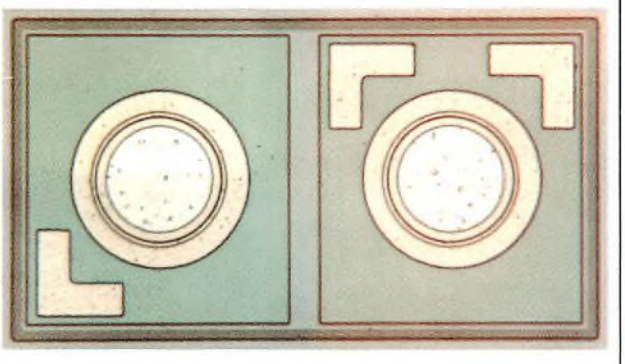

Fig.3 Recognition marks for automatic bonding of a BAV70 diode in SOT 23 package

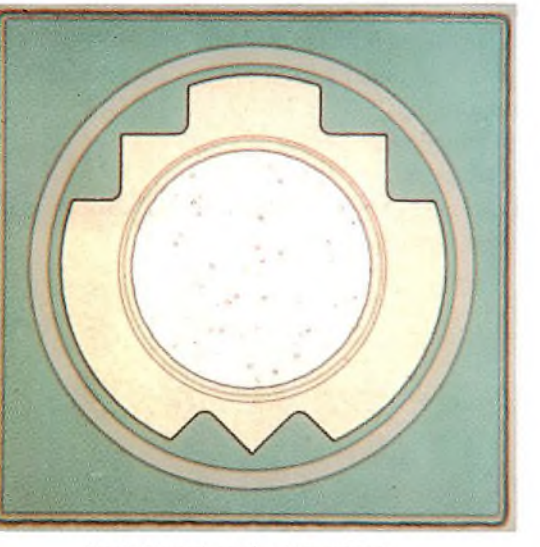

Fig.4 New shape for top contact, to make alignment more reliable

RELIABILITY AND ENDURANCE TESTING

Introducing silicon nitride passivation into transistors greatly improved reliability (Fig.5). A detailed test programme has confirmed that silicon nitride passivation also improves the reliability of small-signal diodes.

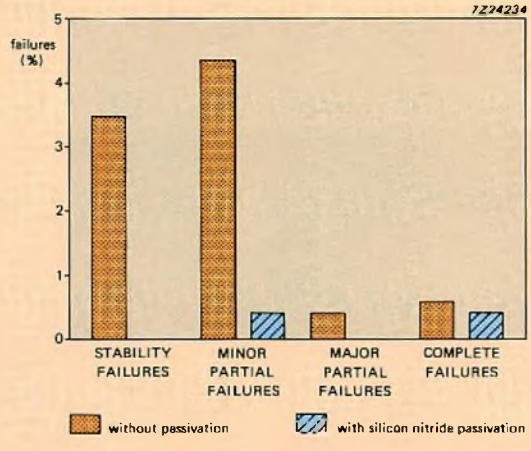

Fig.5 Summarized defects for BF457 transistors, showing no stability failures or major partial failures with silicon nitride passivation

Figure 6 summarizes reliability results for five types of small-signal diode, for the following tests:

- forward current
- thermal fatigue
- reverse bias at high temperature
- reverse bias under humid conditions (85 °C/85% relative humidity)
- high temperature storage
- low temperature storage.

All tests (except at high humidity) were carried out at the maximum published ratings.

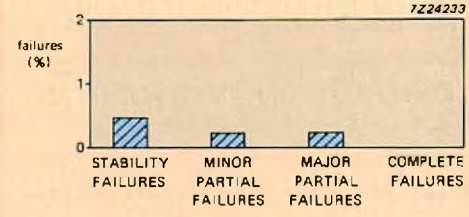

Test conditions:

number of tested devices	430
total tested device hours	430000
observed parameters	I_R, V_F.

Fig.6 Summarized defects for five types of small-signal diode with silicon nitride passivation

Junction temperature is an important parameter in determining lifetime. Figure 7 illustrates the expected useful lifetime of small-signal diodes in plastic encapsulation and with aluminium metallization, as a function of the junction temperature. This figure shows an expected lifetime of 70000 hours at the normal operating temperature of 75 °C.

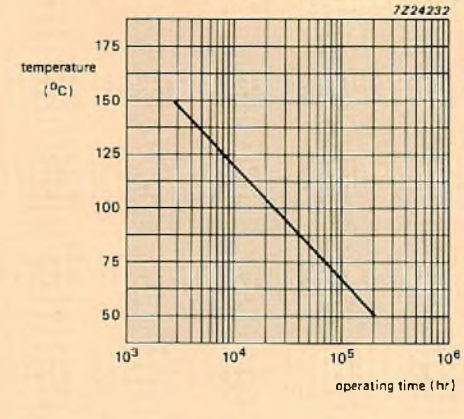

Fig.7 Expected useful life of small-signal diodes in plastic encapsulation and with aluminium top metallization

Blind and buried vias for multilayer PCBs

ALFRED GOBERECHT

The growth of surface-mount devices (SMDs) has had an enormous impact on PCB technologies, not least in the field of interconnection where some of the newest VLSI chips and chip carriers are stretching the expertise of the PCB manufacturer to the limit. Currently, multilayer boards are meeting the interconnection demands – the freedom gained by being able to interconnect layers by plated through vias simplifying component siting and track routing considerably compared with double-sided boards. In addition, impedances are much easier to define in a multilayer than in a double-sided board. And it's easier to protect signal lines from cross-talk – largely the result of being able to have internal as well as external supply and ground planes. Conventional multilayer vias, however, are drilled through *all* circuit layers, even though they may only connect conductors or voltage and earth planes on two layers. Although these plated through vias and lands can be extremely small (now that plated through vias are no longer required to accommodate component leads or pins), the board area they consume still mounts up quickly. A solution to this problem is to interconnect *pairs* of layers by using blind and buried vias, which can save significant amounts of board space. In addition, it can leave both outer layers clear for mounting SMDs at densities comparable to those of hybrid circuits.

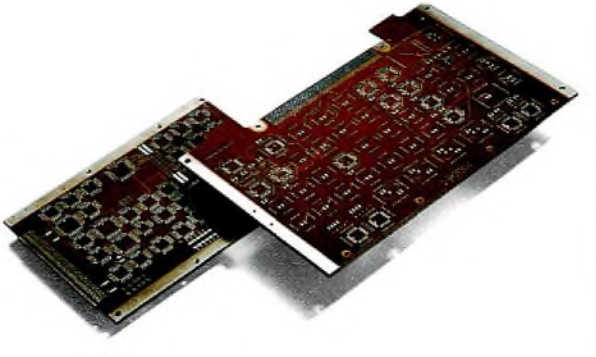

The use of blind and buried vias leaves few signal lines on the external layers of a multilayer – most submerge to internal layers. All that remains are the mounting lands for the SMDs, permitting board designs with extremely high component densities.

WHAT ARE BURIED VIAS?

Buried vias are plated through holes that interconnect two inner layers of a multilayer. Buried vias are not connected to either of the external layers.

WHAT ARE BLIND VIAS?

Blind vias are plated holes that interconnect either of the external layers of a multilayer to one or more internal layers.

ADVANTAGES OF BLIND AND BURIED VIAS

Not widely used to date, buried vias are a useful extension to multilayer technology for dealing with today's high-density printed wiring requirements. They can reduce the number of circuit layers needed, and hence can reduce the thickness and weight of a multilayer. Furthermore, buried vias simplify both manual and computer-aided board design. The use of perpendicular conductors (to provide changes of direction) on different layer pairs connected by buried vias, combined with smaller holes and lands can increase wiring density significantly without having to resort to very-fine conductors, see Fig.1.

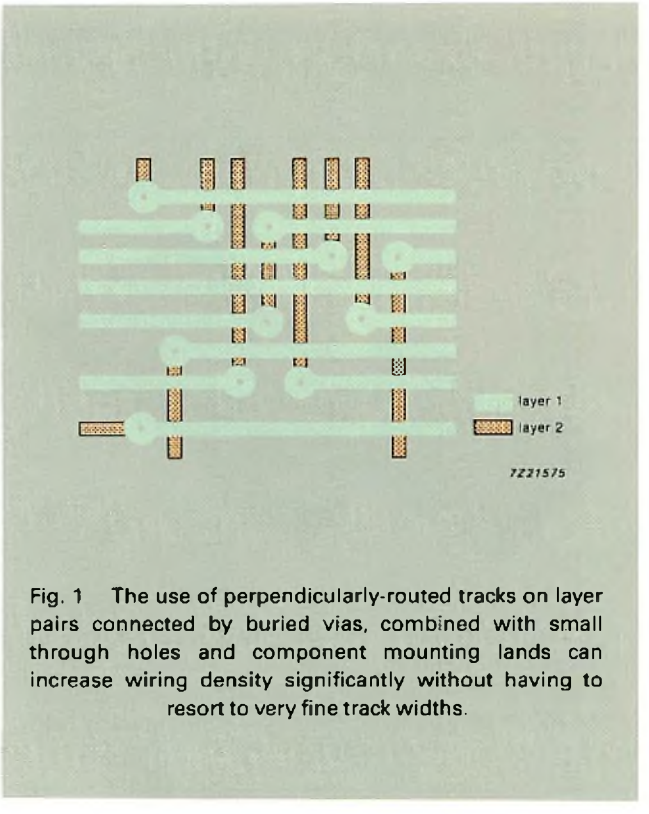

Fig. 1 The use of perpendicularly-routed tracks on layer pairs connected by buried vias, combined with small through holes and component mounting lands can increase wiring density significantly without having to resort to very fine track widths.

MANUFACTURE OF BLIND AND BURIED VIAS

Multilayers with blind and buried vias are manufactured using the same equipment, materials and processes used to manufacture conventional multilayer boards, see Fig.2. The only difference is that inner layers are made in pairs, each with its own drilling tape, and each pair is treated as an individual double-sided board with plated through holes. The additional cost of the two extra steps in manufacture – drilling and plating the inner layer pairs – is usually offset by a reduction in the number of circuit layers required.

Figure 3 shows a section through a multilayer with blind and buried vias. The inner circuit layers are made using double copper-clad laminate (usually about 0.1 mm thick). Layer pairs are connected by small plated holes (buried vias). The inner layer pairs are laminated between copper foil using resin/glass prepeg for bonding and insulation. This process is the same as that in conventional multilayer manufacture, except that the plated holes are filled with resin and buried within the laminate. After lamination, as in conventional multilayer manufacture, holes are drilled and plated to provide through vias, connecting surface layers to internal layers. External layers are imaged and etched to form the external layer wiring and component mounting lands.

External layers with blind vias are treated in a slightly different way to layers with buried vias, namely that the external layers are not etched until after lamination as for a conventional multilayer. Blind vias prevent solder flowing away during the soldering of SMDs, because the plated-through via hole is filled with resin.

Buried vias are used in the first place to gain board space, so they should be as small as drilling techniques permit. At present, we can drill 0.3 mm holes in base materials between 0.1 and 0.4 mm thick. Laser drilling, currently under investigation, will allow even smaller holes to be drilled. Because the aspect ratio (board thickness to hole diameter) of buried vias is low, the holes can be plated easily, a big advantage over through vias in conventional multilayers.

Buried vias can also be manufactured with smaller lands than through vias because the requirements for registration and drilling are less for a double-sided circuit than for a multilayer board with internal lands. Smaller lands allow either wider tracks for high-current applications or fine-line (<0.15 mm) tracks for high-density circuitry to be used. Note, however, that the lands and land diameters of the conventional vias on all the internal layers must be according to the normal rules for multilayer internal layers.

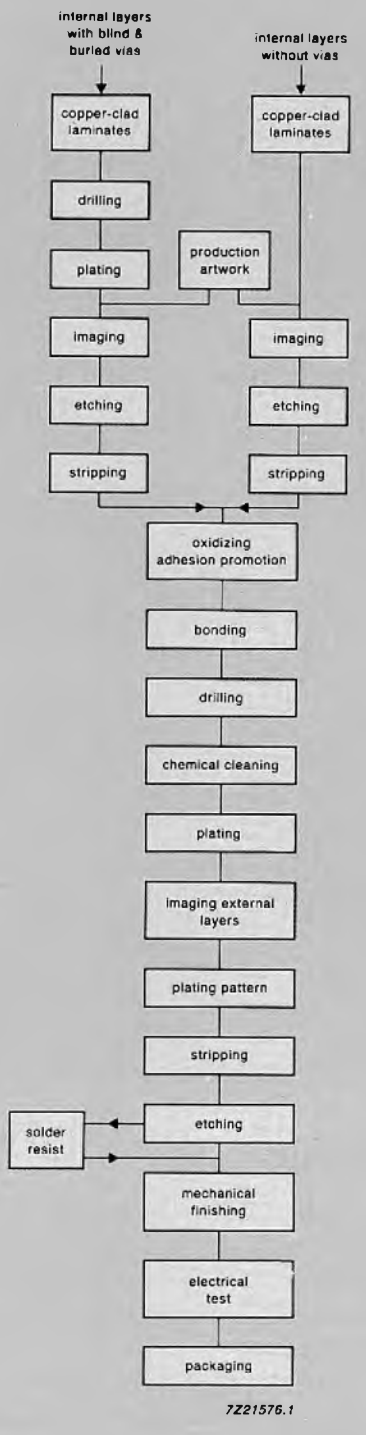

Fig. 2 Manufacturing stages for buried via multilayers.

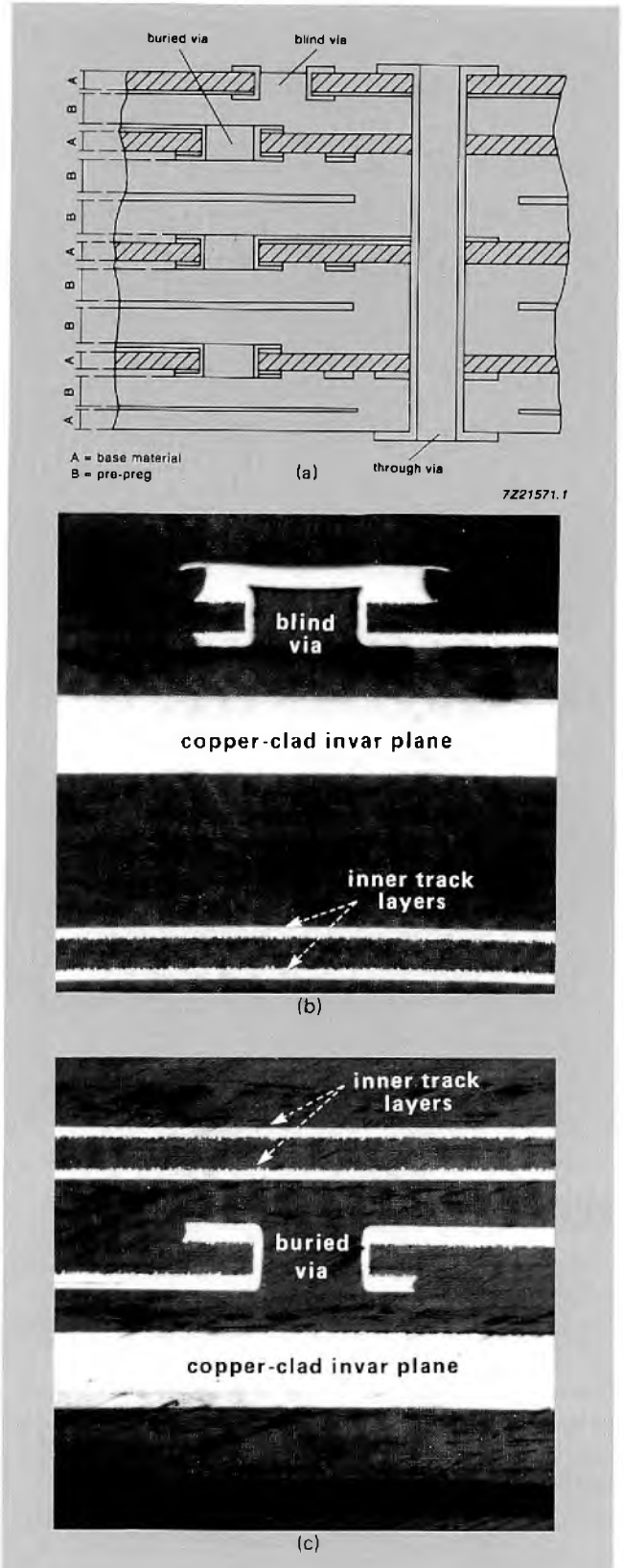

Fig. 3 Sections through a multilayer with blind and buried vias; (a) schematic. For completeness, a through via is also shown; (b) section through a blind via; (c) section through a buried via.

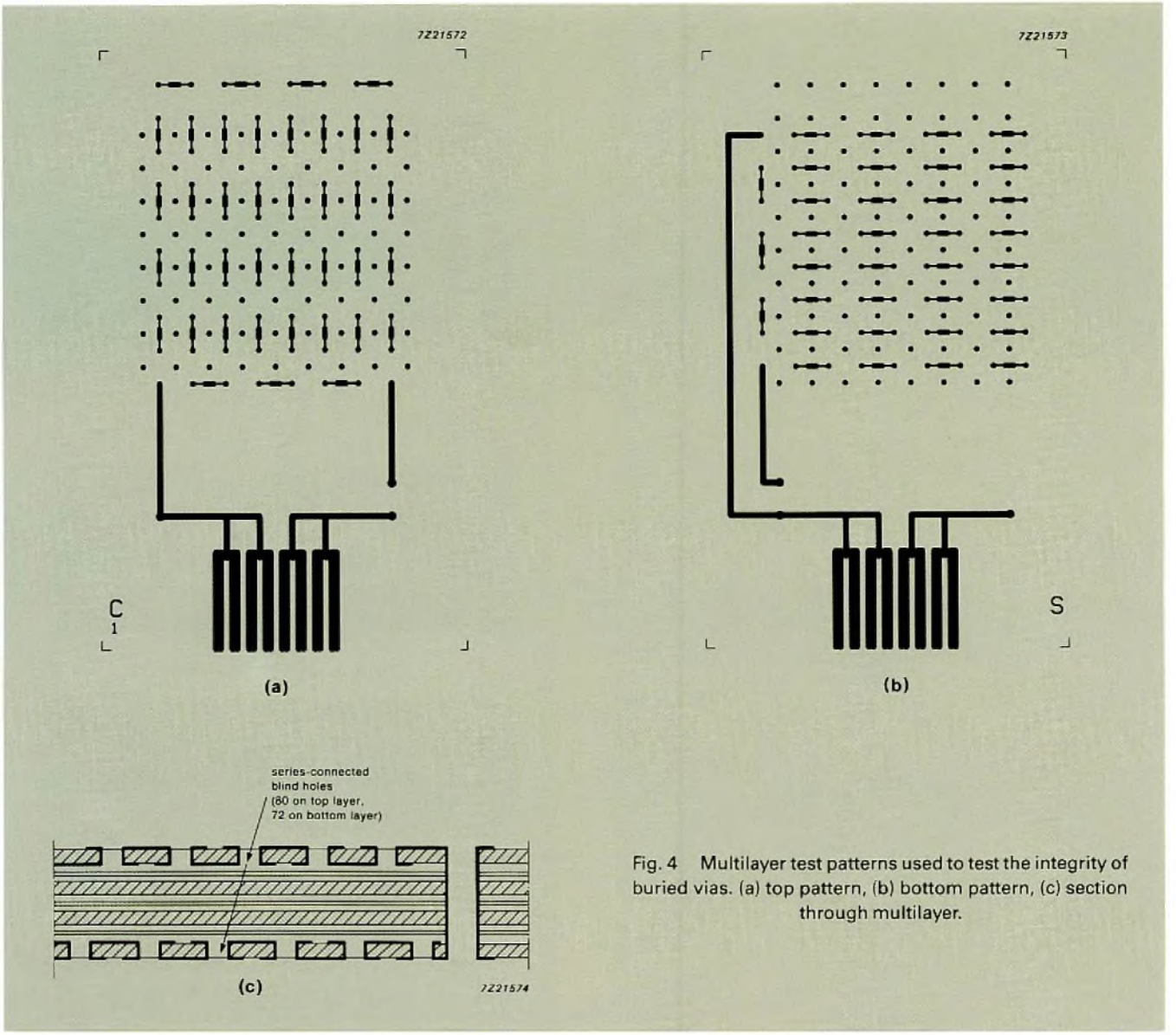

Fig. 4 Multilayer test patterns used to test the integrity of buried vias. (a) top pattern, (b) bottom pattern, (c) section through multilayer.

PROVEN PROCESS

The integrity of our buried via process is checked regularly by manufacturing a multilayer having the test patterns shown in Fig.4. Eighty blind holes on the top layer are electrically connected in series with seventy-two blind holes on the bottom layer. A four-point measurement is used to monitor the interconnection resistance of the plated vias during testing that includes thermal cycling hot oil dip (ten 20-second insertions into oil at 260 °C), thermal stress, solder float (288 °C for 10 s), thermal shock (100 cycles: 125 °C to −65 °C). Any significant resistance variations during testing are investigated thoroughly, the cause isolated and, if necessary, adjustments made to the process.

REFERENCES

1. 'Multilayer printed circuit boards,' Philips Components, Nov. 1986, ordering code 9398 336 30011.
2. 'Laser photo-tool service for printed circuit boards,' Philips Components, Jan. 1988, ordering code 9398 348 40011.
3. 'Printed circuit boards at the heart of the electronics world,' Philips Components, Oct. 1987, ordering code 9398 343 90011.
4. Printed circuit boards for force-fit solderless terminations, Philips Components, Nov. 1986, ordering code 9398 336 40011.
5. 'Photo-defined solder resist for printed circuit boards,' Technical Publication 250, Philips Components, Dec. 1987, ordering code 9398 057 90011.

An angle on the corners

the new approach in shadow-mask suspension systems

CEES ADMIRAAL and HENK BONGENAAR

Since domestic colour television appeared some 35 years ago, the traditional way of suspending the shadow mask in the picture tube has been by means of special mounting springs at or near the centres of each side – even though sound engineering principles dictate that a corner suspension system would be far more satisfactory. The reasons for the traditional system are largely historical, dating back to the early, round colour picture tubes. Shadow masks of these tubes naturally had three mounting springs spaced equally around the circumference, and as these tubes evolved into the rectangular designs of the '60s, it was technically simpler just to add an extra mounting spring and to keep the springs at the centres of each side. And, of course, once the suspension design had been settled, it would have required a major development programme and re-investment to switch to corner suspension, something that, until recently, no manufacturer has felt the incentive for.

The change came with the advent of the flat-square picture tube, which presented designers with new problems in terms of landing and colour purity, problems that could best be solved by introducing a completely new, optimized suspension system. It was at this time, during the introduction of its own Flat-Square (FS) tube when major factory re-tooling was needed in any case, that Philips took the opportunity to perfect and introduce its corner-pin suspension system, a system that has already had dramatic effects on picture tube performance and that's expected to have far-reaching consequences on future picture tube development.

CORNER SUSPENSION – HOW DOES IT COMPARE?

To maintain colour purity, any movement of the shadow mask relative to the screen must be controlled or compensated-for within narrow limits – in the region of microns. These movements may be reversible, such as the thermal expansion of the faceplate glass or of the shadow mask under conditions of high beam current, or irreversible, for example, movement caused by mechanical shock during handling and transport, or irreversible displacement or deformation of the shadow-mask assembly and its suspension system during manufacture. The flatter the mask, the more pronounced will be the mask displacement and hence its effect on colour purity.

For optimum colour purity a mask suspension system has to meet the following requirements:

- highly stable thermal properties for low mask overall doming and rapid compensation, and for low sensitivity to ambient temperature variations
- stable mechanical properties for high stability during manufacture and during life

Excellent thermal stability

The conventional suspension design (Fig.1) is characterized by a heavy mask frame suspended by 3 or 4 bimetal springs engaged in studs located approximately in the middle of the faceplate walls. The frame is required to give strength and rigidity to the assembly and to overcome intrinsic weaknesses in the conventional suspension system. After switch-on, the initial thermal expansion of the mask (due to a temperature rise of about 50 K) is constrained by the frame, leading to mask doming. The required compensation movement of the frame assembly, brought about by the bimetal springs, is slow and delayed owing to the thermal inertia of the assembly and to the indirect nature of the compensation process (thermal conduction from the mask to the bimetal springs). What's more, this compensation movement is in practice never completely symmetrical and leads to landing assymmetries between corners.

Fig.1 In the conventional suspension design a heavy mask frame is suspended by 3 or 4 bimetal springs engaged in studs in the middle of the faceplate walls. After switch-on, the initial thermal expansion of the mask is constrained by the frame, leading to mask doming. The required compensation movement of the frame assembly, brought about by the bimetal springs, is slow and delayed owing to the thermal inertia of the assembly and to the indirect nature of the compensation process (thermal conduction from the mask to the bimetal springs)

Contrast that with the compensation system of the new corner-pin suspension design (Fig.2). Here, 4 mask-supporting pins are embedded in the corners of the faceplate instead of in the middle of the sides. Because of this naturally more stable arrangement, the heavy mask frame can be replaced by a lightweight diaphragm, significantly reducing the mass (by as much as 1 kg) and hence the thermal inertia of the overall assembly.

In addition, as Fig.3 shows, the thermal compensation mechanism relies, not on thermal conduction as with the conventional suspension design, but **directly** on mechanical movement due to the thermal expansion of the mask-diaphragm assembly relative to the faceplate.

Fig.2 In the new corner-pin suspension design, 4 mask-supporting pins are embedded in the corners of the faceplate. Because of this naturally more stable arrangement, the heavy mask frame can be replaced by a lightweight diaphragm, significantly reducing the mass (by as much as 1 kg) and hence the thermal inertia of the overall assembly

The corner suspension element can be considered as a hinge turning around the mask pin as the suspension point. Under thermal load the mask will expand together with the diaphragm which, owing to its low thermal capacity, will rapidly reach its steady state temperature. This expansion in the plane of the shadow mask is transformed by the suspension hinges into the required compensating movement towards the screen by a simple mechanical action.

Figure 3 shows that the mechanism provides optimum compensation of mask expansion for those locations where the incident electron beam is orthogonal to the angle of the hinge plate. In practice, the hinge-plate angle is chosen to give optimum compensation for the E/W border region rather than in the corners (since the E/W region has the lowest landing reserve).

Figure 4 compares the spot movement of a 66 cm (25-inch visible diagonal) corner-pin tube with its conventional counterpart. Stabilization time is halved and, in terms of spot displacement, total transient mask movements are reduced by about 15%. What's more, the nature of the compensation mechanism means that mask movements are completely symmetrical, with practically no lateral or rotational components as in conventional systems, so colour purity is significantly improved.

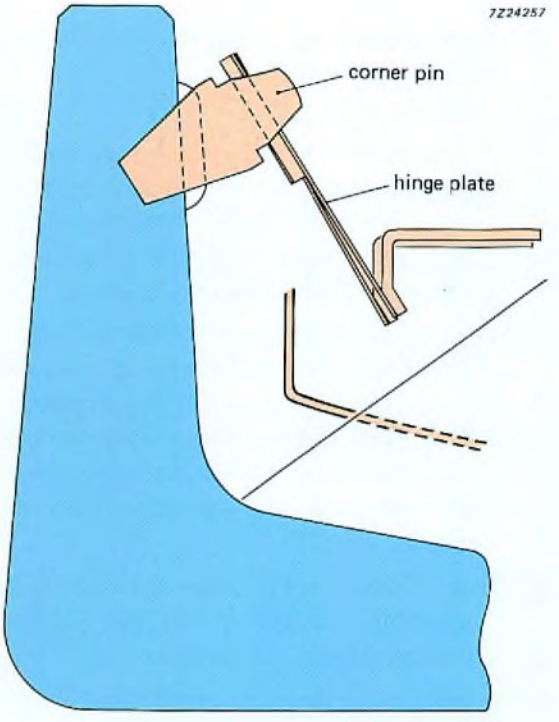

Fig.3 With the corner-suspension design, the thermal compensation mechanism relies, not on thermal conduction as with the conventional suspension design, but **directly** on the thermal expansion of the mask-diaphragm assembly relative to the faceplate

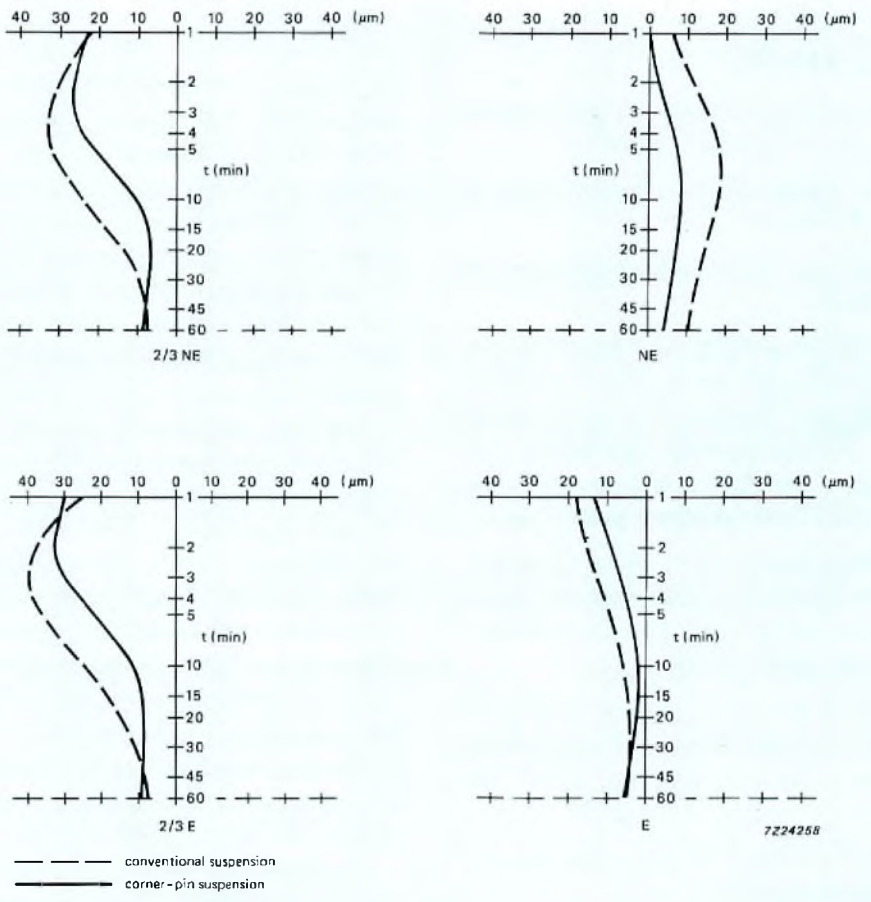

Fig.4 Spot displacement versus time of a 66 cm corner-pin tube (solid lines) and of its conventional counterpart (dashed lines)

Another big advantage of the new compensation mechanism is its response to ambient temperature changes. In the conventional system, expansion or contraction of the glass faceplate relative to the shadow-mask assembly, due to ambient temperature changes, are not compensated and lead to reduced landing reserve. Even worse, if this ambient temperature change gets transmitted to the bimetal strips, it's interpreted as a change in the thermal load of the mask and leads to unwanted movement of the mask-frame assembly (around 0.8 μm/K in a 37 cm/14-inch colour monitor tube). This spurious response is completely absent in the corner-pin suspension system since any relative movement between mask assembly and screen is automatically compensated for.

Finally, although mask suspension systems have no influence on the localized doming behaviour of a shadow mask, the lightweight construction of this new suspension system means that it can easily be produced using low-expansion alloys (invar for example) whose high price has prohibited their use with former, heavier systems.

High mechanical stability

When discussing mechanical stability of a mask suspension system, two areas need to be considered:

- immunity from irreversible deformation and displacement during tube manufacture
- resistance to mechanical shock and vibration (microphony) during tube life.

In tube manufacture, the major causes of degradation in mask-to-screen registration are the thermal processing cycles of frit sealing and pumping. For conventional suspension systems, the high process temperatures and/or temperature gradients may lead to irreversible movement of the mask relative to the phosphor pattern due to:

- relaxation of residual stresses in the mask assembly. To reduce this effect, elaborate process control procedures prior to screening are required (for example, dummy baking of the mask assembly)
- plastic deformation of the bimetal springs and mask frame due to high temperatures and stresses generated by expansion mismatch between glass and metal components
- screen deformations (mainly twisting) that are not followed by the mask assembly
- isotropic contraction of the faceplate glass, which depends on its thermal history

For the corner-pin suspension system, these causes of permanent misregistration are either much less important or completely compensated for.

For example:

- subcomponents and assembly procedures have both been designed to introduce minimum mechanical stress into the finished product, thus minimizing movement due to stress relaxation in the frit seal and eliminating the need for dummy baking
- the lightweight assembly allows the spring force of the suspension elements to be much lower than in conventional systems (around 3 N compared with 15 N). This, combined with the constant spring force and flat characteristic of the 'mousetrap' spring (see Fig.6) prevents plastic deformation of the suspension elements
- any twisting of the screen is transmitted to the mask assembly via the corner pins, greatly reducing misregistration in the corners
- and finally, faceplate contraction (about 150 ppm) is automatically compensated by the hinge mechanism in the same way as it is for thermal expansion of the mask.

At an early stage in the development of this new suspension system, experiments showed that a straight hinge plate, thanks to its high in-plane rigidity, gave the best resistance to shock and vibration. And the use of conical-headed pins with their axes orthogonal to the hinge plates gave optimum insertion repeatability (relocation of the mask upon repeated extraction and insertion during the screening/exposure cycle) with no displacement of the hinge plate from its functional angle (the angle that provides optimum temperature compensation).

Although bent pin designs are possible (to maintain orthoganol pin insertion in the faceplate wall), the simplest solution proved to be a straight conical-headed pin inserted at an angle. This, however, required parallel development of new pin-insertion techniques by our Glass Division. A new mechanism was developed to work in the awkward corner regions of the faceplate, and this now gives process speeds and yields comparable to those for conventional picture tubes. (Note: a ball-headed pin design has recently been perfected that allows orthoganol insertion into the faceplate wall and which provides the same contact area with the mask suspension element as the conical-headed pin.)

Another factor contributing to the system's excellent mechanical stability is the absence of any mechanical interaction between the mask assembly and the internal magnetic shield (IMS), which is supported indepen-

dently on the corner pins and not fixed to the mask assembly as in conventional tubes (Fig.6). Good magnetic shielding is nevertheless maintained by optimizing the form and overlap of the IMS skirt and by close control of the air gap between the IMS and the mask assembly.

Drop tests on properly adjusted tubes have adequately demonstrated the outstanding mechanical stability of this new suspension system by showing no permanent colour impurity for accelerations up to 60g, while microphony behaviour has been shown to be even superior to that of the conventional mask assembly.

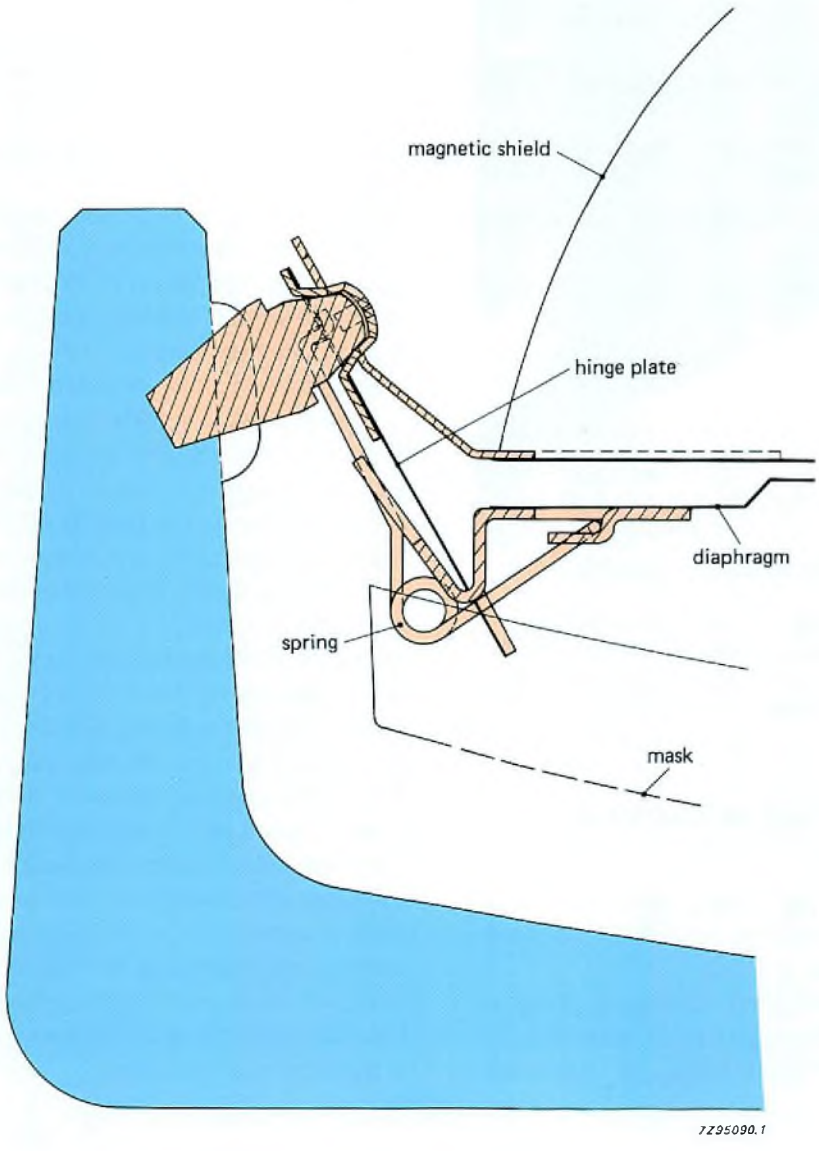

Fig.5 The lightweight assembly allows the spring force of the suspension elements to be much lower than in conventional systems (around 300 g compared with 1500 g). This, combined with the constant spring force and flat characteristic of the 'mousetrap' spring prevents plastic deformation of the suspension elements

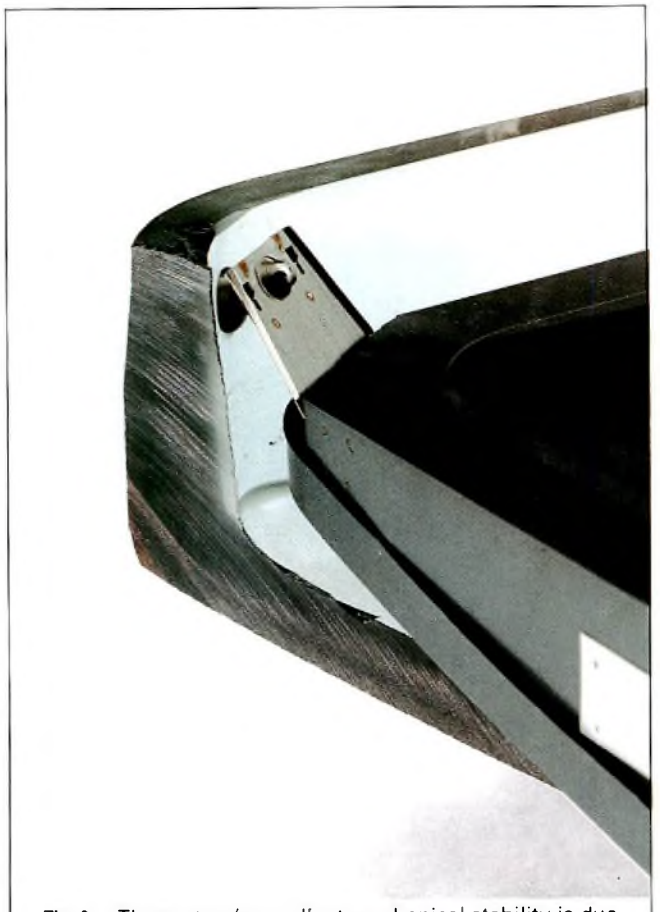

Fig.6 The system's excellent mechanical stability is due in part to the absence of any mechanical interaction between the mask assembly and the internal magnetic shield, which is supported independently on the corner pins and not fixed to the mask assembly as in conventional tubes

AWARD-WINNING MANUFACTURING METHODS

The suspension subcomponents have been designed to allow relatively simple assembly procedures adaptable to full-scale mechanization.

For flat-square tubes with their rectangular phosphor outline and almost straight-edged mask surround, the diaphragm sections are straight L-shaped profiles which, together with the suspension elements (Fig.2) are welded into a rigid framework that's an extremely close fit with the mask. So welding this framework to the mask has little influence on the mask's curvature.

Early investigations of this design indicated some sensitivity to E/W- movements of the mask assembly. This has now been overcome by employing a laser-welding technique to rigidly fix the mask assembly to the corner pins.

The laser-welding system (Fig.7) was developed in co-operation with Lumonix Ltd., UK, and is believed to be one of the first in the world specifically developed for the mass-production environment*. Besides providing the necessary rigid connections to the corner pins, this new system is also considerably faster than conventional welding systems – taking less than a second to weld the four pins of each mask (with four welds per pin). This, of course, minimizes stresses on the mask and also allows a very high throughput (over 200 masks per hour). What's more, the whole welding operation can be performed without any direct contact with the mask, further reducing stresses on the mask and the chances of damage.

Over the last few years, since large-scale production of Philips' Flat- Square picture tube started, the laser welding system has proved outstandingly successful, and we now have more than 30 such systems in full-scale operation at our plants around the world.

To sum up, the development of the Flat-Square picture tube provided Philips with an excellent opportunity to introduce a completely new corner-pin suspension system. Although its development was stimulated by the critical requirements that Flat-Square mask assemblies are required to meet, the new suspension system provided several important bonuses. Bonuses such as significantly reduced microphony and lighter construction, the latter not only reducing the weight of the picture tube itself, but also allowing the mask assembly to be economically manufactured in relatively expensive low- expansion materials like invar. Already, several other manufacturers are moving over to corner suspension, and there's little doubt that the next few years will see a major switch to this new, superior system.

* For the development of this system, Philips and Lumonix Ltd won the 1987 SPOTlight award, presented at the Lasers in Manufacturing SPOT '87 conference in Los Angeles

Fig.7 A Lumonics Nd:YAG laser system is used to weld the bracket holding the glass faceplate to the shadow mask. A special optical head was developed to provide viewing, positioning and beam delivery

The magnetoresistive sensor

a sensitive device for detecting magnetic-field variations

AUGUST PETERSEN

Magnetic-field sensors provide a highly effective means of measuring both linear and angular displacement. This is because even quite small movement of actuating components in machinery (metal rods, gears, cams etc.) can create measurable changes in magnetic field. Examples where this property is put to good effect can be found in instrumentation and control equipment, which often requires position sensors capable of detecting displacements in the region of tenths of a millimetre, and in electronic ignition systems, which must be able to determine the firing positions of an internal-combustion engine with great accuracy.

Formerly, many of these measuring systems were based on Hall-effect sensors, which make use of the property of a current-carrying semiconductor membrane (Hall element) of generating a voltage perpendicular to the direction of current flow when subjected to a magnetic field normal to its surface.

A more recent development for detecting magnetic-field variations, however, is the KMZ10 magnetoresistive sensor which, in many applications, provides an attractive alternative to the Hall-effect sensor. The KMZ10, for example, is more sensitive than the Hall-effect sensor and can operate over an extremely wide temperature range. What's more, its frequency range is much wider: from DC up to several megahertz.

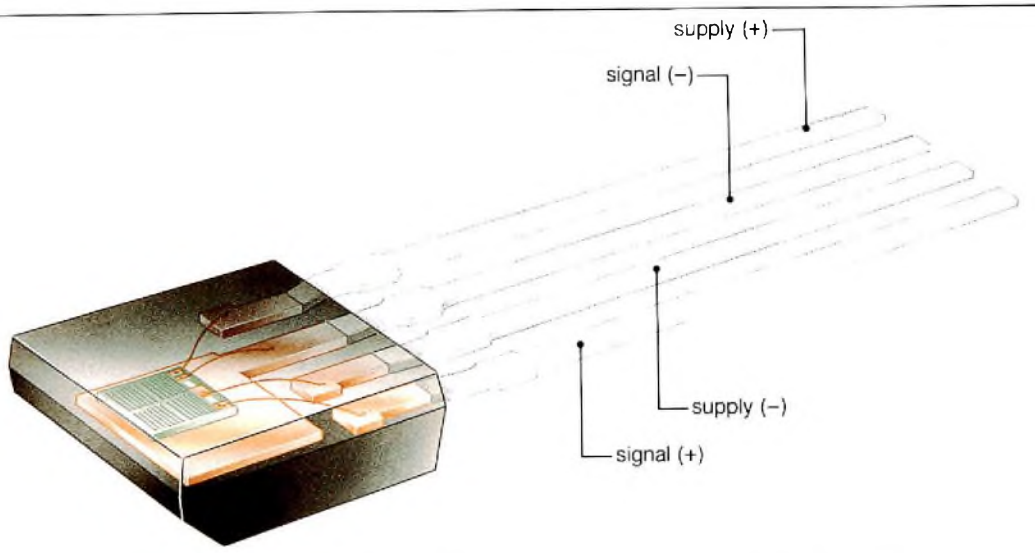

The KMZ10 magnetoresistive sensor – a recent development for detecting magnetic-field variations

The KMZ10 makes use of the **magnetoresistive effect**: the well known property of a current-carrying magnetic material to change its resistivity in the presence of an external magnetic field. This change is brought about by rotation of the magnetization relative to the current direction. In the case of permalloy, for example (a ferromagnetic alloy containing 20% iron and 80% nickel), a 90° rotation of the magnetization (due to the application of a magnetic field normal to the current direction) will produce a 2 to 3% change in resistivity.

In the KMZ10, four permalloy strips are arranged in a meander pattern on a silicon substrate (Fig.1), and connected to form the four arms of a Wheatstone bridge. The degree of bridge imbalance is then used to indicate the magnetic field strength, or more precisely, the variation in magnetic field in the plane of the permalloy strips normal to the direction of current. A proprietary 'barber-pole' configuration, comprising aluminium stripes deposited on the permalloy strips at 45° to their axes, assures a linear characteristic of the bridge (see box).

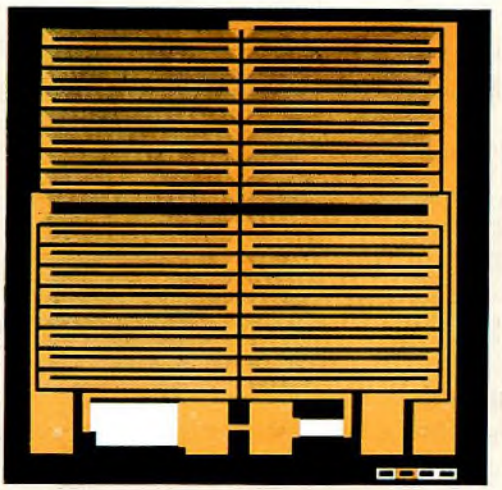

Fig.1 The KMZ10 chip is made up of four permalloy strips arranged in a meander pattern and connected to form the four arms of a Wheatstone bridge. The chip incorporates special resistors that are trimmed during manufacture to give zero offset at 25 °C

LINEAR BEHAVIOUR THANKS TO SPECIAL 'BARBER-POLE' CONFIGURATION

The resistivity of a polycrystalline ferromagnetic alloy such as permalloy is related to the angle θ that the magnetization makes with the current direction by

$$\rho = \rho_o + \Delta\rho_{max}\cos^2\theta \qquad (3)$$

where ρ_o is the isotropic resistivity and $\Delta\rho_{max}$ is the change in resistivity resulting from a 90° rotation of the magnetization (from the direction of current flow).

If this rotation is caused by a magnetic field H normal to the direction of current, and if the field tending to align the magnetization with the current is H_o (comprising the demagnetizing and anisotropic fields), then $\sin\theta = H/H_o$ and

$$\rho = \rho_o + \Delta\rho_{max}(1 - H^2/H_o^2) \qquad \text{for } H < H_o$$

and (2)

$$\rho = \rho_o \qquad \text{for } H \geq H_o$$

It's obvious from this quadratic expression that the resistivity/magnetic-field characteristic is non-linear, and what's more, that each value of ρ is not necessarily associated with a unique value of H.

Fortunately, there are several ways to linearize the characteristic. One is to provide a uniform biasing field H_{bias} in the direction of the field H. Then, provided $H \ll H_{bias}$, ρ will be proportional to H. The KMZ10, however, employs another method that uses aluminium stripes secured to the top of each permalloy strip at an angle of 45° to its axis (Fig.A). This has been called the 'barber-pole' configuration because of its resemblance to the poles traditionally seen outside barber shops.

Since aluminium has a much higher conductivity than permalloy, the effect of these stripes is to rotate the net current direction through 45°, that is, to reduce θ to θ – 45°.

Relation (1) then becomes:

$$\rho = \rho_o + \frac{\Delta\rho_{max}}{2} + \Delta\rho_{max}\frac{H}{H_o}\sqrt{1 - \frac{H^2}{H_o^2}}$$

As Fig.B illustrates, for small values of H (relative to H_o), ρ increases linearly with H.

With the complementary barber-pole configuration to that shown in Fig.2, that is, with the aluminium stripes inclined at – 45° to the axis of the permalloy strip, θ increases to θ + 45° and (1) becomes:

$$\rho = \rho_o + \frac{\rho_{max}}{2} - \Delta\rho_{max}\frac{H}{H_o}\sqrt{1 - \frac{H^2}{H_o^2}}$$

and ρ decreases linearly with H.

The KMZ10 itself comprises two (diagonally opposed) elements in which ρ increases with H, and two in which it decreases. This largely eliminates the effects of ambient variations (temperature etc.) on the individual elements, and moreover, magnifies the degree of bridge imbalance, so increasing the sensitivity of the device.

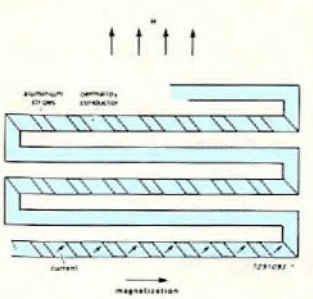

Fig.A

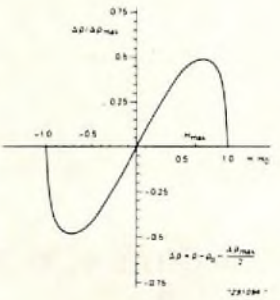

Fig.B

SENSITIVITY – GOVERNING FACTORS

One of the major advantages that the KMZ10 has over other devices like the Hall-effect sensor is the ease with which its sensitivity can be set during manufacture. For small field variations, the sensitivity of the KMZ10 is, from equ (3), given by $\varrho/H = \varrho_{max}/H_o$. The value of ϱ_{max} is determined by the material properties; H_o by, among other things, the strip geometry.

Figure 2 shows how strip geometry governs sensitivity. For a given field strength, the thicker the permalloy strip, the less the magnetization is rotated. So by using different strip geometries, it's possible to produce a range of devices with different sensitivities and measuring ranges. At present, three types are produced: designated types A to C (Table 1).

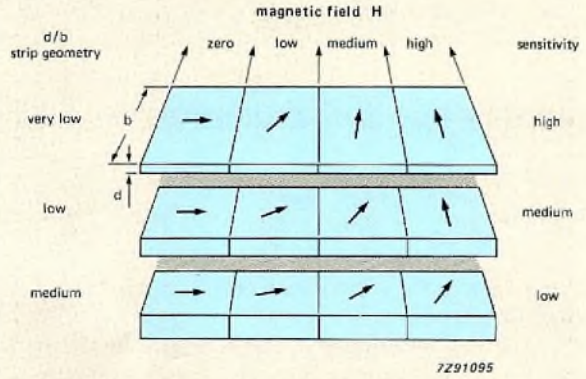

Fig.2 Factors affecting sensitivity. The higher the d/b (depth/breadth) ratio of the aluminium stripes, the less the magnetization will be rotated by a given magnetic field and the lower will be the sensitivity

Table 1
KMZ10 magnetic-field sensors

	KMZ10A	KMZ10B	KMZ10C	units
H_{max}	500	2000	7500	A/m
open-circuit sensitivity (typ)	14.0	4.0	1.5	(mV/V)/(kA/m)

Note: in air, 1 G corresponds to 80 A/m; 1 mT corresponds to 796 A/m. Earth's magnetic field is about 30 A/m

KMZ10 CHARACTERISTIC BEHAVIOUR

During deposition of the strip material (by sputtering), a strong magnetic field is applied parallel to the strip axis. This serves to accentuate the inherent magnetic anisotropy of the strips, so that even in the absence of an external magnetic field, the magnetization will always tend to align with the strips.

The internal magnetization of the sensor strips therefore has two stable positions, so that if the sensor for any reason should come under the influence of a powerful magnetic field opposing the internal aligning field, the magnetization may flip from one position to the other, and the strips become magnetized in the opposite direction (from say the +x to the −x direction). As Fig.3 shows, this can lead to changes in sensor characteristics.

In Fig.3, the unbroken line shows the characteristics of a normal sensor (with the sensor magnetization oriented in the +x direction), and the broken line shows the characteristics of a 'flipped' sensor.

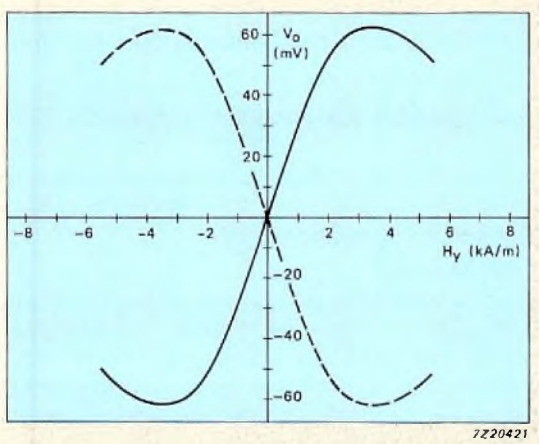

Fig.3 Sensor characteristic. The unbroken line shows the characteristic of a 'normal' sensor (with the magnetization oriented in the +x direction), and the broken line shows the characteristic of a 'flipped' sensor

The field, H_{-x} say, needed to flip the sensor magnetization (and hence the characteristic) depends on the magnitude of the transverse field H_y: the greater the field H_y, the smaller the field H_{-x}. This is quite reasonable since the greater the field H_y, the closer the magnetization's rotation approaches 90°, and hence the easier it will be to flip it into a corresponding stable position in the −x direction.

This is illustrated in Fig.4, which shows sensor output signal V_o versus H_x for several values of H_y. Take the curve for H_y = 0.5 kA/m. For such a low transverse field, sensor characteristic is stable for all positive values of H_x, and a reverse field of around 1 kA/m is required before flipping occurs.

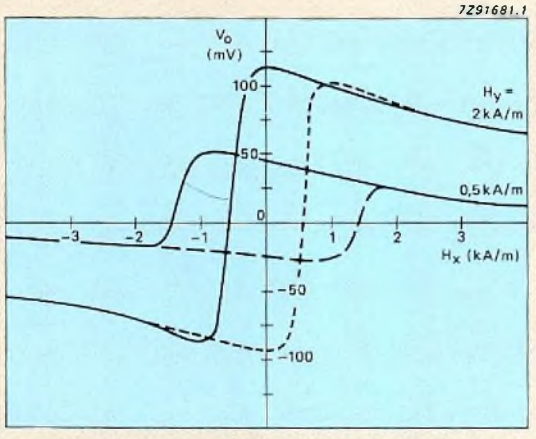

Fig.4 Sensor output V_o versus H_x for several values of H_y (sensor KMZ10B). The curves illustrate several things: first, that the sensor exhibits hysteresis, second, that the flipping is not instantaneous, and third, that sensitivity falls with increasing H_x.

Figure 4 also shows that the flipping itself is not instantaneous; this is because not all the permalloy strips flip at the same rate. Also in Fig.4 you can see the hysteresis effect exhibited by the sensor.

Finally, Figs 3 and 4 show that the sensitivity of the sensor falls with increasing H_x. This again is reasonable since the moment imposed on the magnetization by H_x directly opposes that imposed by H_y, thereby reducing the degree of bridge imbalance and hence the output signal for a given value of H_y.

Internal magnetization

As a precaution against the sensor flipping, it can be provided with a stabilizing magnetic field parallel to the internal aligning field. This stabilizing field will, however, reduce sensitivity slightly, but since it need not be too strong, the effect is only slight. The stabilizing field may be provided by an auxiliary magnet close to or even glued to the sensor with its axis parallel with the x-axis of the sensor. In some applications, especially where the sensor is used to measure the field of say a moving permanent magnet (as in linear position sensors), the magnet itself may be oriented to provide the auxiliary field.

This field should not be confused with the linearizing field H_{bias} (see box), which is unnecessary with the KMZ10 owing to its barber-pole configuration, and which anyway is applied perpendicular to the internal aligning field.

Effect of temperature on behaviour

Figure 5 shows that the bridge resistance increases linearly with temperature. This variation comes, of course, from the fact that the resistance of the bridge resistors themselves (i.e. the permalloy strips) varies with temperature. Figure 5 shows only the variation for a typical KMZ10B sensor. The data sheets show also the spread in this variation due to manufacturing tolerances, and this should be taken into account when incorporating the sensor into practical circuits.

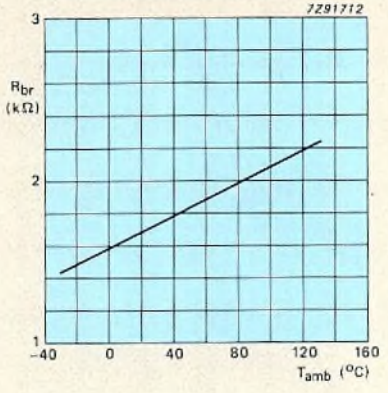

Fig.5 Bridge resistance as a function of temperature (KMZ10B)

Not just the bridge resistance but the sensitivity too varies with temperature. This can be seen from Fig.6 which plots output voltage against transverse field H_y for various temperatures. The figure shows that sensitivity falls with increasing temperature. The reason for this is rather complicated and is connected with the energy-band structure of the permalloy strips.

In general, temperature dependence of sensor characteristics presents no problem since it's relatively easy to incorporate effective compensating networks in the operating circuitry.

Figure 7 is similar to Fig.6 but with the sensor powered by a constant-current supply. The figure shows that with a constant-current supply, the temperature dependence of sensitivity is significantly lower. This is a direct result of the increase of bridge resistance with temperature (Fig.5) which partially compensates the fall in sensitivity by increasing the voltage across the bridge and hence the output voltage. The figure, therefore, adequately demonstrates the advantages of operating with constant current.

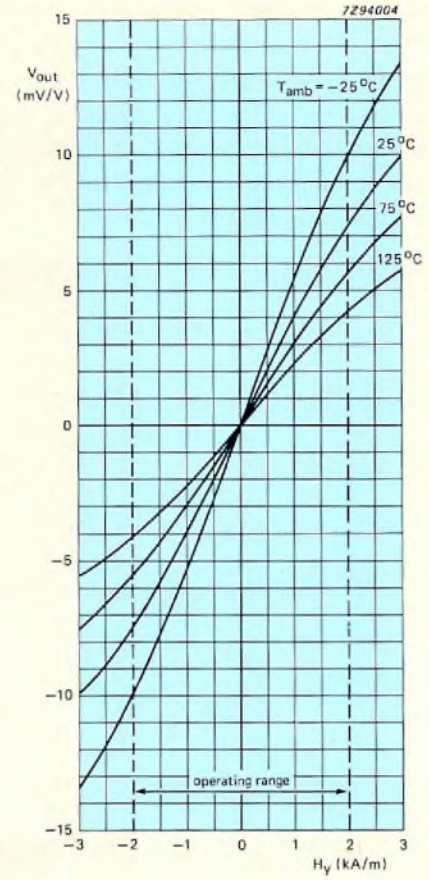

Fig.6 Output voltage V_o versus transverse field H_y for several temperatures (sensor KMZ10B). The figure illustrates that, for a constant supply voltage, sensitivity falls with increasing temperature

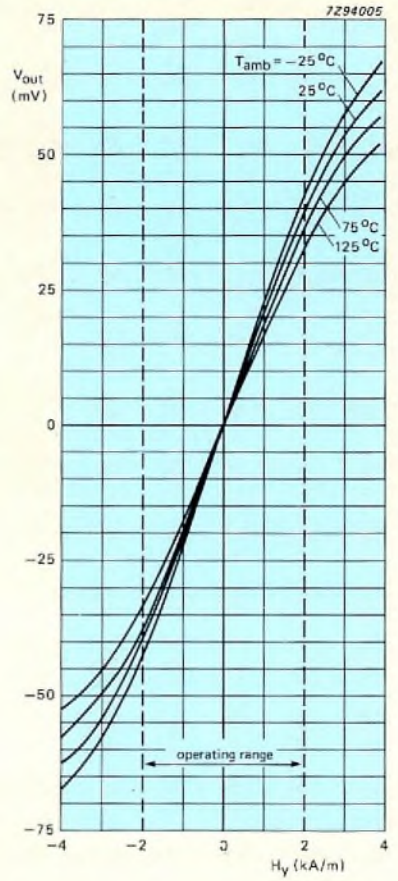

Fig.7 Output voltage V_o versus transverse field H_y for several temperatures, with the sensor powered by a constant-current supply (KMZ10B, current 3 mA). The reduction in temperature dependence of sensitivity is a result of the increase of bridge resistance with temperature, which increases the bridge voltage to partially compensate the fall in sensitivity

KMZ10 VERSUS THE OTHERS – HOW DOES IT COMPARE?

With the broad range of magnetic-field sensors currently available, the question of which to use for a particular application is often a confusing one. In many instances the choice is dictated by familiarity – designers familiar with say, the Hall-effect sensor, will quite naturally choose it for their system even when other sensors, like, for example, the magnetoresistive sensor, might prove more appropriate. Table 2 lists the essential features of some of the more common magnetic-field sensors and should help in choosing the right sensor for a given application.

From Table 2 it can be seen that for applications requiring high sensitivity and low drift, and where mechanical stresses may be high, the KMZ10 magnetoresistive sensors are clear favourites.

We'll now look at some typical application examples to find areas where the KMZ10 can be used to advantage.

Automotive navigation systems

This is an area currently generating a lot of interest, particularly with the imminent introduction of compact-disc based navigation systems (such as the Philips

Table 2
Essential characteristics of some magnetic-field sensors

	operating temp range (°C)	supply voltage (V)	sensitivity at 1 kA/m (mV)	offset (mV)	offset drift (μV/K)	frequency range (Hz)	sensitivity to mechanical stress
magnetoresistive							
KMZ10A	–40 – 150*	10	140	+ 15	+ 20	0 – 1 M	low
KMZ10B	–40 – 150*	10	40	+ 15	+ 10	0 – 1 M	low
KMZ10C	–40 – 150*	10	15	+ 15	+ 10	0 – 1 M	low
Hall-effect							
In	–40 – 100	1	7			0 – 1 M	high
GaAs	–40 – 150*	5	1.2	± 25		0 – 1 M	high
Si (with signal conditioning)	–40 – 150	12	94	6000	± 1600	0 – 100 k	high
flux-gate	–40 – 100					0 – 1 k	
Wiegand-effect	–40 – 125					0 – 25 k	insensitive
induction coil	–40 – 190					1 – 50 k	insensitive
'magnetic' transistor	–40 – 150**	20	up to 20				
'magnetic' diode	–40 – 90	6	12.5	± 1000	± 80	0 – 4 k	

*175 °C possible **estimated

CARIN system) into top-end domestic motor cars. The requirement here is for robust compass systems with an accuracy of around 1°. Likely candidates for this application are the magnetoresistive sensor and the flux-gate sensor. The former, however, is significantly cheaper and is currently attracting a lot of attention from automotive system designers.

Current sensors

This is an area in which Hall-effect sensors have been prominent for some time, generally because of their small size which compensates, to some extent, their low sensitivity. Typical Hall-effect current sensors use the current to be measured to energize an electromagnet, and the strength of the resulting magnetic field, measured by the Hall-effect sensor, provides a measure of the current. A disadvantage of such systems, of course, is that they inevitably affect the current they are measuring. The magnetoresistive sensors, on the other hand, thanks to its high sensitivity, can measure the magnetic field of a current-carrying wire directly, so its use has no effect on the current to be measured. It could, therefore, be a powerful rival in this area.

Angular and linear displacement measurement.

Again this is an area where the high sensitivity of the magnetoresistive sensor makes it a clear favourite, allowing it to operate in the far-field region of a magnetic system, giving better linearity and reproducibility than its main rival – the Hall-effect sensor. It's also a cheaper solution since its high sensitivity allows the use of relatively cheap ferrite magnets. It is, however, more sensitive to disturbing magnetic fields (the earth's field for example), so care must be taken to avoid or compensate for these.

Movement detectors

For detecting moving magnets or iron parts in hydraulic systems, or flywheels, the magnetoresistive sensor is an excellent candidate. Its high sensitivity means that it can detect these moving objects at relatively large distances (compared with other sensing systems), and even through (non-ferrous) walls. The sensor can also be easily combined with a comparator to provide digital outputs provided operating temperatures don't exceed say 150 °C.

This speed control, based on a rotating magnet and a magnetic-field sensor, is used in some of the latest VCR systems. The KMZ10 is an excellent candidate for the sensor in such applications

Table 3
Magnetoresistive sensors – advantages and main application areas

advantages	
high sensitivity	– simplifying magnetic circuits for lower costs
	– allowing operation over relative great distances
	– allowing the use of cheaper magnetic circuits and ferrite-based magnets instead of metal magnets
low source resistance	– giving low sensitivity to electrical interference
high-temperature operation	– 150 °C continuous, 175 °C peak (chip alone can withstand 175 °C continuous)
operation over a wide frequency range	– from DC up to several MHz
metal-film technology	– giving excellent long-term stability
low sensitivity to mechanical stress	– facilitating mounting of the sensor and allowing its use in relatively rough environments
application areas	
traffic control	– detection of vehicles
low-cost navigation	– allowing the production of simple compass systems with an accuracy of around 1°, ideal for automotive applications
long-distance metal detection	– for the detection of, for example military vehicles (tanks etc.) by measuring disturbances in the earth's magnetic field
motion detectors	– by measuring position changes relative to the earth's magnetic field
current detection	– for example, earth-leakage switches
general magnetic-field measurement	– from 10 A/m to 10 kA/m
direct-current measurement	– starting currents in motor vehicles (in engine-management system for example), where they afford simplicity since the high currents involved eliminate the need for magnetic circuits
angular or position measurement	– sensing of accelerator pedal or throttle position (again in engine-management systems)
	– position sensing in industrial automation systems (commercial sensor arrays that can measure positions with an accuracy of ± 30 μm)
	– force/acceleration/pressure measurement using a moving magnet, for example: engine-intake-manifold pressure sensors, fluid-level sensors, low-cost weighing systems, geosonic (seismic) sensors, accelerometers
mark detection and counting	– camshaft or flywheel position sensors for engine ignition systems
	– end-point sensors
	– wheel-speed sensors for anti-blocking systems
	– rpm counters (0 to 20 kHz) for engine tachometers and for electronic synchromesh systems
	– flow meters
	– zero speed detectors (for spin dryers or drum washing machines)
	– rpm control in electric motors
	– general instrumentation

USING THE KMZ10

The MRS in circuit

For some applications it's not necessary to compensate for temperature dependence of bridge characteristics, and it's sufficient to operate the KMZ10 from a simple constant-voltage source. For many applications, however, temperature compensation is essential and Fig.8(a) shows a simple set-up for doing this using just a single opamp (an NE5230N).

The circuit provides the following facilities:

- **compensation of sensitivity drift with temperature** via a negative feedback loop incorporating a KTY83-110 silicon temperature sensor
- **offset adjustment** by means of potentiometer R7
- **gain adjustment**

Figure 8(b) shows the output of this circuit for various temperatures and clearly demonstrates the effectiveness of the temperature compensation. The circuit does not compensate for spread of sensitivity drift and offset. What's more, in this circuit, the temperature sensor draws relatively high current so self-heating effects may result in incomplete temperature compensation.

Figure 9 shows a more elaborate circuit, embodying the functions of Fig.8. The circuit provides for adjustment of gain (R22) and of offset voltage (R21) from the magnetic-field sensor, and although it largely compensates for the sensor's temperature coefficient of sensitivity, it provides no compensation for the (relatively small) temperature variation of offset voltage. Compared with the circuit of Fig.8, however, it does allow the use of higher supply voltages and hence can generate higher output signals.

The circuit can be divided into two stages: an amplification stage that produces a symmetrical output signal derived from the magnetoresistive sensor, and an output stage that also provides a reference to ground for the amplification stage.

The magnetoresistive sensor has a negative temperature coefficient of sensitivity, the precise value of which can be obtained from its data sheet. To compensate this the amplification stage is given an equal but positive temperature coefficient by means of a KTY81 (or KTY85) silicon temperature sensor in the feedback loop of opamp U1a.

The gain A of the amplification stage is:

$$A = 1 + \frac{R6(T) + R10}{R_A}$$

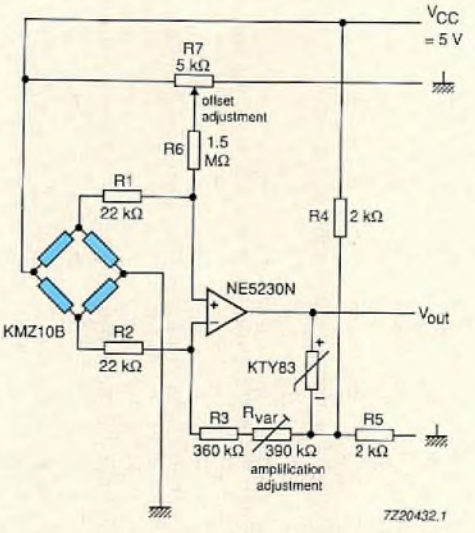

(a)

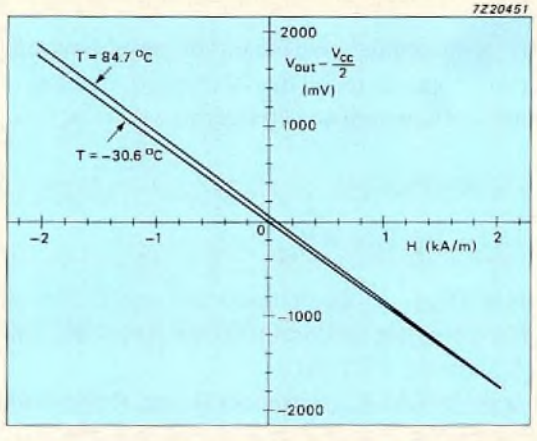

(b)

Fig.8 (a) Simple drive circuitry for the KMZ10 incorporating temperature compensation; (b) output [V_{out} - V_{cc}/2] of circuit of Fig.8(a) for two temperatures, clearly demonstrating the effectiveness of the temperature compensation

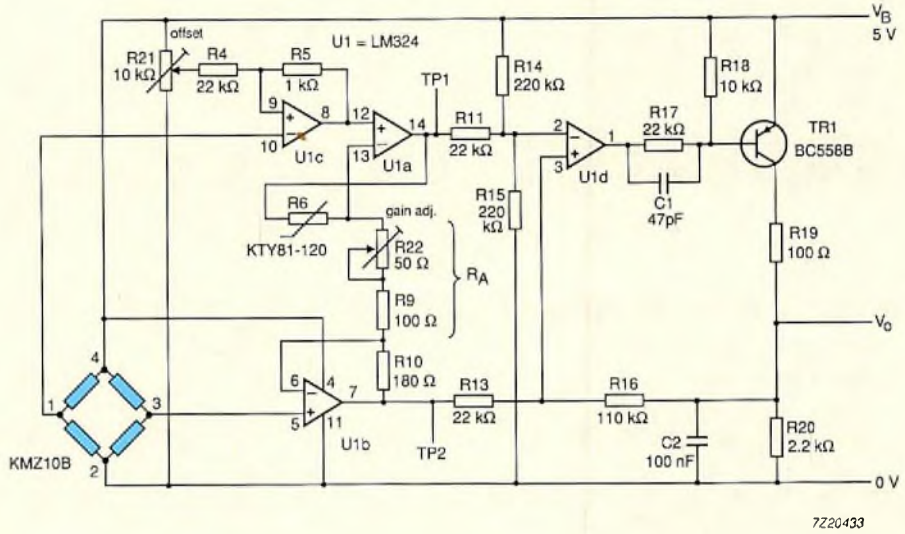

Fig.9 KMZ10 drive circuitry with a quad opamp.
The circuit provides for adjustment of gain, offset voltage and temperature coefficient of sensor sensitivity

and its temperature coefficient of amplification TC_A (equal and opposite to the magnetoresistive sensor's temperature coefficient of sensitivity) is:

$$TC_A = \frac{R6(T)\,TC_{KTY}}{R_A + R6(T) + R10}$$

in which TC_{KTY} is the temperature coefficient of the silicon temperature sensor (0.0078/K for the KTY81 and 0.0075/K for the KTY85).

For a given gain A, resistances R_A and R10 can then be calculated from:

$$R10 = R6(T)\left\{\frac{TC_{KTY}}{TC_A}\left(1-\frac{1}{A}\right)-1\right\}$$

$$R_A = \frac{R6(T) + R10}{A-1}$$

In Fig.9, the output stage has a maximum gain of 5 and gives an output voltage of half the supply voltage V_B for zero differential output voltage of the amplification stage (between test points TP1 and TP2). Output voltage will vary from zero to slightly less than V_B.

One point position measurement with the KMZ10

Figure 10(a) shows how a KMZ10B may be used to make position measurements of a metal object, a steel plate for instance. The sensor is located between the plate and a permanent magnet oriented with its magnetic axis normal to the axis of the plate. A discontinuity in the plate's structure, such as a hole or region of non-magnetic material, will disturb the magnetic field and produce a variation in the output signal from the sensor.

This is shown in Fig.10(b) which gives the sensor output signal versus hole/sensor offset x, for two values of magnet/plate spacing d. The interesting point of this figure is that the crossover point, i.e. the point where the hole and sensor precisely coincide, is independent of d. The obvious advantage of this set-up is that precise location of the sensor/magnet combination is unimportant for one-point position measurements, so adjustment procedures in a practical device would be greatly simplified. Although not shown in Fig.10(b), the crossover point is also independent of temperature. This is not surprising since it is effectively a null measurement, and it could be a major advantage in practical applications.

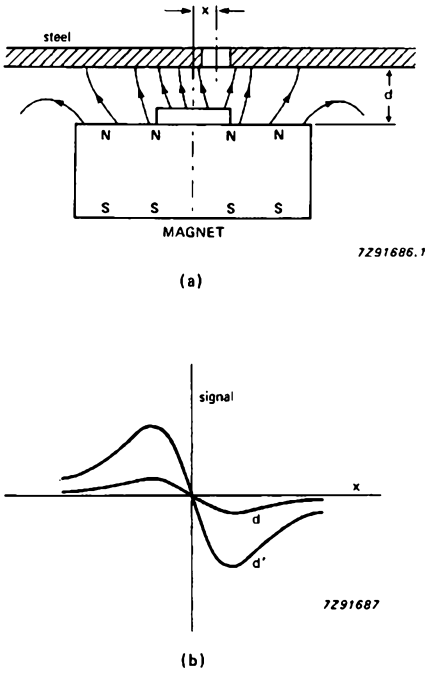

Fig.10 One-point measurement with the KMZ10.
(a) The sensor is located between a metal plate and a permanent magnet oriented with its magnetic axis normal to the axis of the plate. A discontinuity in the plate's structure, such as a hole or region of non-magnetic material, will disturb the magnetic field and produce a variation in the output signal from the sensor.(b) Output signal versus hole/sensor offset x for two values of magnet/plate spacing d. The figure shows that the crossover point is independent of d, which greatly simplifies adjustment procedures

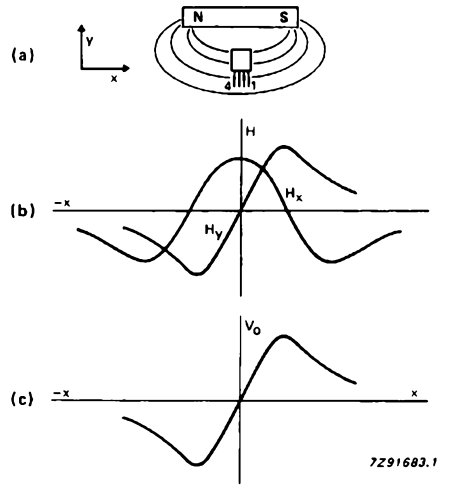

Fig.11 Sensor output in the field of a permanent magnet as a function of its displacement x parallel to the magnetic axis. The magnet provides both the auxiliary and transverse fields

Linear position measurement

Figure 11 shows probably one of the simplest arrangements for measuring linear displacement using a KMZ10 sensor and a permanent magnet.

When the sensor is placed in the field of a permanent magnet, it's exposed to magnetic fields in both the x and y directions. If the magnet is oriented with its axis parallel to the sensor strips (that is, in the x direction) as shown in Fig.11(a), H_x then provides the auxiliary field and the variation in H_y can be used as a measure of x displacement. Figure 11(b) shows how both H_x and H_y vary with x, and Fig.11(c) shows the corresponding output signal as a function of x.

An excellent example of how this arrangement can be put to practical use, making use of the circuit of Fig.9, is shown in Fig.12(a). Here, the linear displacement of the magnet provides a measure of the movement of a pressure-sensing membrane. Figure 12(b) shows that the

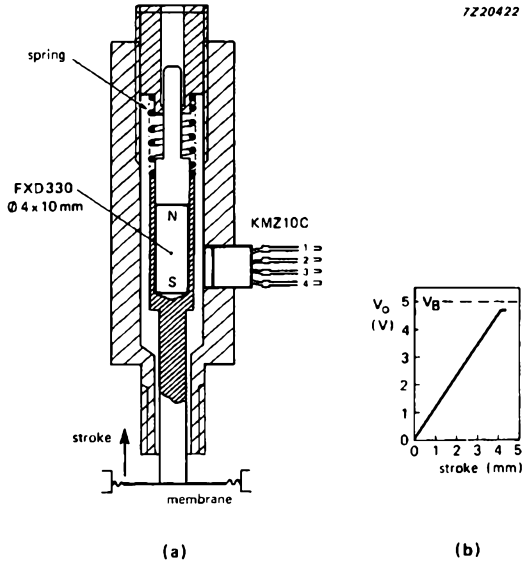

Fig.12 (a) Pressure sensor in which the movement of a membrane is transmitted to a permanent magnet from which it can be detected by a KMZ10C magnetoresistive sensor
(b) Amplified bridge output voltage versus membrane displacement (using the circuit of Fig.9)

(amplified) bridge output voltage V_o is substantially a linear function of membrane displacement. A typical application for such an arrangement would be for sensing inlet manifold pressure in engine-management systems.

Angular position measurement with the KMZ10

Figure 13(a) shows a set-up for measuring angular position using a KMZ10C. The sensor itself is located in the magnetic field produced by two RES190 permanent magnets fixed to a rotatable frame. The output of the sensor will then be a measure of the rotation of the frame (Fig.15). Taking the zero position for measurement to be parallel to the x axis of the sensor (that is with the magnetic field in the H_x direction), then the device can measure angular rotation up to around +85 °. Beyond that the sensor is in danger of flipping.

Figure 14 shows a circuit for measuring the sensor output in the set-up of Fig.13. The output signal of the sensor bridge is amplified by opamps A_1 and A_2. A KTY81 silicon temperature sensor in the feedback loop of A_2 varies the gain of the opamp to provide temperature compensation for the output signal. Figure 15 shows the effectiveness of this temperature compensation by comparing the output V_2 of A_2 with the direct output V_1 from opamp A_1 for a range of temperatures.

Figure 13(b) shows a more practical arrangement for measuring angular position. This arrangement is, in effect, a contactless potentiometer and could be used, for example, as a throttle or accelerator pedal position detector in engine management systems.

Fig.13 (a) Angular measurement with the KMZ10
(b) Contactless potentiometer with the KMZ10

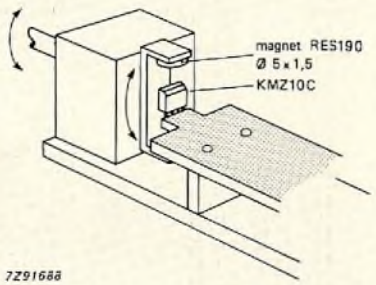

(a)

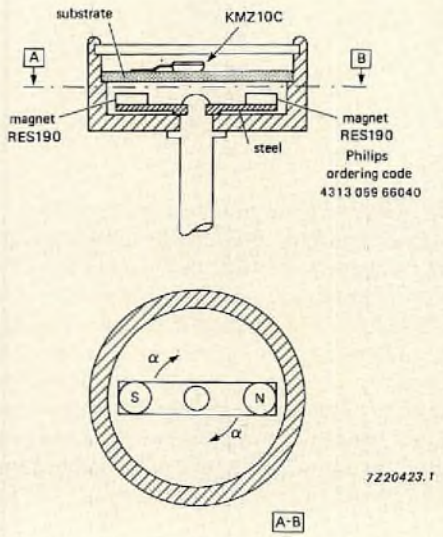

(b)

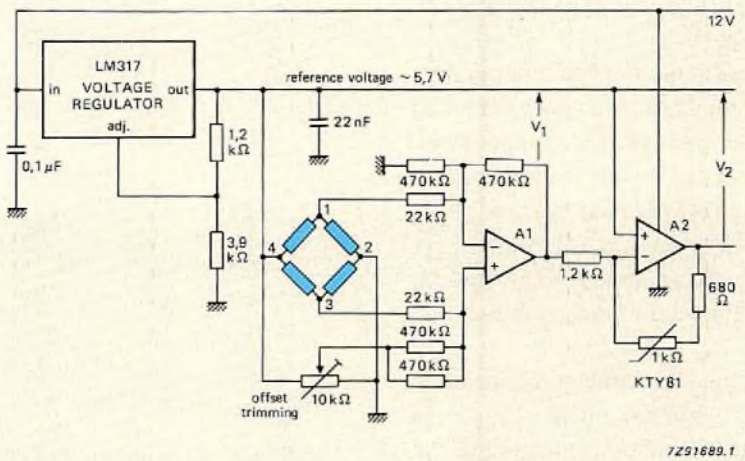

Fig.14 Circuit for measuring sensor output in the setup of Fig.13.

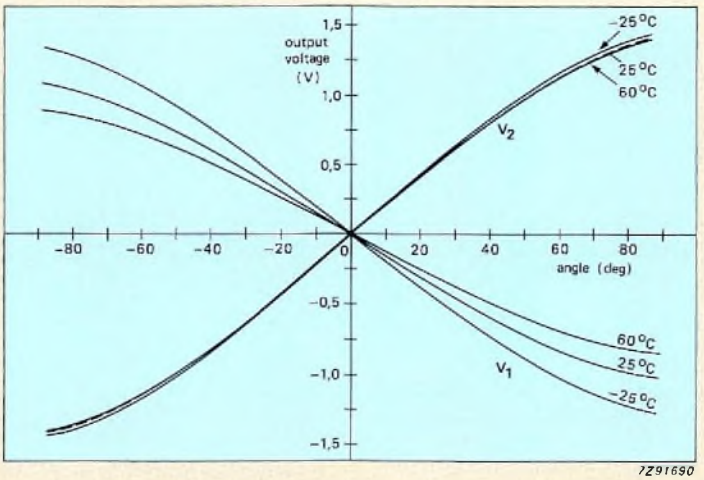

Fig.15 Effect of temperature compensation in the circuit of Fig.14. The figure compares the uncompensated output V_1 of opamp A_1 with the compensated output V_2 of opamp A_2.

Current measurement with the KMZ10

Figures 16 and 17 show two ways in which the KMZ10B can be used to measure electric current. This could be useful, for example, in headlamp-failure detection systems in motor vehicles or in clamp-on (non-contacting) meters as used in the power industry.

Figure 16 is a rather simple set-up in which the sensor measures the magnetic field generated by the current-carrying wire. Figure 17(a) shows how the sensitivity of the sensor varies with distance d from the wire and Fig.17(b) shows sensor output versus current for various values of d.

Not surprisingly, sensor sensitivity rises as d decreases. For relatively large values of d (say 5 mm), the increase in sensitivity is substantially linear, but at closer spacings, when the magnetic field generated by the current is no longer uniform over the sensor, the rate of increase drops off. For higher currents, a similar drop off from linearity would be observed at quite large distances, but this is due to the magnetic field generated by the current saturating the sensor.

The sensor can also be laid directly onto a conductor of a printed-circuit board, and Fig 17(a) also shows the sensitivity of the sensor for three PCB conductor widths.

Figure 18 is a more sophisticated arrangement in which the magnetic field generated by the current-carrying wire is compensated by a secondary circuit wrapped around a ferrite core. At the null-field point, detected by a KMZ10 sensor located in the air gap between the ends of the core, the magnitude of the current in the secondary circuit is a measure of the current in the main circuit. This arrangement provides a more accurate means of measuring current and lends itself more to precision applications.

What's important to bear in mind in both these examples is that they allow current measurement without any break in or interference with the circuit.

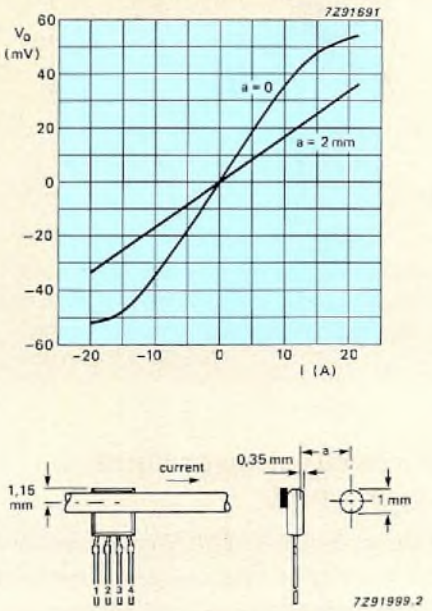

Fig.16 Simple setup for measuring current with a KMZ10B sensor plus auxiliary magnet. The sensor simply measures the magnetic field generated by a current-carrying wire.

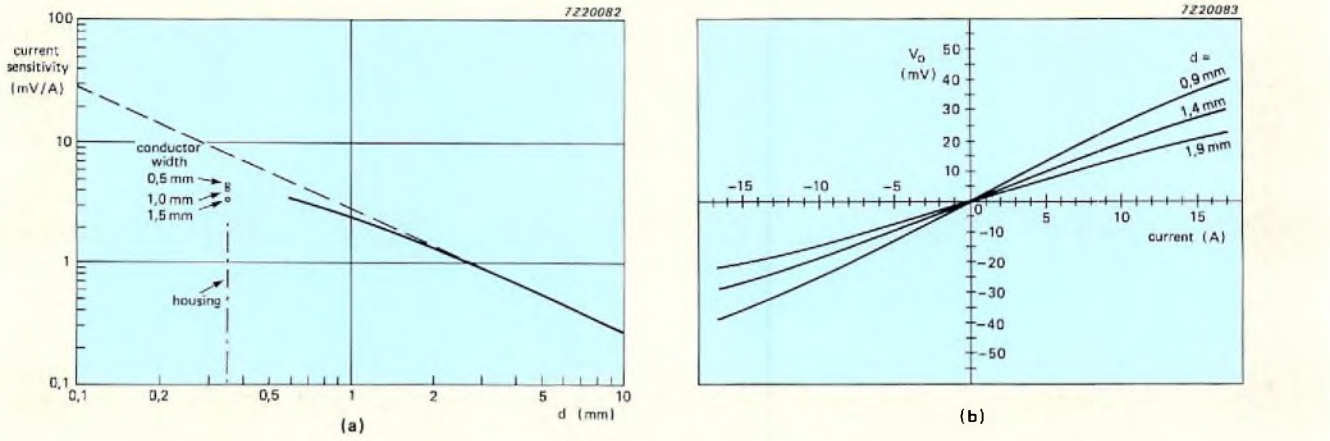

Fig.17 (a) Sensor sensitivity (in mV/A) versus distance d between the axis of the wire and the plane of the sensor chip. The figure also shows, for three conductor widths, the sensitivity of the sensor when laid directly onto a conductor of a printed-circuit board
(b) Sensor output versus current for various distances d

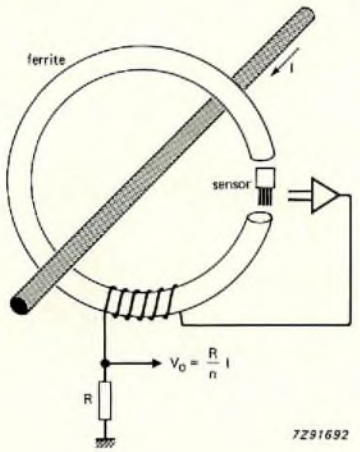

Fig.18 Current measurement. In this setup a current-carrying wire is wrapped around a ferrite core, with the sensor located in the air gap between its ends.

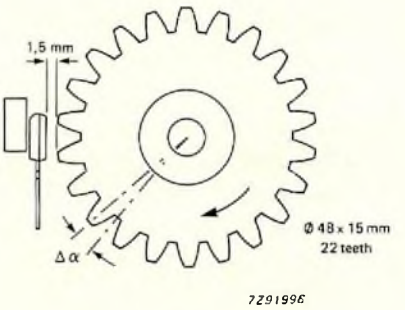

Fig.19 Measuring the rpm of a ferrous gear wheel using the KMZ10B sensor with the FXD100 8 x 8 x 4,35 magnet

Angular-velocity measurement – ferrous gear wheel

Figure 19 shows how a KMZ10B can be used to measure the angular velocity of a ferrous gear wheel, and Fig.20 shows the sensor output as an oscilloscope trace.

As the wheel's rpm increases, so will the frequency of the oscilloscope trace. This setup therefore provides a very sensitive means of measuring rpm and could be used, for example, in anti-lock breaking systems (ABS) for motor vehicles.

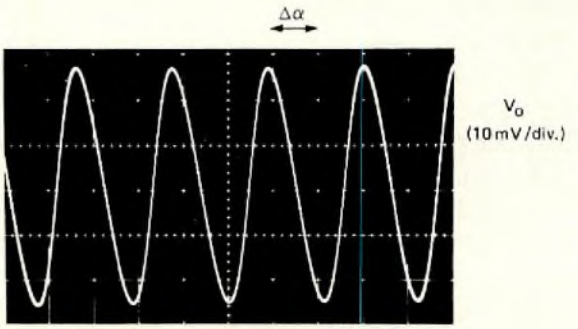

Fig.20 Oscilloscope trace for the setup of Fig.19. As you increase the wheel's rpm the frequency of the trace on the oscilloscope will also increase

Angular-velocity measurement – eddy-current effect

A KMZ10B sensor can also measure the speed of a rotating non-ferrous metal object (for example, a copper wheel) using eddy-current detection. Figure 21 shows a simple arrangement for doing it, and Fig.22 shows how the sensor output varies with rpm.

The sensor measures the magnetic field produced by eddy currents induced in the copper wheel by the auxiliary magnet. The faster the wheel rotates, the greater the eddy currents and the higher the sensor's output signal.

This arrangement would enable the sensor to operate as an extremely simple tachometer unit which could be permanently mounted in a wide range of mechanisms.

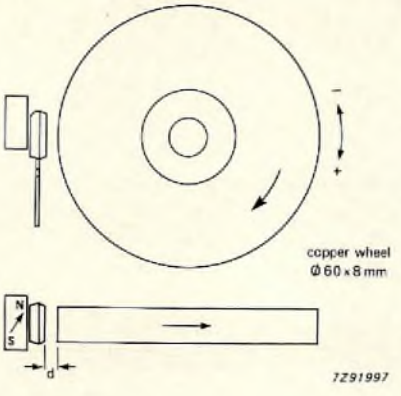

Fig.21 Measuring the rpm of a copper wheel using eddy currents.

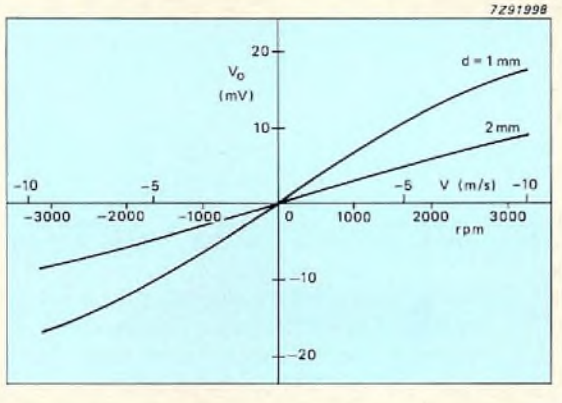

Fig.22 Sensor output versus rpm. The sensor measures the magnetic field produced by eddy currents induced in the copper wheel by the auxiliary magnet

Proximity switch

Figure 23 shows a simple arrangement, that, together with a comparator, can be used as a proximity switch.

By orienting the sensor axis at 45° to the axis of the permanent magnet, the sensor gives a negative signal (Fig.24) for both axial arrangements of the magnet, which could, in a practical circuit, be applied to the input of a comparator. Experience indicates that with a supply of 5 V, a KMZ10C sensor with a switching level above 10 mV is probably the best choice for this application. Below this switching level, strong external fields may disturb the sensor and give ambiguous results. Switching level may be set by means of offset adjustment in the comparator circuit.

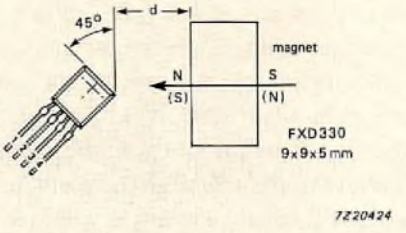

Fig.23 By orienting the sensor axis at 45° to the axis of the permanent magnet, a negative signal can be obtained from the sensor which can be applied to the inverting input of a comparator

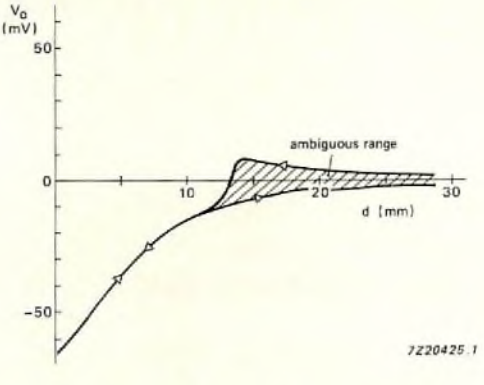

Fig.24 Sensor output as a function of distance d between the sensor and the permanent magnet

General magnetic-field measurements

Thanks to its high sensitivity, the KMZ10 sensor is ideal for measuring magnetic fields by so-called 'null-field' methods, in which the field to be measured is compensated by a coil, the current through which serves as a measure of the field. The advantage of such methods is that since they operate around a null-field position, tolerances and drift of sensitivity can be ignored, as can slight non-linearities in sensor characteristics. The high sensitivity of the sensor also means that the compensating coils can do without ferromagnetic cores (and the inevitable hysteresis effects that these would introduce). It does, however, limit the number of turns and the current that can be used, and restricts the measuring range to a few kA/m.

Figure 25(a) shows the sensor/coil arrangement and Fig.25(b) the drive circuitry. With zero external field applied to the sensor (by, for example, arranging the sensor's y-axis perpendicular to the earth's magnetic field), bridge offset is initially set by potentiometer R4 to just below the switching voltage of the comparator (which has a gain of around 10^5). An external field applied to the sensor will then cause the comparator to switch and current to pass through the coil L1. This then sets up a magnetic feedback system in which the magnetic field generated by the coil almost compensates the external field but leaves a small residual field that's sufficient to maintain the current through the coil and hence the compensating field generated by it. The output voltage V_o is thus a direct measure of the magnetic field generated by the coil and hence of the external field to be measured.

Figure 25(b) is suitable for measuring magnetic fields in only one direction. For bi-directional field measurement, the circuit of Fig.25(c) should be used.

Finally, Table 4 suggests some coils suitable for this application.

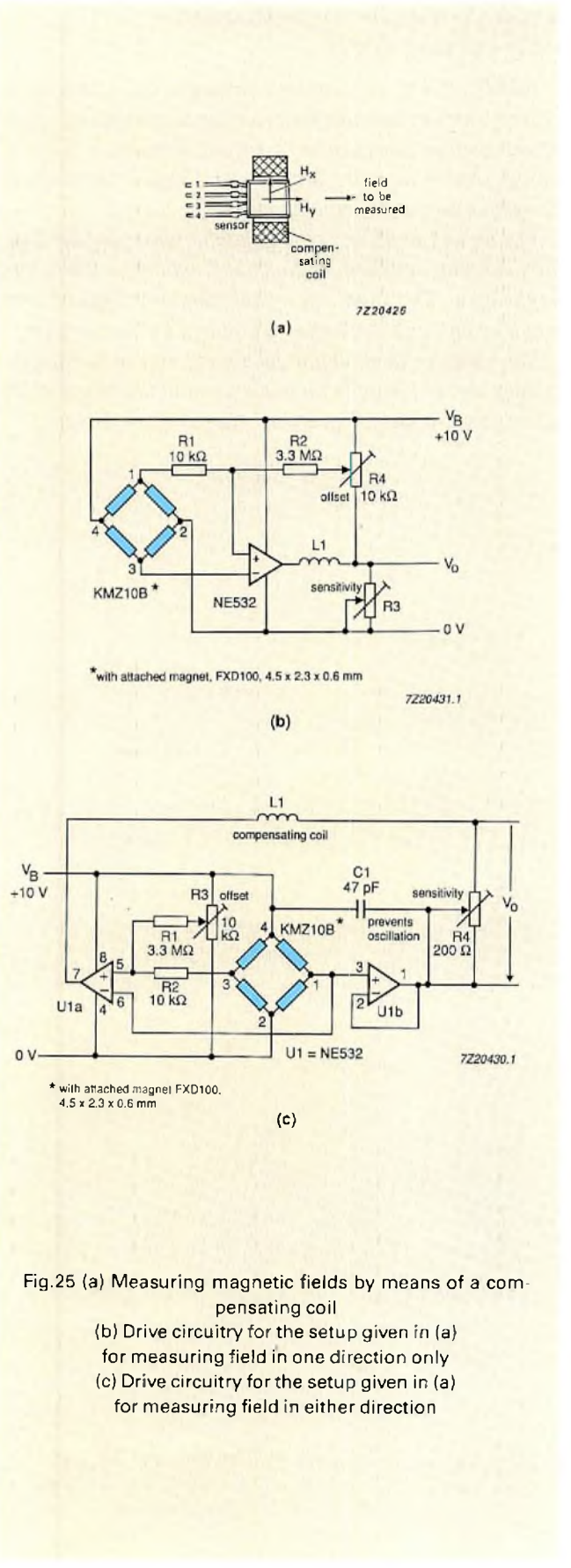

Fig.25 (a) Measuring magnetic fields by means of a compensating coil
(b) Drive circuitry for the setup given in (a) for measuring field in one direction only
(c) Drive circuitry for the setup given in (a) for measuring field in either direction

Table 4
Compensating coils

coil	turns	wire dia (mm)	resistance (Ω)	H/i* ([A/m]/mA)
1	365	0.10	18	48
2	720	0.07	75	100

* H - magnetic field i - current coil former Philips 4322 021 30240

Detecting and measuring weak magnetic fields – magnetic compass

In the measurement of weak magnetic fields (for example the earth's field), it's often advantageous to omit the auxiliary magnet in order to get maximum sensitivity from the sensor. The sensor, however, is then in danger of being flipped by any stray magnetic field. The circuit of Fig.26 shows an excellent way of removing this danger by the use of a coil to periodically reset the sensor's polarity.

The circuit is intended only for *detecting* weak magnetic fields (some hundreds of A/m). A constant current via R13 generates a weak stabilizing field of about 0.5 kA/m for high sensitivity, and the sensor is periodically reset by current pulses generating more than 3 kA/m. The circuit, therefore combines high sensitivity with relative insensitivity to disturbing magnetic fields.

Another problem of measuring weak magnetic fields is that precision is limited by drift in both the sensor and amplifier offset. In these instances it's possible to take advantage of the 'flipping' characteristic of the KMZ10 series to generate an output that's independent of offset.

The sensor, located in a coil (Fig.27(a)) whose axial field is periodically reversed by alternate positive and negative going pulses (Fig.27(b)), is continually flipped from its normal to its reversed polarity and back again. The polarity of the offset, however, remains unchanged, so the offset itself can be eliminated by passing the two output signals (Fig.27(c)) through a comparator circuit.

For the most sensitive sensor, the KMZ10A, the switching field should not be less than 3 kA/m. Since there's no auxiliary field in this arrangement, the sensitivity of the KMZ10A is about 22 mV/V/(kA/m), and fields up to around 250 A/m can be measured without stability problems.

The normal KMZ10A sensor chip is encapsulated with its x axis (the axis of its permalloy strips) perpendicular to its leads, and this is rather inconvenient for locating it in a coil with its x axis aligned with the coil axis. A special 'turned' sensor, with its x axis parallel with its leads, type KMZ10A1, is therefore available for this application.

Figure 28 shows how a magnetic compass can be made using two mutually perpendicular 'turned' sensors inside a coil. As in the previous example, the magnetic field is periodically reversed to produce an output that's independent of offset. What's more, the compass needs no temperature correction since the determination of field direction relies on the ratio of the two signals and not on their absolute values.

A suitable coil for this compass would be 100 turns of 0.35 mm copper wire wound on a Philips 4322 021 30270 coil former – giving a resistance of 0.6 Ω, an inductance of 87 μH and a axial magnetic field of 8.3 (kA/m)/A.

Figure 29 gives a circuit for delivering the current pulses (50 μs) and for processing the outputs of the two sensors. The current pulses for the coil L1 (70 Hz) are

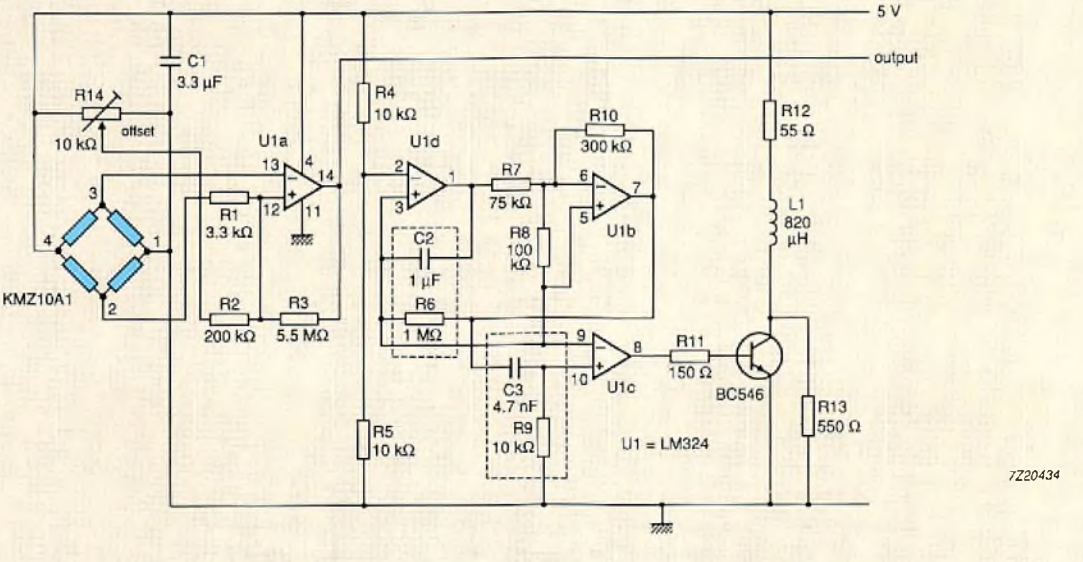

Fig.26 To remove the danger of flipping when the sensor is used without an auxiliary magnet (for maximum sensitivity), the sensor's polarity can be periodically reset by a coil L1

generated by transistors TR1, TR2 driven by a 140 Hz pulse generator via a 2:1 frequency divider.

Capacitor C4 differentiates the output signal from the transistors to ensure zero current through the coil between the current pulses.

Capacitors C5 and C6 suppress the offset of the two sensor signals. These are then amplified and fed to two synchronous demodulators which generate output voltages V_x and V_y proportional to the x and y components of the earth's magnetic field.

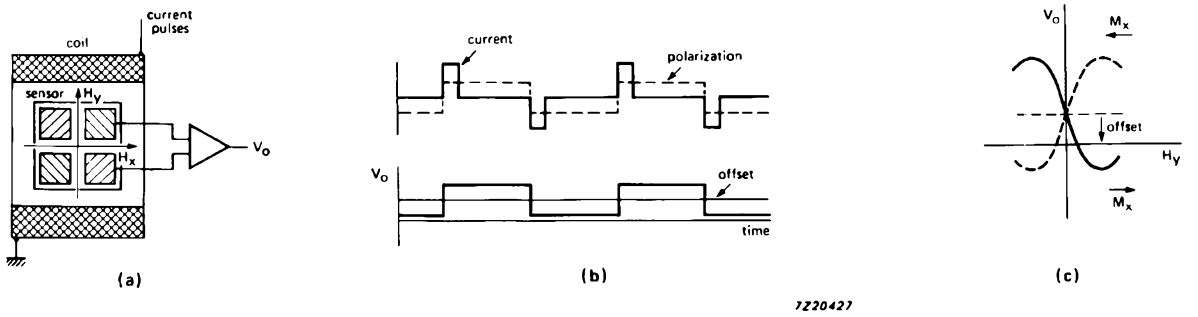

Fig.27 (a) Setup for measuring weak magnetic fields using a coil whose magnetic field is periodically reversed to continually flip the sensor's polarity and eliminate the effects of offset
(b) Pulse diagram
(c) Sensor output

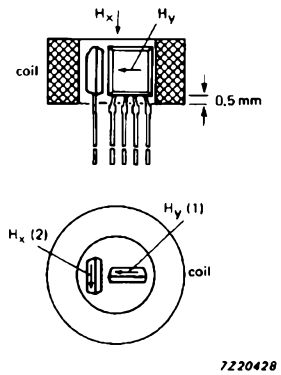

Fig.28 Magnetic compass using two mutually perpendicular 'turned' sensors inside a coil. As in the previous example, the magnetic field is periodically reversed to produce an output that's independent of offset

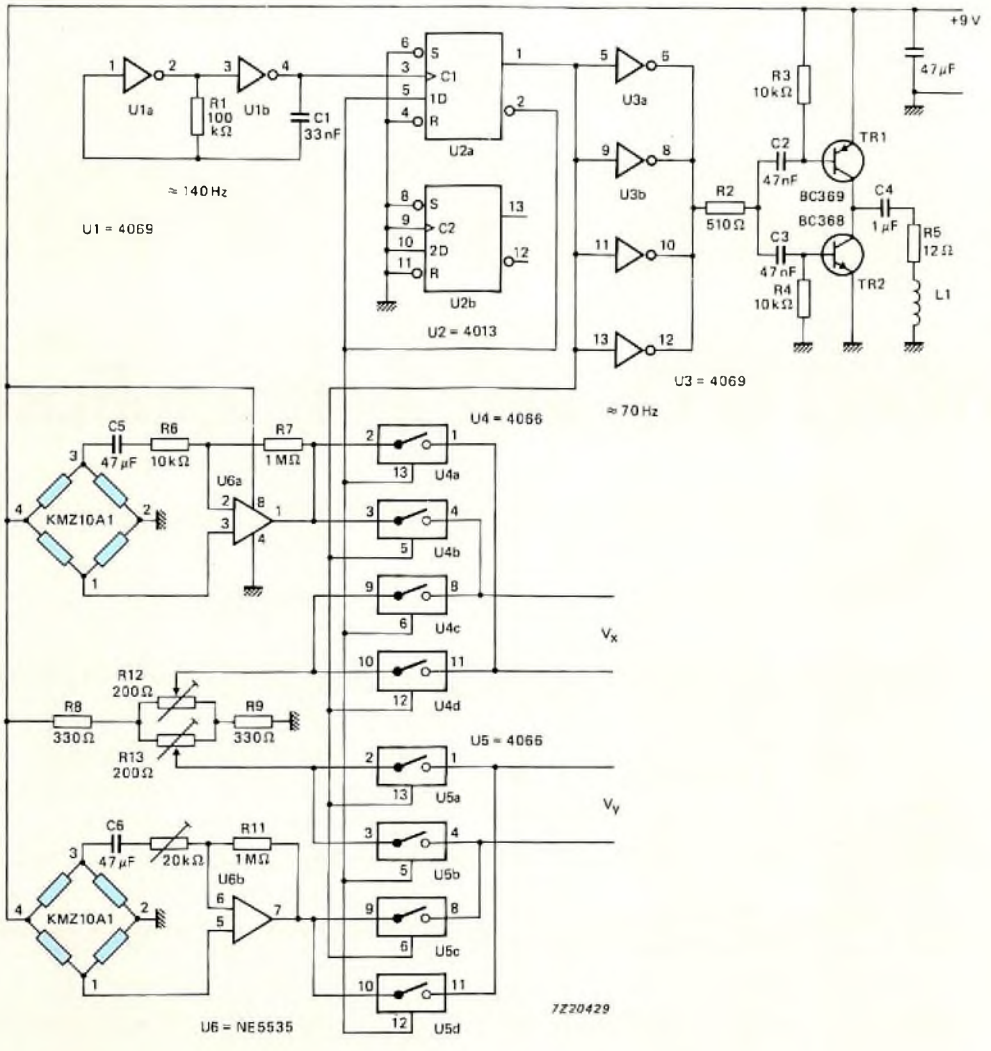

Fig.29 Circuit for delivering the current pulses and for processing the outputs of the two sensors

HCMOS FIFOs and their applications

ROB VOLGERS

When data is transferred between digital sub-systems which can operate at different maximum baud rates, the rate at which the overall system can transfer data is limited to the baud rate of the slowest sub-system. A PC for example, has a serial input which can accept data at 9600 baud but the keyboard connected to it sends its data at only 4800 baud. The difference between the two data rates creates problems - the computer doesn't understand the keyboard. Other examples are data fed to a VDU screen and data exchanges via telephone lines. In such cases, the performance of the overall system can be improved by using a First-In/First-Out (FIFO) buffer to temporarily store blocks of data from one sub-system and read them out at a rate that the other sub-system can handle when it's ready.

Our HCMOS family of logic ICs includes two FIFO registers, both of which operate at a guaranteed maximum frequency of 18 MHz; the PC74HC/HCT40105 (sixteen 4-bit words) and the PC74HC/HCT7030 (sixty-four 9-bit words). Like all other HCMOS ICs, they operate from a supply of 2 V to 6 V (CMOS compatible ICs with PC74HC prefix) or 5 V ± 10% (TTL compatible ICs with PC74HCT prefix). Features of our HCMOS family, especially its low power consumption, ability to work at low voltages, wide operating temperature range (−40 to +125 °C for PC74HC/HCT) and high noise-immunity makes these FIFOs ideal for upgrading system performance, especially with regard to operation in electrically noisy environments and meeting battery-powered standby requirements.

FIFO BUFFER OPERATING PRINCIPLES

A FIFO buffer is a memory buffer with completely independent input and output clocks. As shown in Fig.1, it can be used to interface two asynchronous sub-systems A and B. Instead of being transferred directly to sub-system B, data from sub-system A is first accumulated in the FIFO memory buffer and then read into sub-system B in the same sequence but at a different rate.

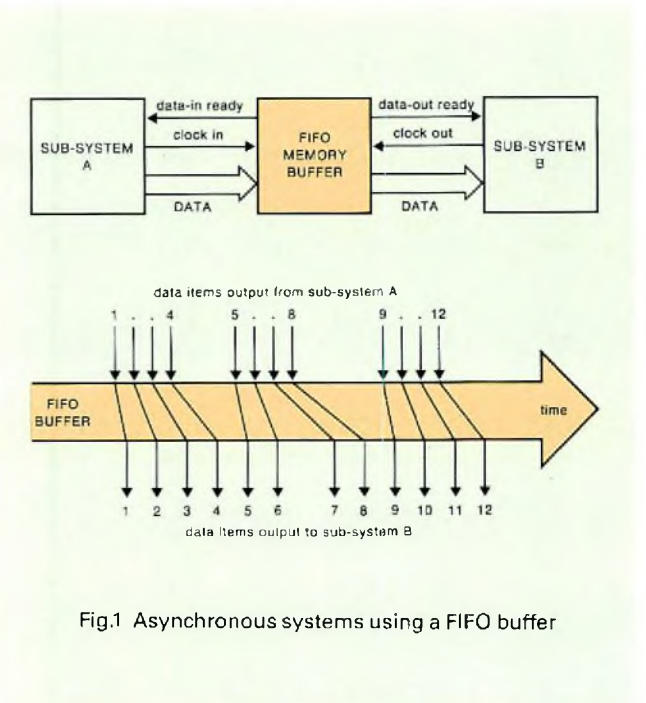

Fig.1 Asynchronous systems using a FIFO buffer

Since sub-system A needs to know whether the FIFO is busy or full, it receives a Data-In Ready (DIR) input. A Data-Out Ready (DOR) input to sub-system B indicates that output data is available.

At present, there are two basic ways to implement a FIFO memory buffer. The first is simply a series chain of flip-flops with data entering at one end and exiting at the other with the 'ripple-through' process controlled by an internal clock. The other method is to store the data in a RAM so that it can be directly accessed without any 'ripple-through' delay. However, this method has the drawbacks of high current consumption and relatively slow speed due to the RAM access time. The operation of our HCMOS FIFO register ICs is therefore based on the 'ripple-through' principle which will now be explained more in more detail.

INTRODUCTION TO HCMOS FIFO REGISTER ICs

As shown in Fig.2, an HCMOS FIFO register has two stacks of shift-registers to move data through the IC. One stack (data latches) contains the data. Data is entered at the top of this stack and proceeds downwards to emerge from the bottom. The other stack of shift-registers (control flip-flops), operates in parallel with the data latches. It contains control flags to indicate whether the segment of data in the associated data latch is valid.

When data is written into the top of the stack, a true flag is placed in the first control flip-flop, and the data, together with its control flag, then proceeds downwards (ripples-through) the stack until it reaches the lowest location. This process eventually forms a full stack of valid data.

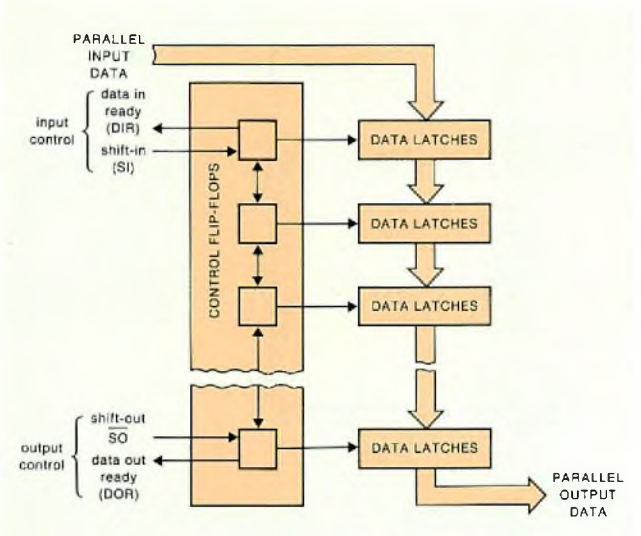

Fig.2 Operating principle of the HCMOS FIFO register ICs

The timing of the ripple-through process is controlled by an internal clock. The maximum ripple-through time is the product of the number of levels in the stack and the internal clock period. The DOR flag, which tells the system that data is present, is fed out together with the associated data.

If the entire word length isn't used, the unused data inputs must be pulled up/down to either V_{CC} or GND and the corresponding data outputs left open-circuit.

Because of the ripple-through process, the entire output sequence is shifted by at least one ripple-through period, but this won't be a problem for most applications.

4-bit x 16-word FIFO PC74HC/HCT40105

These are expandable HCMOS FIFO registers that can store sixteen 4-bit words. The 40105 has two status flags, one to indicate that the FIFO is not full or busy (DIR = data-in ready), and the other to indicate that valid data is present at the output (DOR = data-out ready).

They also have an active-HIGH master reset (MR) and an active-LOW output enable ($\overline{OE}$) input. When $\overline{OE}$ is HIGH, the outputs are in the high-impedance OFF-state. MR clears the control flip-flops and the data content is declared invalid. The contents of the output data latches then remains in the state associated with the last word that was shifted out, or in the random state existing at power-up.

The HCMOS 40105 is pin-compatible with the LSTTL 74LS224, but the latter has an active-LOW master reset. Features of the PC74HC/HCT40105 are:

- expandable in multiples of 16 words or of 4 bits
- very low power consumption (V_{CC} = 5.0 V)
  I_{CC} (static) < 8 μA
  I_{CC} (dynamic) at 18 MHz = 21 mA (all outputs loaded with 50 pF)
- 3-state outputs
- guaranteed maximum speed of 18 MHz at V_{CC} = 4.5 V
- fully asynchronous operation
- reset capability
- maximum ripple-through delay of 500 ns at V_{CC} = 4.5 V
- operates from 2 V to 6 V (PC74HC40105) or 4.5 V to 5.5 V (PC74HCT40105)
- available in SO-16(150-mil) and DIL-16 packages
- low cost

9-bit x 64-word FIFO PC74HC/HCT7030

These are expandable HCMOS FIFO registers that can store sixty-four 9-bit words. The facilities described for the 40105 also apply to this IC except that, unlike the 40105, the 7030 has an active-LOW $\overline{MR}$ input. The 9-bit wide array of the 7030 allows for an optional control or parity bit. This feature is especially useful in data communications applications where it's necessary to use a parity bit for transmission/reception error checking. The 7030 is pin- and function-compatible with the bipolar TDC1030 FIFO but the latter consumes about 250 mA in the standby mode. Features of the PC74HC/HCT7030 are:

- expandable in multiples of 64 words or of 9 bits
- very low power consumption (V_{CC} = 5.0 V)
  I_{CC} (static) < 50 μA
  I_{CC} (dynamic) at 18 MHz = 80 mA (all outputs loaded with 50 pF)
- 3-state outputs
- guaranteed maximum speed of 18 MHz at V_{CC} = 4.5 V
- fully asynchronous operation
- maximum ripple-through delay of 2 μs at V_{CC} = 4.5 V
- operates from 2 V to 6 V (PC74HC7030) or 4.5 V to 5.5 V (PC74HCT7030)
- available in SO-28 and DIL-28 packages
- low cost

FUNCTIONAL DESCRIPTION OF HCMOS FIFO REGISTER ICs

Figure 3 is a functional block diagram of an HCMOS FIFO register IC.

Data input

After power-up, the Master Reset input is pulsed to clear the FIFO memory. The DIR flag is set HIGH to indicate that the FIFO input stage is empty and ready to receive data. As long as DIR is HIGH, data present at the input can be shifted-in using the Shift-In (SI) control input. With SI HIGH, data is shifted into the input latches and a busy indication is given by DIR going LOW.

If the FIFO isn't full after the SI pulse, DIR again becomes HIGH to indicate that space is available. The DIR flag remains LOW if the FIFO is full. With the FIFO full, SI can be held HIGH until a Shift-Out (SO) pulse occurs. Then, after data is shifted-out, the input latches are empty and DIR goes HIGH to allow the next data to be shifted-in. The SI pulse must be made LOW to end the shift-in process.

Data transfer

After data has been transferred from the input latches to the main FIFO register, it moves through the FIFO asynchronously and is stored at the output end of the register stack. Empty locations occur at the input end of the FIFO as the data moves down the stack.

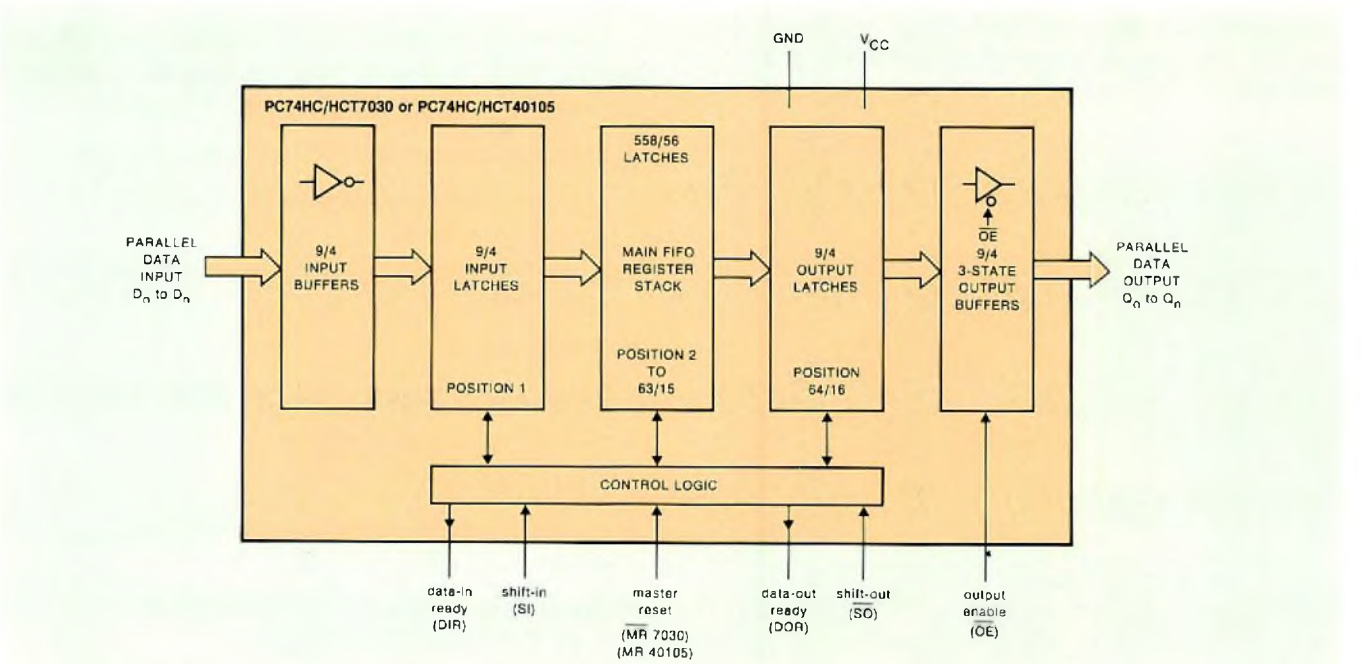

Fig.3 Functional block diagram of an HCMOS FIFO register

Data output

The initial master reset at power-on sets DOR LOW. After a reset pulse, data shifted into the FIFO ripples-through to the output latches causing DOR to go HIGH, thereby indicating that there is valid data at the outputs.

When the DOR flag goes HIGH, data can be shifted-out by setting the $\overline{SO}$ control input HIGH. A busy indication is then given by DOR going LOW. When $\overline{SO}$ is set LOW, data ripples-through the FIFO to fill the output latches and an empty location appears at the input.

When the output latches are loaded, DOR goes HIGH, but, if the last of the valid data has been shifted-out leaving the FIFO empty, the DOR flag remains LOW.

With the FIFO empty, the last word that was shifted-out is latched at the outputs. In this state, the $\overline{SO}$ input can be held HIGH until the SI control input is used. Following an SI pulse, data ripples-through the FIFO to the output latches, resulting in the DOR flag going HIGH and the data being shifted-out. The $\overline{SO}$ control input must be set LOW before additional data can be shifted-out.

High-speed burst mode

If the shift-in/shift-out pulses (SI and $\overline{SO}$) aren't applied until the respective status flags (DIR and DOR) are valid, the shift-in/shift-out rates are determined by the status flags. However, without the status flags, a high-speed burst mode can be implemented. In this mode, the burst-in/burst-out rates are determined by the duration of the pulses at the shift-in/shift-out inputs. Shift pulses can be applied irrespective of the state of the status flags, but shift-in pulses that would cause the FIFO to overflow are not allowed.

Increasing word length

The word length of the FIFO can easily be increased by simply adding another FIFO and two AND gates to generate composite DIR/DOR flags as shown in Fig.4. The basic operation and timing of this arrangement are identical to a stand-alone FIFO, except that there is an extra gate delay on the flag outputs.

However, if a particular application causes SI to be held HIGH when the FIFO is full, or $\overline{SO}$ to be held HIGH when it's empty, differences in the ripple-through times of the two FIFOs caused by process variations can cause the flag signals of FIFOs A and B to occur at different instants, thereby preventing the AND-gates from generating composite flag signals. Extra logic circuitry as shown in Fig.5 must then be used to generate the composite DIR/DOR pulses. Note that, if the 40105 FIFO is used, the extra circuitry is only needed for the composite DIR flag.

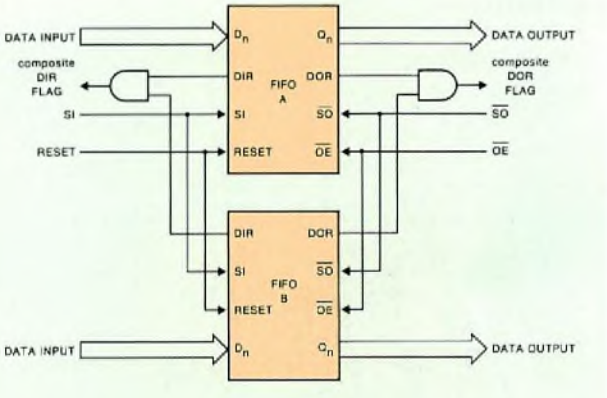

Fig.4 Using two FIFO registers to increase word length. The timing is the same as that for a single FIFO except that the flags are subject to an additional gate delay

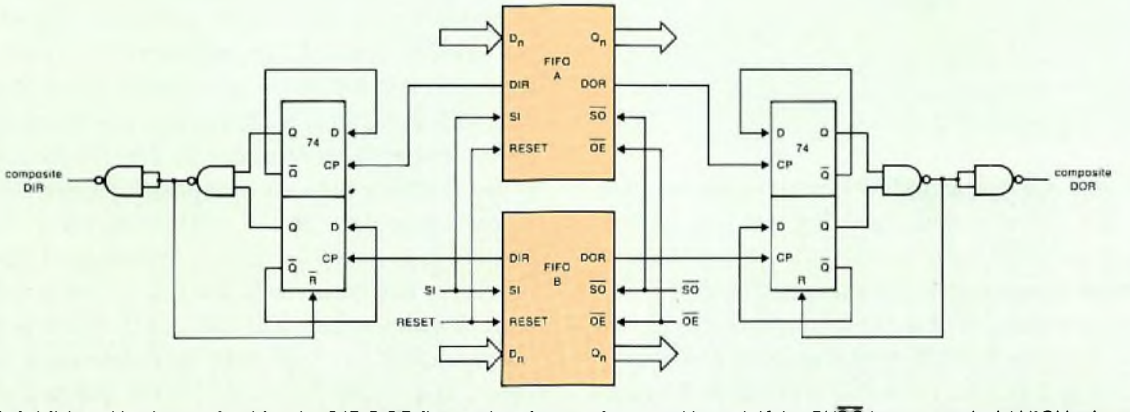

Fig.5 Additional logic required for the DIR/DOR flags when increasing word length if the SI/$\overline{SO}$ inputs are held HIGH when the FIFO registers are empty/full so that an automatic shift-in/out cycle is started. If the 40105 FIFO register is used, the extra logic is only needed for the DIR flag

Increasing word capacity

FIFOs can also be cascaded to increase their word capacity without using extra components. In the cascaded configuration, all necessary communications and timing are performed by the FIFOs themselves. The data transfer rate is determined by the minimum durations and delays of the flag pulses. The typical data transfer rate for cascaded FIFOs is 23 MHz.

Figure 6 shows two FIFOs cascaded to double the word capacity. After a ripple-through delay, data arrives at the output of FIFO A. Because $\overline{SO}$ is HIGH, a DOR A pulse is generated. After a second ripple-through delay, data arrives at the outputs of FIFO B. After the $\overline{SO}$ B pulse has been applied with both FIFOs full, there is a delay for an empty location to bubble-up to the input. A DIR B pulse which acts as an $\overline{SO}$ A pulse for FIFO A is then generated. One word is transferred from the output of FIFO A to the input of FIFO B. After a second bubble-up delay, an empty space arrives at D_n A and DIR A then goes HIGH.

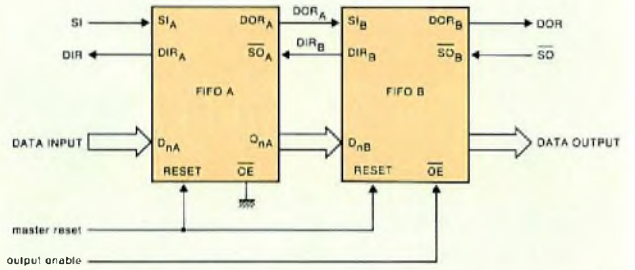

Fig.6 Cascading two FIFO registers to double the word capacity.

If FIFO A is very fast and FIFO B is very slow because they are from different manufacturing lots, the DIR B flag applied to the $\overline{SO}$ input could be too narrow to allow FIFO A to function correctly. On the other hand, if FIFO A is much faster than FIFO B, the DOR A pulse could be too narrow to trigger the SI B input. The circuitry in Fig.7 improves the performance of cascaded FIFOs by lengthening the narrow DOR/DIR pulses. Because of the forward voltage-drop of the diode, this network can only be used with supply voltages greater than 4.5 V.

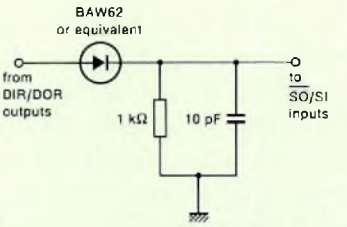

Fig.7 Circuit arrangement for improving the performance of cascaded FIFOs

FIFO APPLICATIONS

As previously stated, the classical application for a FIFO is to match the instantaneous data rates of two digital systems in a simple and economical manner. For reasons of design economy or even of sheer necessity, one of the systems may read or write data words in ultra high-speed bursts, whereas the other operates at a slow, constant data rate or even at a rate which varies between ultra-slow and fast. Asynchronous HCMOS FIFOs 40105 and 7030 can smooth-out these data rate variations as long as the FIFO input and output data rates coincide for long enough periods to prevent the FIFO from being completely filled or emptied.

There are, however, some other uses for FIFOs which arise from other, rather different circumstances. For instance, they can be used in a system which must accumulate a block of 16 or 64 bits and then use some scanning logic, or perhaps even a microprocessor which is otherwise occupied most of the time, to search the block for the presence of a control character.

A less obvious but interesting application for FIFOs is to use them as automatic bus-monitors for recording the jump-history for hardware or software diagnostic purposes. A FIFO whose inputs are connected to a minicomputer's program counter or microprogram counter, or to a microcomputer's main address bus, can be used to record every new jump address generated by the program. Thus, if the hardware fails, or the operating system crashes, a record exists of the last 16 or 64 jumps which were taken before the system was halted. Assuming of course, that provision has been made for the system to sense that something is wrong and halt itself. Such a record of jumps can be very valuable for determining what happened just before the crash. FIFOs can be used in this way, either as part of a built-in self-monitoring feature of a digital system, or as part of various kinds of external test equipment.

FIFOs can also be used as controllable delay elements for digital information which can't be used immediately it's received. For example, it may first have to be compared with other information which isn't yet available, or be synchronized with other streams of information with different phase relationships. An example of the latter situation is de-skewing of several bit-streams from a densely recorded parallel-format magnetic tape. Although one FIFO is required for each bit-stream, this may still be a more reliable and economical method of solving the problem than using other digital circuitry.

For some applications, it's advantageous to operate a FIFO with all its input and output cycles synchronized, so that it merely delays the data for a number of clock periods.

File server

It's cheaper and more efficient to use high-speed FIFOs in a file server than to adopt other hardware or software approaches. Consider a system like the one in Fig.8 in which the file server is connected to a local area network (LAN) on one side and to a Winchester disk on the other. To prevent loss of data, both I/O connections demand attention at unpredictable intervals and must be serviced on demand.

A possible software solution would be to form the data into software FIFO queues as it arrives and, when a full record is buffered, start processing the data. To implement this, the data rates of both interfaces would have to be low enough to allow the software code to poll the status of either I/O port. The ports would also have to be monitored in case another user of the LAN made a request. These time-consuming tasks would degrade the performance of the system.

One hardware method of moving data in a file server uses hardware interrupts. Here, an interrupt mechanism calls routines to move data between the I/O ports and the software FIFO queues. Interrupts allow one task to run at a time and can switch to an I/O service routine at any instant. An interrupt system must therefore be so designed that the data of the interrupted task isn't destroyed. Extra code is required to maintain the state of the machine. This overhead could prevent an interrupt being made at a critical time for a particular piece of code and would, in turn, require code to disable and re-enable interrupts around the critical sections. Also, the programmer would have to spend extra time verifying that all possible sequences caused by random interrupts produced desirable results. In most cases, these complications outweigh the advantage of the faster execution offered by hardware interrupts.

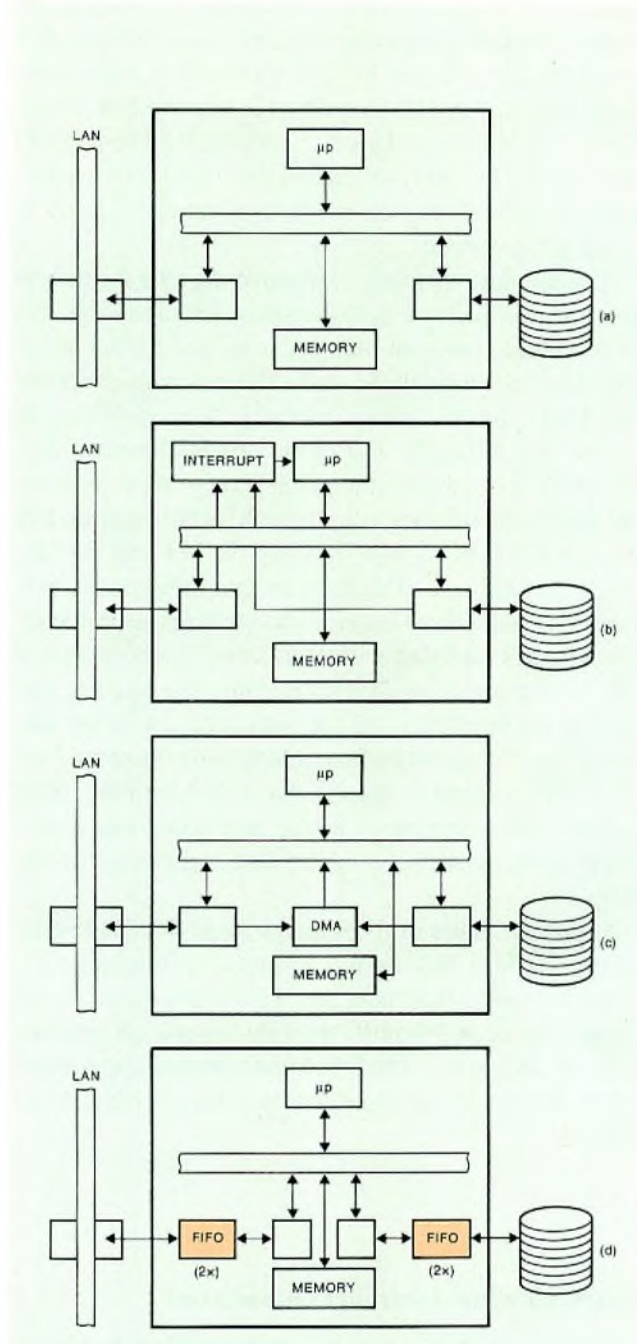

Fig.8 Methods of implementing a file server (a) with software (b) with interrupts (c) with DMA (d) with FIFOs

Direct memory access (DMA) is another hardware method of moving data in file servers. Here, a block of circuitry monitors the I/O ports and, when the port requires attention, the DMA logic interrupts the current task at the bus transfer level and steals a memory cycle to transfer the data between the port and the FIFO queue in memory. Although memory cycles are lost, this affects

performance much less than hardware interrupt schemes in which a whole subroutine of many cycles is executed to transfer each element of data. However, a significant disadvantage of the DMA method is that the DMA controllers are complex and must be programmed and implemented in the bus structure. Also, since the DMA mechanism can only serve one source at a time, it causes a throughput bottleneck.

With all these methods of transferring data in file servers, the mechanism that transfers data between the FIFOs and the program memory is shifted further away from the software and closer to the I/O port. Because both FIFO queues are in memory, the memory bus remains a bottleneck. Hardware FIFOs eliminate this bottleneck and enhance the performance of the system. The processor still interfaces to the FIFO through an I/O port, but the FIFO is now between the I/O port and the rest of the hardware. The software can service data at a steady rate without losing any, and without the problems or overhead associated with more complicated schemes such as interrupts or DMA. Because the queues are between the controller and the peripheral, the latter can load or read the queue without interrupting the controller. Since the controller doesn't have to maintain both queues, there's no risk of losing data when one of the queues is being serviced whilst data is arriving for the other.

A special feature of the 9-bit 64-word HCMOS FIFO register 7030 is that its use results in a minimum IC count. Assuming that there are two FIFOs (transmit and receive) for each I/O port, the FIFO approach requires only four 28-pin ICs. The DMA and interrupt approaches require at least one 40-pin IC and several bus buffer/control ICs.

Communications controller bus interface

Another example of a rate mismatch problem occurs in the interface between a CRT terminal and a CPU. A communications controller is used so that the CPU doesn't have to be burdened with the task of monitoring the UARTs of multiple CRTs and printers. As shown in Fig.9, the communications controller serves as a communications multiplexer and data concentrator.

The communications controller must buffer received data words so that, if several words from different terminals are received close together, they won't be lost as more data words arrive. The obvious structure for storing the data words is a FIFO queue. The CPU can then respond to them without having to wait for the controller to finish inputting other words. There should therefore be two FIFOs; one for transmitting and one for receiving. To simplify the design, the two FIFOs can be connected back-to-back and placed between the CPU and the controller. When data words are received, they're written into the receive FIFO and read from the other end of it by the CPU. As the CPU prepares the data words for transmission, it writes them into the transmit FIFO from which the controller reads them and sends them to the terminal through a UART.

It is conceivable that there could be a separate pair of FIFOs for each UART to make it easier for the controller and CPU to identify data words associated with a particular UART. The DIR/DOR flags of the FIFOs would then be used as status flags. For example, the status of both sides of the transmit FIFO would have to be monitored. As the CPU prepared a data word for transmission, it would examine the full flag (DIR) to check if the transmit FIFO was full and, if it was, would delay entering that word. If the transmit FIFO wasn't full, the CPU would enter the data word. The empty flag (DOR) of the transmit FIFO would be monitored by the communications controller and would change to 'false' as soon as the first word was entered into the FIFO by the CPU. The communications controller would then know that the transmit FIFO was holding a word which could be transmitted. It would continue to read words from the transmit FIFO as long as the DOR (empty) flag remained 'false' indicating that the transmit FIFO contained one or more words.

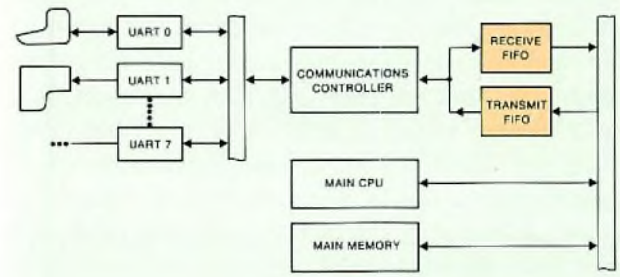

Fig.9 Using FIFOs in a communications controller

Optimizing the DIR/DOR flags

As long as a FIFO register IC is only partially full and is shifting data in or out, the DIR/DOR flags are both pulsed at the shift frequency. This may be inconvenient if the DIR/DOR flags are used to indicate that the FIFO is empty or full. The arrangement shown in Fig.10 uses a steady-state full (DIR) flag and converts a slow-continuous data rate to a fast-burst one.

The monostable multivibrator prevents the full flag (DIR) from interrupting the CPU until 100 ns after the data has been shifted into the FIFO by the Shift-In (SI) command. If there hasn't been a DIR signal to reset the flip-flop within this period, the interrupt is issued because the FIFO is full. The CPU then empties the FIFO before the next character from the tape drive is entered. The waveforms associated with this circuit are given in Fig.11.

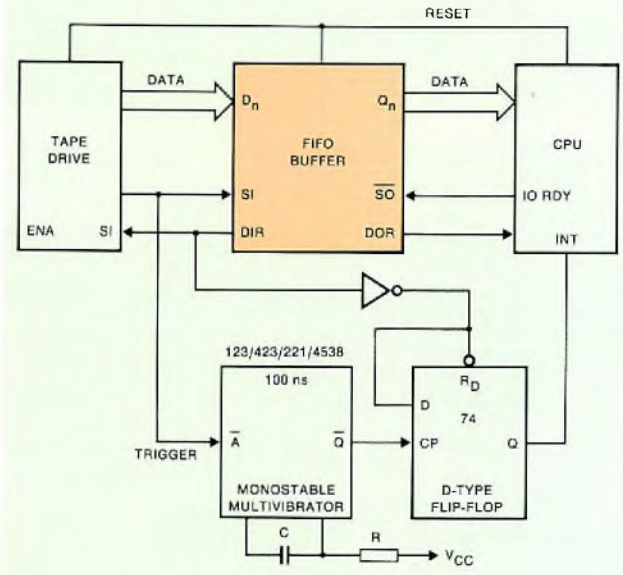

Fig.10 Using a steady-state FIFO full flag to convert a slow continuous data rate to a fast burst rate

If the full flag is used to interrupt the CPU so that it loads data from the FIFO to make space in its front-end, the bubble-up time can sometimes be a limiting factor if the input rate is too high. This can be solved if two FIFOs are cascaded to generate a half-full flag as shown in Fig.12. With this arrangement, there's always a guard-band of 16 or 64 words before both FIFOs are full.

Figure 13 is a much simpler circuit, which replaces both the monostable and/or the D-flip-flop in the previous examples. The waveforms for the circuit are given in Fig.14. The value of R depends on the rate of the Shift-in Input (SI) pulses (and therefore of the DIR/DOR pulses). If R is too low, the level at point A will reach the switching threshold of the Schmitt-trigger during a single pulse and false spikes will be generated. On the other hand, if R is too high, the output of the Schmitt-trigger will not switch until after the 65th pulse and data may be lost.

The RC time-constant must be such that the level at point A exceeds the Schmitt-trigger switching level during the HIGH period of DIR or DOR, but falls below it within the complete HIGH and LOW period of DIR or DOR. The circuit can only be used if the shift-in or shift-out rates are constant, or constant within a burst. The following Table gives typical values for R as functions of the frequency of the Shift-in Input (SI) pulse when C = 100 pF.

f_{SI} (MHz)	0.5	1.0	2.0	3.0	4.0	5.0	10.0	20.0
R (Ω)	3000	500	760	490	360	290	120	52

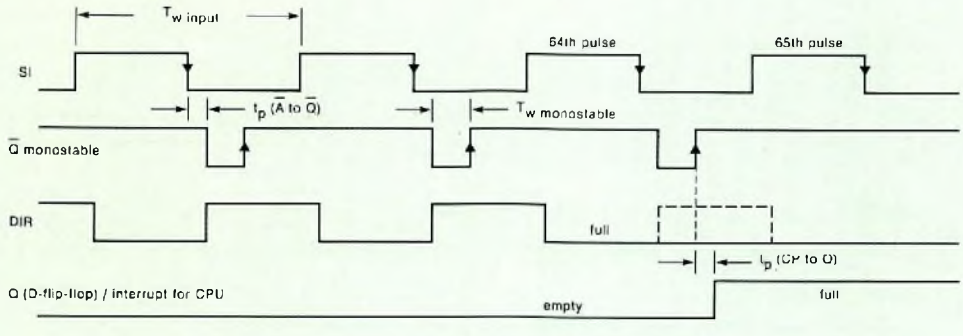

Fig.11 Waveforms associated with Fig.10 Period $T_{w\,input}$ must be longer than the sum of the bubble-up delay, $T_{w\ monostable}$ and tp (CP to Q) to empty the first location of the FIFO in time. The tape unit will then be able to generate a continuous data stream without filling the FIFO

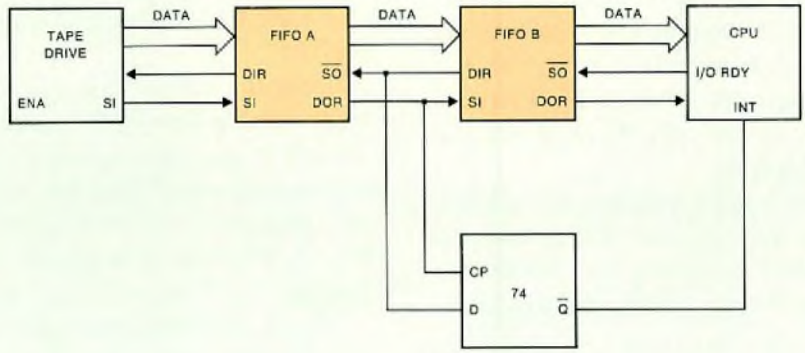

Fig.12 Half-full flag generation

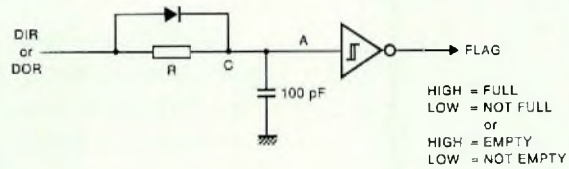

Fig.13 Steady-state full/empty flag generation

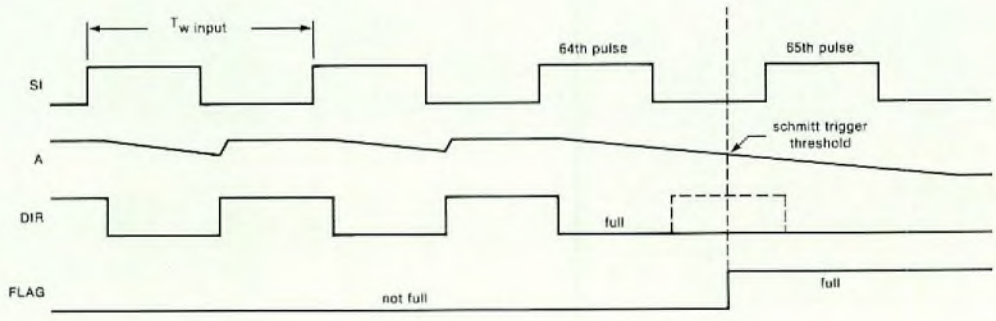

Fig.14 Waveforms associated with Fig.13

Increasing word capacity without increasing ripple-through time

Figure 15 is an arrangement for doubling the number of data words that can be handled by a FIFO buffer by multiplexing the data beween two 7030s. The associated waveforms are given in Fig.16. The advantage of this arrangement, which can only be used with the 7030, is that the ripple-through and bubble-up times are the same as those for only one FIFO. If the two FIFOs were to be simply cascaded, these delays would be doubled.

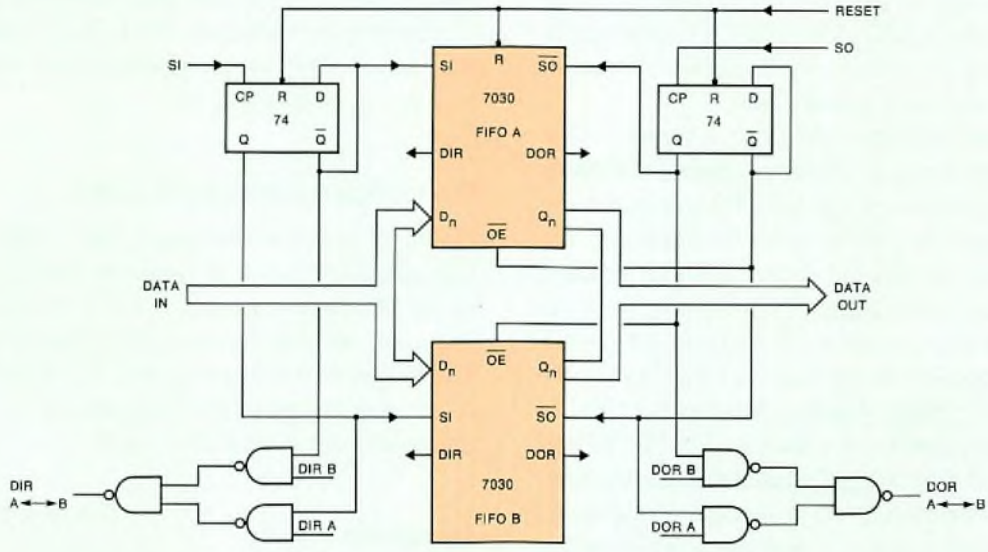

Fig.15 Using two FIFO registers to double the word capacity of a FIFO buffer without increasing ripple-through time or bubble-up delay. The waveforms for this arrangement are given in Fig.16

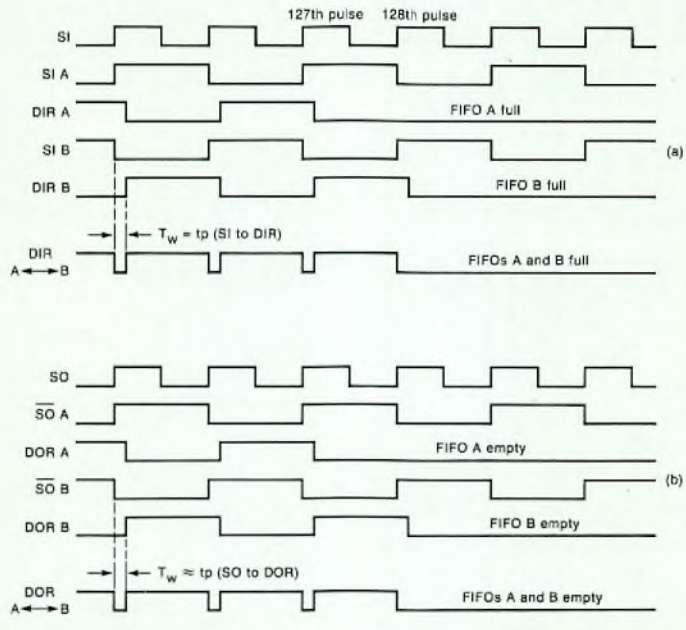

Fig.16 Waveforms associated with Fig.15 (a) shifting in (b) shifting out

A COMPLETE INTERSPEEDER

Block diagram description

The interspeeder shown in block form in Fig.17 uses two PC74HC/HCT7030 FIFO registers and two UARTs, each of which contain a serial-in/parallel-out receiver and a parallel-in/serial-out transmitter. The baud rates at which words are shifted-in or shifted-out are determined by separate clocks. The UARTs also allow pre-selection of the number of stop bits, parity mode and the number of bits per word by hard-wiring some pins.

The Interspeeder regulates the flow of two-way data between a computer and a slower peripheral such as a VDU, floppy disk drive or a tape unit. When transferring the slow data from the peripheral to the computer, the difference in data rate doesn't cause problems because the computer can do other things whilst waiting for a signal that the next word is ready. To increase the overall speed, it is also possible to introduce a FIFO in the peripheral to computer path, thereby allowing the CPU to check for incoming data at a convenient time. To prevent loss of data when transferring the fast data from the computer to the slower peripheral, it is necessary for the data to be divided into blocks of words by a FIFO buffer which stores them until the slow peripheral is ready to receive them,. While the peripheral is busy emptying the FIFO buffer, the computer can continue with other tasks.

Two cascaded PC74HC/HCT7030 FIFO registers, which can each store sixty-four 9-bit words, together form the 128-word FIFO buffer that also generates a half-full flag. This flag indicates whether the FIFO is being filled, half-full, being emptied or empty, and is used to determine when to tell the computer to stop or resume transmission. As long as the peripheral operates at a speed that's no more than half that of the computer, this can be done by adding an ASCII Xoff or Xon code in the data stream from the peripheral to the computer without waiting for an empty space.

Operating principles of the UART

Figure 18 is a block diagram of the UART. Some operating conditions, such as baud rate, bits per word, parity mode and number of stop bits are externally selectable and apply to both the transmitter and receiver sections. The frequency of the transmitter clock signal (TCP) and receiver clock signal (RCP) must be 16 times the required transmitting/receiving baud rates.

Transmitter

After resetting the UART at switch-on, outputs Transmitter Buffer Empty (TBMT), End Of Character (EOC) and Serial Output (SO) go HIGH. Data can then be applied to

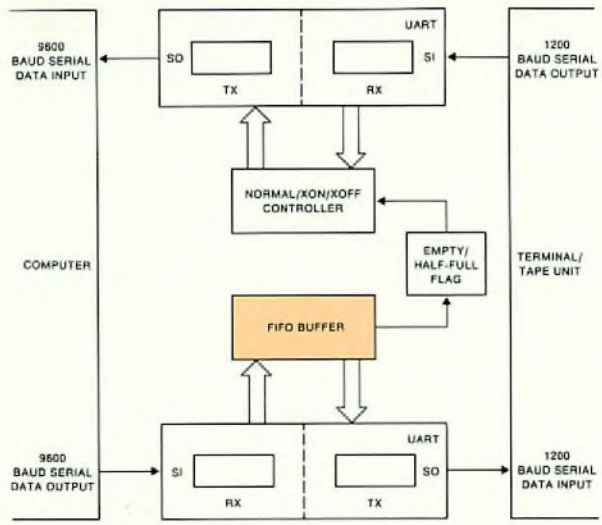

Fig.17 Block diagram of an Interspeeder

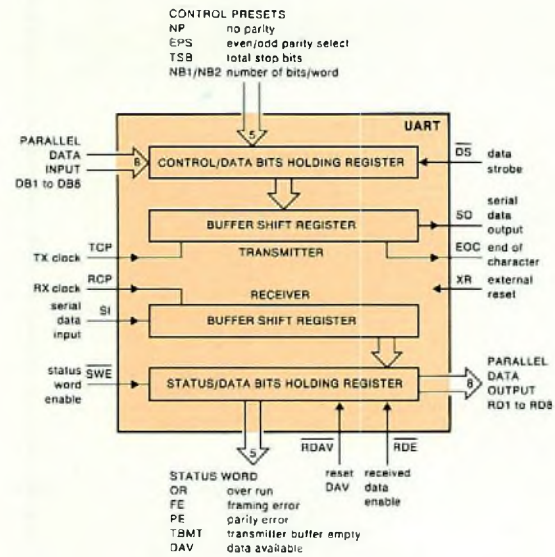

Fig.18 Functional block diagram of the UART

the parallel input of the UART transmitter. When the DS input goes HIGH, parallel data is read into the data bits holding register and the TBMT output goes LOW to indicate that a new parallel data word cannot be read-in because the data-bits holding register is occupied. When the data word has been transferred into the buffer shift register from where it is immediately transmitted in serial form, TBMT goes HIGH again to indicate that new parallel data can be accepted.

As soon as the buffer shift register is empty, any further data in the data-bits holding register is immediately transferred into it and transmitted. The EOC signal is LOW while each complete word is being shifted out in serial form. From this description, it's clear that a new parallel data word can be offered to the UART transmitter while it's still serially transmitting the previous word.

Receiver

When the UART is reset at switch-on, its Data Available (DAV) output goes LOW and its receiver is ready to accept the first serial data word in its buffer from where it's immediately transferred into the data bits holding register. The word is read-out in parallel form by setting the Received Data Enable ($\overline{RDE}$) input HIGH.

Before the next serial data word is read-in and transferred to the data bits holding register, the internal logic looks at the DAV signal to check whether the previously received word has been read-out in parallel form (DAV LOW). If it hasn't, the Over-Run (OR) bit of the status word is set HIGH.

Since the serial data input waits for a negative start bit, the Serial Input (SI) must remain HIGH if no data is incoming. When stop and parity bits are received, they are checked against the control presets and, if an error is detected, the Parity Error (PE), Total Stop Bits (TSB) or Framing Error (FE) bit of the status word output goes HIGH. If a parity check is not required, the No Parity (NP) control preset can be hard-wired HIGH or left open-circuit.

Data handling in the computer to peripheral path

A full circuit diagram of the computer to peripheral path of the Interspeeder is given in Fig.19. Shifting parallel data into the data-bits holding register of the transmitter section of UART1 for immediate transmission via the Serial Output (SO) is simple. It occurs if valid data is available at the output of the FIFO buffer and the Data Strobe ($\overline{DS}$) input of UART1 is set HIGH. If a continuous flow of serial data is to be shifted out, a new $\overline{DS}$ signal must be generated for each word. This is done by C5/R5 using the positive flank of the EOC (End Of Character) signal of the previous word. However, the DOR flag from FIFO B is also applied to the input of NAND gate N5 to prevent further $\overline{DS}$ pulses being generated if the FIFOs are empty (DOR B = LOW).

The question now arises as to which of the signals at the input of gate N5 (EOC or DOR B) initiates the first $\overline{DS}$ signal. The first time that DOR B goes HIGH is a sign that data is present in the FIFO. C4/R4 then makes a pulse from the positive-going flank of DOR B and the first $\overline{DS}$ pulse is presented to the $\overline{DS}$ input of UART1 via N5, N4 and INV8. The EOC signal at the other input to the gate N5 initiates the subsequent $\overline{DS}$ pulses.

The right data must be present at the output of the FIFO buffer when a $\overline{DS}$ pulse occurs. This is ensured by signal TBMT (Transmitter Buffer Empty) from UART1. When a $\overline{DS}$ pulse occurs, TBMT goes LOW to indicate that new data must not be sent to the UART input. When the present data has been transferred from the data-bits holding register of the UART transmitter to the output buffer shift register, TBMT goes HIGH again. Network C7/R7 then makes a pulse from the rising flank of TBMT and feeds it to the Shift Out ($\overline{SO}$) input of FIFO B. The UART completely handles shifting-in of serial asynchronous data as long as it includes start and stop bits and arrives at the right baud rate. When the word has been received and is available in parallel form, the UART issues a DAV (Data Available) signal. This signal is used as an SI (Shift In) pulse for the FIFO buffer.

Empty/half-full flag

Flip-flops FF1 and FF2 in Fig.19 keep track of the state of the FIFOs. The following conditions are important:

- If FIFO B is full and data continues to arrive (DOR A = HIGH), an Xoff code must be sent to the computer
- If FIFO B is empty (DOR B = LOW), an Xon code must be sent to the computer
- The computer mustn't transmit data while the FIFOs are being emptied (DOR B = pulsed).

As long as FIFO B isn't full, FIFO A will continue to generate DOR A pulses. However, FF1 will not be set because filter C6/R6, which doesn't have to be adapted for different baud rates, blocks any short pulses that occur during 'ripple-through'.

If FIFO B becomes full and data continues to arrive, DOR A remains HIGH and FF1 is set (half-full). The

negated output of FF1 then goes LOW and triggers FF5 in Fig.20 so that the Xoff code is set on the data path selector. This Xoff code is sent to the computer to stop it transmitting further data. However, this can take some time, during which the computer will transmit some extra words into FIFO A. How long the computer takes to stop transmitting data depends on its response time. Also, if the ratio of the peripheral/computer baud rates is less than 1:2, the Xoff word has to wait for an empty space in the data stream. However, no data will be lost because the second FIFO can store another 64 words, which will give sufficient time for the computer to respond to the Xon/Xoff interrupt.

When FIFO B is empty, DOR B remains LOW so that no further $\overline{DS}$ pulses pass via gate N5 and, at the same time, FF2 is set and immediately reset again causing FF1 to be reset and its negated output to go HIGH to generate an Xon signal.

Data handling in the peripheral to computer path

If an Xon/Xoff command isn't generated by FF1 in Fig.19, flip-flops FF4 and FF5 in Fig.20 remain reset and the output from NAND gate N1 is LOW. The DAV2 output from UART2 goes HIGH and sets S HIGH ('normal' mode) via FF3 when an entire word has been received from the peripheral and transferred to the data-bits holding register of the UART2 receiver. The DAV2 signal constantly resets itself via INV1 and the Reset DAV ($\overline{RDAV2}$) input of UART2. The output from INV1 is also used to generate the Data Strobe ($\overline{DS2}$) for UART2 via INV1, N3 and INV2. The serial data from the peripheral is then passed to the computer via Serial Input SI2 of UART2, the parallel output of UART2, the data path selector, the parallel input of UART2 and the Serial Output (SO2) of UART2. When the word has been completely read-out, the End Of Character (EOC2) signal resets FF3 via INV3 to restore the system to the waiting state.

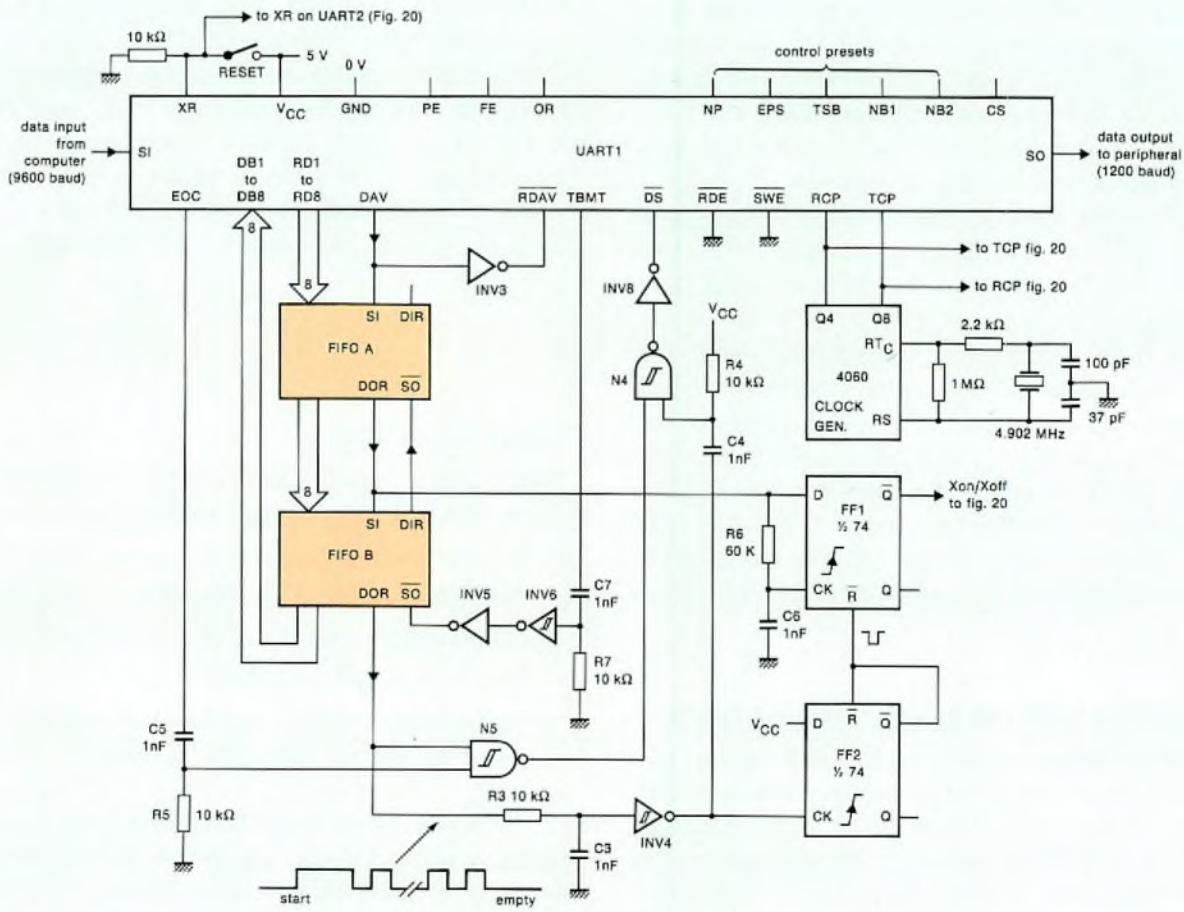

Fig.19 The computer to peripheral path of the Interspeeder

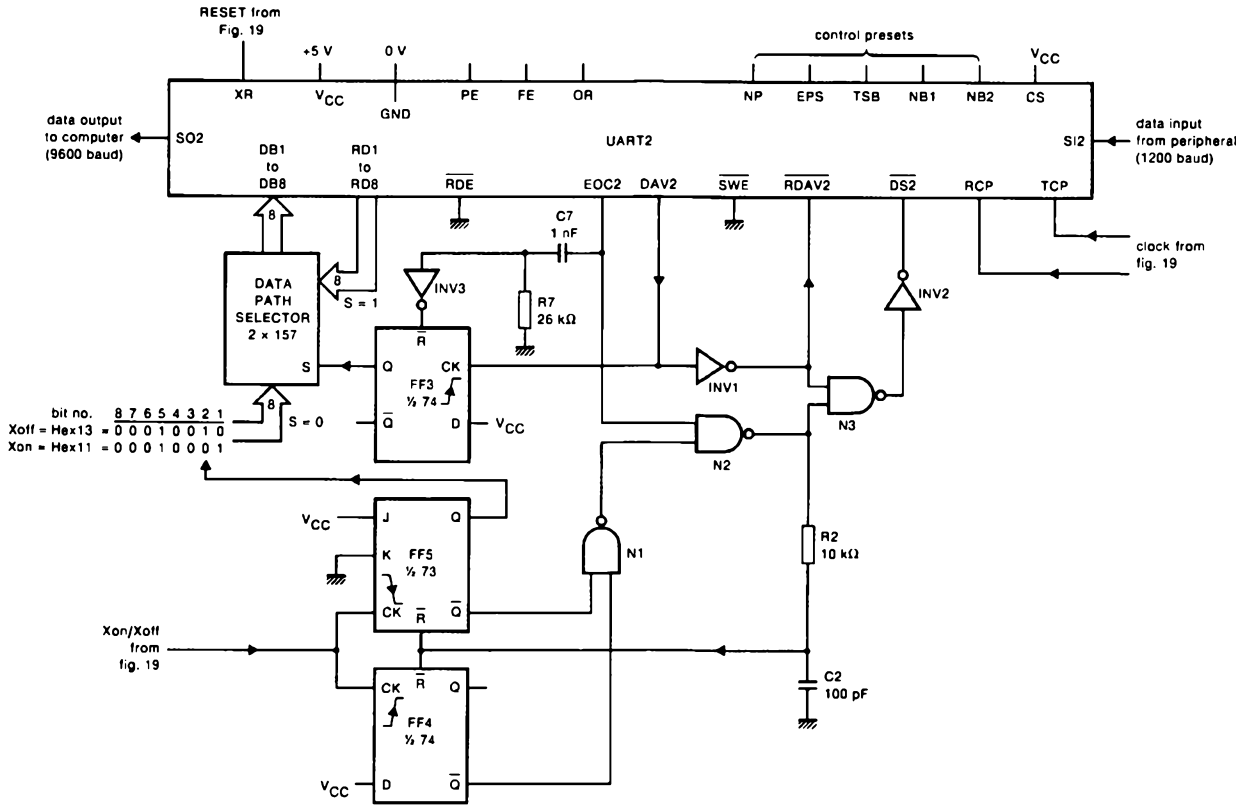

Fig.20 The peripheral to computer path of the Interspeeder

Normal/Xon/Xoff controller

The data path selector comprises two quad two-input multiplexers type PC74HC/HCT157 and allows selection of either the 'normal' mode of transmission from the peripheral to the computer as just described (S = HIGH), or transmission with an Xoff or Xon code (S = LOW).

When an Xon/Xoff command is received at the clock inputs of FF4 and FF5, these flip-flops determine whether a positive flank is received (FF4 set = Xon code to be transmitted), or a negative flank (FF5 set = Xoff code to be transmitted). The Q output of FF5 generates the second bit of the Xon/Xoff code applied to the data path selector, the other seven bits being hard-wired because they're common to both codes.

The negated outputs of FF4 and FF5 are passed to the inputs of NAND gate N1, thereby making its output HIGH to indicate that an Xon or Xoff code must be transmitted. If the End Of Character (EOC2) flag is HIGH (UART ready for transmission), the output of NAND gate N2 is HIGH and so is the output of INV1 because the DAV2 signal has reset itself via the $\overline{\text{RDAV2}}$ input of UART2. The output of NAND gate N3 is therefore LOW and a data strobe ($\overline{\text{DS2}}$) is generated via INV2. The rising edge of SO sets EOC2 LOW when the Xon/Xoff word has been transmitted. If EOC2 were to be LOW during reception of the Xon/Xoff command, NAND gate N2 would be blocked until the UART had finished transmitting the previous word. The rising edge of the EOC2 pulse would then reset FF3, thereby setting the data path selector back into the right state (S = LOW) and allowing flip-flop FF4 or FF5 to start a $\overline{\text{DS2}}$ strobe. The purpose of the delay obtained with C2/R2 is to lengthen the $\overline{\text{DS2}}$ strobe to at least 200 ns as required by the UART.

Abstracts

SAL capacitors for automotive applications

Electronic equipment is an important and growing part of the automotive industry, which requires components and assemblies that can operate under very demanding conditions. Solid aluminium (SAL) capacitors are ideal for these harsh conditions: they have no known failure mechanisms, can tolerate a variety of electrical loads, operate under extremes of temperature, and can withstand mechanical shock and vibration. This article describes the construction and properties of SALs, and highlights their automotive applications.

Redesign of small-signal switching diodes in SOT packages

Philips have completely redesigned their small-signal diodes in SOT23 and SOT143 packages. The redesign incorporates silicon nitride passivation to protect the active areas of the crystal; a single layer of aluminium, instead of a Ti/Pt/Au triple-layer, as the top metallization; adding recognition marks and changing the shape of the top contact, making it easier to align and bond the crystals with automatic wire bonding machines. The result: greatly improved reliability.

Blind & buried vias for multilayer PCBs

Not widely used to date, blind and buried vias are a useful extension to multilayer technology for dealing with today's high-density printed wiring requirements. They can reduce the number of circuit layers needed, making multilayer boards thinner and lighter. Furthermore, buried vias simplify both manual and computer-aided board design. Finally, the low aspect ratio (board thickness to hole diameter) of buried vias makes the plating of holes easy, a big advantage over through vias in conventional multilayers.

An angle on the corners
the new approach in shadow-mask suspension systems

The new Flat-Square colour picture tube of Philips uses a corner-pin suspension system for its shadow masks. A major advantage of this new system is that the thermal compensation mechanism relies, not on the reaction of bimetal elements as with conventional designs, but directly on mechanical movement of the mask-diaphragm assembly relative to the faceplate. The result, faster, more positive, more symmetrical temperature compensation. Other advantages are significantly better microphony and lighter construction. Already, several other manufacturers are moving over to corner suspension, and there's little doubt that the next few years will see a major switch to this new, superior system.

The magnetoresistive sensor
– a sensitive device for detecting magnetic-field variations

The KMZ10 magnetoresistive sensor is a recent development for detecting magnetic-field variations, and in many applications, provides an attractive alternative to the Hall-effect sensor. The KMZ10, for example, is more sensitive than the Hall-effect sensor and can operate over an extremely wide temperature range. What's more, its frequency range is much wider: from DC up to several megahertz. For applications requiring high sensitivity and low drift, and where mechanical stresses may be high, the KMZ10 magnetoresistive sensors are clear favourites. This article describes the operation of the sensor, compares it with its main rivals and gives a large number of application examples.

HCMOS FIFOs and their applications

To allow a slow peripheral to transmit to a faster computer, it's necessary to connect a UART between the computer and the peripheral. On the other hand, to allow the faster computer to transmit to the slower peripheral, its necessary to interpose a UART and a buffer between them. Important requirements for the buffer are low power consumption, wide operating temperature range, CMOS/TTL compatibility, low supply voltage and high noise immunity. Since these are all features of Philips' HCMOS logic ICs, FIFO buffers PC74HC/HCT7030 and PC74HC/HCT40105 are ideal for the purpose. This article describes the operating principles of the FIFOs, explains how to increase their word length and capacity and gives several application examples. The article concludes with a description of a complete bidirectional interspeeder for connection between a fast computer and a slower peripheral.

Al-Elkos mit festem Elektrolyten (SAL) für Anwendungen in der Automobiltechnik

Die elektronische Ausstattung spielt in der Automobilindustrie, die an Bauelemente und Zusammenstellungen höchste Ansprüche stellt, eine wichtige und zunehmende Rolle. Trockenaluminium-Kondensatoren (SAL-Kondensatoren) sind für diese harten Einsatzbedingungen optimal geeignet: Sie haben keine bekannten Ausfallmechanismen, sind geeignet für unterschiedliche elektrische Belastungsanforderungen, funktionieren bei extremen Temperaturen und sind beständig gegen mechanische Stöße und Schwingungen. In diesem Artikel werden Aufbau und Eigenschaften von Trockenaluminium-Kondensatoren beschrieben und ihre Anwendungen in der Automobiltechnik hervorgehoben.

Neuer Entwurf von Kleinsignal-Schaltdioden in SOT-Gehäusen

Philips hat seine Kleinsignal-Schaltdioden in den Gehäusen SOT23 und SOT143 vollkommen neu entworfen. Der neue Entwurf umfaßt eine Siliziumnitrid-Passivierung zum Schutz der wirksamen Flächen des Kristalls und eine einzige Aliminiumschicht als obere Metallisierung anstatt der dreifachen Schicht aus Ti/Pt/Au. Außerdem wurden Kennmarken hinzugefügt und die Form des oberen Kontakts geändert, so daß sich die Kristalle leichter ausrichten und mit automatischen Bondmaschinen bonden lassen. Das Ergebnis ist eine wesentlich verbesserte Zuverlässigkeit.

Sacklöcher und vergrabene Löcher für Multilayer-Leiterplatten

Sacklöcher und vergrabene Löcher – bis heute noch nicht weit verbreitet – tragen in der Multilayer-Technologie dazu bei, die Anforderungen der hohen Bauelementdichte zu erfüllen. Bei Anwendung dieser Löcher sind weniger Lagen erforderlich, so daß die Multilayer-Leiterplatten dünner und leichter werden. Außerdem machen vergrabene Löcher sowohl den manuellen als auch den computergestützten Leiterplatten-Entwurf einfacher. Schließlich lassen sich auch die Löcher aufgrund des geringen Größenverhältnisses (Leiterplattendicke zu Lochdurchmesser) leicht galvanisieren, was ein großer Vorteil gegenüber den Durchkontaktierungen in herkömmlichen Multilayer-Leiterplatten ist.

Der Winkel in der Ecke
– die neue Lösung bei der Lochmasken-Aufhängung

Bei der neuen Flat-Square-Farbbildröhre von Philips wird die Lochmaske an einer selbstkompensierenden Eckenaufhängung befestigt. Der Hauptvorteil dieses neuen Systems besteht darin, daß die Kompensation der Wärmeausdehnung nicht von der Reaktion von Bimetall-Elementen abhängt, wie bei herkömmlichen Entwürfen, sondern direkt von der mechanischen Bewegung der Masken-Rahmen-Zusammenstellung in bezug auf den Glasschirm. Damit erfolgt der Ausgleich der Maskenausdehnung aufgrund der Betriebstemperatur schneller, sicherer und symmetrischer. Weitere Vorteile sind erheblich bessere Mikrophonie-Eigenschaften und leichtere Konstruktion. Einige andere Hersteller übernehmen bereits die Eckenaufhängung, und höchstwahrscheinlich wird man in naher Zukunft größtenteils auf dieses neue, überlegene System übergehen.

Der Magnetfeldsensor
– ein empfindliches Bauelement zur Detektion von Magnetfeldern

Der Magnetfeldsensor KMZ10 ist ein Bauelement zur Detektion von Magnetfeldern und stellt in vielen Anwendungsbereichen eine Alternative zum Halleffekt-Sensor dar. Der KMZ10 ist z.B. empfindlicher als der HalleffektSensor und eignet sich für einen großen Temperaturbereich. Sein Frequenzbereich reicht von Gleichstrom bis zu Wechselstrom von einigen MHz. Bei Anwendungen, die hohe Empfindlichkeit und geringe Drift erfordern und bei denen hohe mechanische Beanspruchung auftreten kann, bieten die Magnetfeldsensoren KMZ10 deutliche Vorteile. In diesem Artikel wird die Funktion des Sensors beschrieben und der Sensor mit Sensoren anderer Technologien verglichen; außerdem werden zahlreiche Anwendungsbeispiele aufgeführt.

HCMOS-FIFOs und ihre Anwendungen

Für die Datenübertragung von einem 'langsamen' Peripheriegerät an einen 'schnelleren' Computer muß zwischen Computer und Peripheriegerät ein UART (universeller asynchroner Empfänger/Sender) geschaltet werden, für die Datenübertragung in Gegenrichtung - vom schnellen Computer zum langsameren Peripheriegerät - hingegen sind ein UART und ein Pufferspeicher zwischenzuschalten. Wichtige Anforderungen an den Pufferspeicher sind dabei geringe Stromaufnahme, großer Arbeitstemperaturbereich, CMOS/TTL-Kompatibilität, niedrige Versorgungsspannung und hohe Rauschimmunität. Die HCMOS-Logik-ICs von Philips, die FIFO-Pufferspeicher PC74HC/HCT7030 und PC74HC/HCT40105, erfüllen die oben aufgeführten Anforderungen und eignen sich daher hervorragend für diese Aufgabe.
Im vorliegenden Beitrag wird das Arbeitsprinzip der FIFOs beschrieben. Außerdem werden Möglichkeiten zur Steigerung von Wortlänge und Kapazität aufgezeigt und einige Anwendungsbeispiele aufgeführt. Die Beschreibung eines kompletten bidirektionalen 'Interspeeders' für die Verbindung eines schnellen Computers mit einem langsameren Peripheriegerät schließt diesen Beitrag ab.

Condensateurs aluminium à électrolyte solide pour l'industrie automobile

L'équipement électronique est une part importante et croissante de l'industrie automobile dont les composants et assemblages doivent pouvoir fonctionner dans des conditions sévères. Les condensateurs aluminium à électrolyte solide (ALUSOLID) répondent parfaitement à ces exigences: ils n'ont pas de défaut mécanique connu, tolèrent diverses charges électriques, fonctionnent à des températures élevées et résistent aux chocs mécaniques et aux vibrations. Cet article décrit la construction et les caractéristiques de ces condensateurs et met en valeur leur utilisation dans l'industrie automobile.

Nouvelle conception des diodes de commutation pour de petits signaux des boîtiers SOT

Philips a procédé à une refonte complète des cristaux pour les diodes petits signaux pour encapsulation en boîtiers SOT23 et SOT143. Cette conception nouvelle des cristaux comprend une couche de passivation au nitrure de silicium destinée à protéger les zones actives du cristal, une seule couche d'aluminium pour la métallisation supérieure (au lieu de la triple couche au Ti/Pt/Au), l'adjonction de repères et la modification de la forme du contact supérieur facilitant l'alignement et la soudure des cristaux par des machines automatiques. Il en résulte une fiabilité extrêmement accrue.

Trous borgnes et enterrés pour circuits multicouches

D'une utilisation restreinte à ce jour, les trous borgnes et enterrés représentent une extension intéressante de la technologie des multicouches permettant de répondre aux contraintes dues à la forte densité des liaisons des circuits imprimés actuels. Grâce à eux, il est possible de réduire le nombre des couches et de produire ainsi des cartes moins épaisses et plus légères. De plus, les trous enterrés simplifient la conception des cartes, qu'elle soit manuelle ou assistée par ordinateur. Pour finir, le faible rapport entre l'épaisseur de la carte et le diamètre des trous enterrés facilite la métallisation de ces derniers, un avantage sérieux sur les trous débouchants des multicouches classiques.

Suspension souple

Nouvelle approche pour la fixation des masques perforés

Le nouveau tube couleur Philips à écran plat est équipé d'un masque perforé suspendu par les coins. L'avantage principal de ce nouveau dispositif réside dans le fait que le mécanisme de compensation thermique ne repose pas sur la réaction de deux éléments bimétalliques comme dans la conception classique, mais directement sur le mouvement mécanique du cadre du masque par rapport à l'écran. Il en résulte une compensation de température plus rapide, positive et symétrique. Il s'ajoute à cela un meilleur effet microphonique et une construction plus légère. De nombreux autres constructeurs ont déjà adoptés la suspension souple et les prochaines années verront sans aucun doute la généralisation de son utilisation.

Le capteur magnétorésistif

Un dispositif sensible détectant les variations de champs magnétiques

Le capteur magnétorésistif KMZ10 est un dispositif récent de détection des variations de champs magnétiques qui, dans de nombreuses applications, fournit une solution de rechange intéressante au capteur à effet Hall. Le KMZ10 est entre autre plus sensible que ce dernier et fonctionne dans une gamme de températures extrêmement large. De plus, sa gamme de fréquence est plus étendue: du continu jusqu'à plusieurs mégahertz. Les capteurs magnétorésistifs KMZ10 partent grands favoris pour les applications exigeant une grande sensibilité et une faible déviation et subissant éventuellement de fortes contraintes mécaniques. Cet article décrit le fonctionnement du capteur, le compare à ses principaux concurrents et donne un grand nombre d'exemples d'applications.

Les registres FIFO HCMOS et leurs applications

Pour permettre la transmission de données d'un périphérique lent vers un ordinateur plus rapide, il faut connecter un émetteur-récepteur asynchrone universel (UART) entre ces deux éléments. Dans le sens inverse (de l'ordinateur vers le périphérique) il faut prévoir la connexion d'un UART et d'une mémoire-tampon. Les principales caractéristiques de la mémoire-tampon sont: une faible consommation d'énergie, une gamme de températures de fonctionnement étendue, la compatibilité CMOS/TTL, une faible tension d'alimentation et une grande immunité au bruit. Les circuits logiques HCMOS de Philips réunissant toutes ces caractéristiques, les registres FIFO PC74HC/HCT7030 et PC74HC/HCT40105 conviennent parfaitement à cet usage. L'article décrit les principes de fonctionnement des registres FIFO, explique comment augmenter leur longueur de mot et leur capacité et fournit plusieurs exemples d'applications. En conclusion, ils donnent la description d'une interface bidirectionnelle complète à connecter entre un ordinateur rapide et un périphérique lent.

Condensadores SAL para automóviles

El equipo electrónico desempeña cada vez más un papel muy importante en la industria del automóvil que utiliza componentes y conjuntos que han de funcionar en condiciones muy exigentes. Los condensadores de aluminio sólido (SAL) son idóneos para estas rigurosas condiciones por no conocer mecanismos que fallen, tolerar una gran variedad de cargas eléctricas, funcionar bajo temperaturas extremas y resistir golpes y vibraciones mecánicas. En este artículo se describe la construcción y propiedades de los condensadores SAL y se enumeran sus aplicaciones en el automóvil.

Rediseño de diodos de conmutación de pequeña señal en encapsulado SOT

Philips ha diseñado completamente de nuevo sus diodos de pequeña señal en encapsulados SOT23 y SOT143. La nueva fórmula incluye la pasivación de nitruro de silicio para proteger las zonas activas del cristal; una sola capa de aluminio en lugar de una triple Ti/Pt/Au, como metalización de la parte superior; se han adicionado marcas de reconocimiento y se ha cambiado la forma del contacto superior, lo que simplifica la alineación y soldadura de los cristales mediante máquinas automáticas. El resultado de todo ello es una notable mayor fiabilidad de funcionamiento.

Vías ciegas y simuladas para multicapas

Aunque de uso no muy divulgado, las vías ciegas y simuladas son un complemento útil en la tecnología de las multicapas por cumplir los requisitos hoy en día impuestos a los circuitos impresos de alta densidad. Entre otras cosas son capaces de reducir el número de capas necesarias, por lo que las placas de varias capas son más finas y ligeras. Y lo que es aún más, las vías ciegas simplifican el diseño manual y computerizado de las placas. Por último, la baja relación de aspecto (espesor de la placa con respecto al diámetro del orificio) de las vías ocultas facilita la metalización de orificios, lo que supone una gran ventaja sobre las vías directas en las multicapas corrientes.

Angulo en las esquinas

nuevo método en los sistemas de suspensión de máscara de sombra

El nuevo tubo de imagen color de Philips 'Flat-Square' utiliza un sistema de suspensión mediante pivote en las esquinas para sus máscaras de sombra. La principal ventaja de este nuevo sistema radica en el mecanismo de compensación térmica que descansa, no en la reacción de elementos bimetálicos como es el caso en los diseños corrientes, sino directamente en el desplazamiento mecánico del conjunto del diafragma de la máscara con respecto a la chapa frontal. El resultado es una compensación más duradera, más positiva y más simétrica de la temperatura. Otras ventajas son una microfonía notablemente mejor y construcción más ligera. Son ya varios los fabricantes que han optado por la suspensión en las esquinas, y no cabe duda que dentro de unos años se observará una cierta preferencia por este nuevo sistema superior.

Sensor magnetorresistivo

un dispositivo útil para detectar variaciones en los campos magnéticos

El sensor magnetorresistivo KMZ10 es algo completamente nuevo que sirve para detectar las variaciones en los campos magnéticos y en muchas otras aplicaciones y constituye una interesante alternativa para el sensor de efecto Hall. Así por ejemplo, el KMZ10 es de mayor sensibilidad que el de efecto Hall y admite un margen de temperatura sumamente amplio. Y lo que es aún más, tiene un margen de frecuencias mucho mayor: desde C.C. hasta varios megaherzios. Para aquellos usos que requieren una alta sensibilidad y baja desviación y allí donde pueden haber fuertes tensiones mecánicas, los sensores magnetorresistivos KMZ10 merecen una clara preferencia. En el presente artículo se describe el funcionamiento del sensor, se compara con sus principales competidores y se cita gran número de aplicaciones.

FIFO'S HCMOS y sus aplicaciones

Para que un equipo periférico lento pueda transmitir datos a un ordenador más rápido hay que conectar un UART entre ambos. Pero cuando es a la inversa, hay que intercalar un UART y una memoria. Requisitos importantes para la memoria son: bajo consumo, amplio margen de temperaturas de funcionamiento, compatibilidad CMOS/TTL, baja tensión de alimentación y gran inmunidad al ruido. Por ser éstas las características de los CI lógicos HC MOS de Philips, las memorias intermedias FIFO PC74HC/HCT7030 y PC74HC/HCT40105 son ideales para este fin. El presente artículo describe los principios de funcionamiento de las FIFO, explica como aumentar su longitud de palabra y capacidad al mismo tiempo que se citan varios ejemplos de aplicación. Termina el artículo con una descripción de un regulador de velocidad intermedio bidireccional para interconectar un ordenador rápido a un equipo periférico más lento.

Authors

Cees B. Admiraal was born in Renesse, The Netherlands. He studied physics at the University of Nijmegen and joined Philips in 1984. He is currently working on the development of shadow-mask suspension systems at the Technology Centre for Display Components, Eindhoven.

After joining Philips in 1964, **Chris J. Hartman** filled several functions in development, quality assurance and technical/commercial management in both the Glass and Lighting Divisions. He moved to Philips Components in 1985, first in the assembly factory at Stadskanaal, The Netherlands, and subsequently in Eindhoven as International Product Marketing Manager for small-signal diodes and zeners.

Henk Bongenaar was born in Hilversum, The Netherlands in 1935, and graduated in mechanical engineering from Breda University. After military service he joined the Development Department for TV picture tubes of Philips Components, Eindhoven, and is currently involved in the development of metal components.

Michiel W. Hillen graduated in physics from the University of Groningen, The Netherlands, and was awarded a PhD by the same university for his work on semiconductor physics. After working on CMOS technology at the ESAT Laboratory of the Katholieke Universiteit, Leuven, Belgium, he joined Philips Components, Nijmegen where he is currently involved in diode development.

Evert H.L.J. Dekker received his doctorate in solid-state chemistry from the University of Technology, Eindhoven, The Netherlands, in 1975. He then joined Philips' Research Laboratories where he worked on magnetic bubble circuit and memory design. From 1979 to 1986 he was responsible for solid electrolytic capacitor development at Philips' Electronic Components and Materials Division, Zwolle, and is currently innovative manager in charge of development and engineering of electrolytic capacitors and capacitor foils.

August Petersen was born near Flensburg, Germany, in 1937, and graduated in physics from the University of Kiel in 1964. The same year he joined the Valvo Application Laboratory, Hamburg, initially working on applications of passive components, especially piezo-electric ceramics. As a member of the Industrial Electronics Group, he is currently responsible for developing sensor control circuitry.

Alfred Goberecht was born in 1938 and in 1961 he received a chemical-industrial engineering degree from RHIK, Brussels, Belgium. The following year he joined MBLE, Brussels, working initially on non-linear resistors. In 1965 he became a process engineer for printed-circuit boards and for the last 15 years he has been involved in PCB technology development. More recently he has also been involved in international customer service.

Rob Volgers was born in Zutphen, The Netherlands, in 1956, and graduated in electrical engineering from Arnhem Polytechnic in 1980. The same year he joined Philips Components, Nijmegen, initially working on the design of 4000 CMOS series ICs. He is now involved in product support for CMOS logic.

Philips Components – a worldwide Group of Companies

Argentina: PHILIPS ARGENTINA S.A., Div. Components, Vedia 3892, 1430 BUENOS AIRES, Tel. (01) 541 - 7141 to 7747.
Australia: PHILIPS INDUSTRIES LTD., Components Division, 11 Waltham Street, ARTARMON, N.S.W. 2064, Tel. (02) 439 3322.
Austria: ÖSTERREICHISCHE PHILIPS INDUSTRIE G.m.b.H., UB Bauelemente, Triester Str. 64, 1101 WIEN, Tel. (0222) 60 101-820.
Belgium: N.V. PHILIPS PROF. SYSTEMS – Elcoma Div., 80 Rue Des Deux Gares, B-1070 BRUXELLES, Tel. (02) 525 6111.
Brazil: CONSTANTA-IBRAPE; (Active Devices): Av. Brigadeiro Faria Lima, 1735-SAO PAULO-SP, Tel. (011) 211-2600. CONSTANTA-IBRAPE; (Passive Devices & Materials): Av. Francisco Monteiro, 702 – RIBEIRAO PIRES-SP, Tel. (011) 459-8211.
Canada: PHILIPS ELECTRONICS LTD., Philips Components, 601 Milner Ave., SCARBOROUGH, Ontario, M1B 1M8, Tel. (416) 292-5161.
Chile: PHILIPS CHILENA S.A., Av. Santa Maria 0760, SANTIAGO, Tel. (02) 77 38 16.
Colombia: IND. PHILIPS DE COLOMBIA S.A., c/o IPRELENSO LTD., Cra. 21, No. 56-17, BOGOTA, D.E., Tel. (01) 2 49 76 24.
Denmark: MINIWATT A/S, Strandlodsvej 2, P.O. Box 1919, DK 2300 COPENHAGEN S, Tel. (01) 54 11 33.
Finland: PHILIPS COMPONENTS, Sinikalliontie 3, SF-02631 ESPOO HELSINKI 10, Tel. 09 +358-0-50 261.
France: RTC-COMPELEC, 117 Quai du Président Roosevelt, 92134 ISSY-LES-MOULINEAUX Cedex, Tel. (01) 40 93 80 00.
Germany (Fed. Republic): VALVO, UB Bauelemente der Philips G.m.b.H., Valvo Haus, Burchardstrasse 19, D-2 HAMBURG 1, Tel. (040) 3296-0.
Greece: PHILIPS HELLENIQUE S.A., Elcoma Division, No. 15, 25th March Street, GR 17778 TAVROS, Tel. (01) 48 94 339/4894 911.
Hong Kong: PHILIPS HONG KONG LTD., Elcoma Div., 15/F Philips Ind. Bldg., 24-28 Kung Yip St., KWAI CHUNG, Tel. (0)-24 51 21.
India: PEICO ELECTRONICS & ELECTRICALS LTD., Elcoma Dept., Band Box Building, 254-D Dr. Annie Besant Rd., BOMBAY – 400 025, Tel. (022) 493 0311/493 0590.
Indonesia: P.T. PHILIPS-RALIN ELECTRONICS, Elcoma Div., Setiabudi II Building, 6th Fl., Jalan H.R. Rasuna Said (P.O. Box 223/KBY) Kuningan, JAKARTA 12910, Tel. (021) 51 79 95.
Ireland: PHILIPS ELECTRICAL (IRELAND) LTD., Components Division, Newstead, Clonskeagh, DUBLIN 14, Tel. (01) 69 33 55.
Italy: PHILIPS S.p.A., Div. Componenti, Piazza IV Novembre 3, I-20124 MILANO, Tel. (02) 6752.1.
Japan: NIHON PHILIPS CORP., Shuwa Shinagawa Bldg., 26-33 Takanawa 3-chome, Minato-ku, TOKYO (108), Tel. (03) 448-5611. (IC Products) SIGNETICS JAPAN LTD., 8-7 Sanbancho Chiyoda-ku, TOKYO 102, Tel. (03) 230-1521.
Korea (Republic of): PHILIPS ELECTRONICS (KOREA) LTD., Elcoma Div., Philips House, 260-199 Itaewon-dong, Yongsan-ku, SEOUL, Tel. (02) 794-5011.
Malaysia: PHILIPS MALAYSIA SDN BHD, Components Div., 345 Jalan Gelugor, 11700 PULAU PINANG, Tel. (04) 87 00 44.
Mexico: ELECTRONICA, S.A de C.V., Carr. México-Toluca km. 62.5, TOLUCA, Edo. de México 50140, Tel. Toluca 91 (721) 613-00.
Netherlands: PHILIPS NEDERLAND, Marktgroep Elonco, Postbus 90050, 5600 PB EINDHOVEN, Tel. (040) 78 37 49.
New Zealand: PHILIPS NEW ZEALAND LTD., Components Division, 110 Mt. Eden Road, C.P.O. Box 1041, AUCKLAND, Tel. (09) 605-914.
Norway: NORSK A/S PHILIPS, Electronica Dept., Sandstuveien 70, OSLO 6, Tel. (02) 68 02 00.
Pakistan: PHILIPS ELECTRICAL CO. OF PAKISTAN LTD., Philips Markaz, M.A. Jinnah Rd., KARACHI-3, Tel. (021) 72 57 72.
Peru: CADESA, Av. Pardo y Aliaga No. 695, 6th Floor, San Isidro, LIMA 27, Tel. (014) 70 70 80.
Philippines: PHILIPS INDUSTRIAL DEV. INC., 2246 Pasong Tamo, P.O. Box 911, Makati Comm. Centre, MAKATI-RIZAL 3116, Tel. (02) 868 951 to 59.
Portugal: PHILIPS PORTUGUESA S.A.R.L., Av. Eng. Duarte Pacheco 6, 1009 LISBOA Codex, Tel. (019) 68 31 21.
Singapore: PHILIPS PROJECT DEV. (Singapore) PTE LTD., Elcoma Div., Lorong 1, Toa Payoh, SINGAPORE 1231, Tel. 35 02 000.
Spain: MINIWATT S.A., Balmes 22, 08007 BARCELONA, Tel. (03) 301 63 12.
Sweden: PHILIPS KOMPONENTER A.B., Lidingövägen 50, S-11584 STOCKHOLM, Tel. (08) 782 1 000.
Switzerland: PHILIPS A.G., Components Dept., Allmendstrasse 140-142, CH-8027 ZÜRICH, Tel. (01) 488 22 11.
Taiwan: PHILIPS TAIWAN LTD., 150 Tun Hua North Road, P.O. Box 22978, TAIPEI, Taiwan, Tel. (02) 71 20 500.
Thailand: PHILIPS ELECTRICAL CO. OF THAILAND LTD., 283 Silom Road, P.O. Box 961, BANGKOK, Tel. (02) 233-6330-9.
Turkey: TÜRK PHILIPS TICARET A.S., Components Department, Inönü Cad., No. 78-80, 80090 Ayazpasa ISTANBUL, Tel. (01) 143 59 10.
United Kingdom: PHILIPS COMPONENTS Ltd., Mullard House, Torrington Place, LONDON WC1E 7HD, Tel. (01) 580 6633.
United States: AMPEREX ELECTRONIC CORP., 230 Duffy Avenue, P.O. Box 560, HICKSVILLE, L.I.N.Y. 11802, Tel. (516) 931-6200. (Active Devices & Materials) AMPEREX SALES CORP., Providence Pike, SLATERSVILLE, R.I. 02876, Tel. (401) 762-9000. (Colour picture tubes – Monochrome & Colour display tubes) PHILIPS DISPLAY COMPONENTS, 50 Johnston St., SENECA FALLS, N.Y. 13148, Tel. (315) 568-5881. (IC Products) SIGNETICS CORPORATION, 811 East Arques Avenue, SUNNYVALE, CA 94088-3409, Tel. (408) 991-2000. (Passive & Electromech. Dev.) MEPCO/CENTRALAB, INC., 2001 West Blue Heron Blvd, RIVIERA BEACH, Florida 33404, Tel. (305) 881-3200.
Uruguay: LUZILECTRON S.A., Avda Uruguay 1287, P.O. Box 907, MONTEVIDEO, Tel. (02) 98 53 95.
Venezuela: IND. VENEZOLANAS PHILIPS S.A., c/o MAGNETICA S.A., Calle 6, Ed. Las Tres Jotas, App. Post. 78117, CARACAS, Tel. (02) 239 39 31.

For all other countries apply to: Philips Components Division, International Business Relations, P.O. Box 218, 5600 MD EINDHOVEN, The Netherlands, Telex 35000 phtcnl

AX65

Printed in The Netherlands 9398 705 20011

Philips Components

PHILIPS

PHILIPS